

Alma Mater Studiorum – Università di Bologna

DOTTORATO DI RICERCA IN  
**SCIENZE BIOCHIMICHE E BIOTECNOLOGICHE**

**Ciclo XXVIII**

Settore Concorsuale di afferenza: **05/E1 – Biochimica generale e biochimica clinica**

Settore Scientifico disciplinare: **BIO/10 Biochimica**

**Modulation of tumor cell metabolism by the ATP  
synthase inhibitor protein (IF<sub>1</sub>) and role of the  
miRNAs as drivers of drug resistance**

Presentata da: **Dott.ssa SIMONA BARBATO**

**Coordinatore Dottorato**

**Prof. Santi Mario Spampinato**

**Relatore**

**Prof. Giancarlo Solaini**

**Correlatore**

**Prof.ssa Alessandra Baracca**

**Esame finale anno 2016**



# Index

---

<b>Index</b> .....	<b>1</b>
<b>Abstract</b> .....	<b>5</b>
<b>Introduction</b> .....	<b>7</b>
<b>1- Cancer and metabolism</b> .....	<b>7</b>
<b>1.1- Mitochondria</b> .....	<b>9</b>
<b>1.1.1- Mitochondrial structure</b> .....	<b>11</b>
<b>1.1.2- Mitochondrial homeostasis: fission and fusion</b> .....	<b>14</b>
<b>1.1.3- Mitochondrial genome</b> .....	<b>16</b>
<b>1.1.4- ETC</b> .....	<b>18</b>
<b>1.1.5- Oxidative phosphorylation</b> .....	<b>23</b>
<b>1.1.6- ATP synthase: structure and function</b> .....	<b>25</b>
<b>1.1.6.1- Regulation of ATP synthase</b> .....	<b>26</b>
<b>1.1.6.2- Dimerization of ATP</b> .....	<b>27</b>
<b>2- IF<sub>1</sub></b> .....	<b>29</b>
<b>2.1- IF<sub>1</sub> in dimerization</b> .....	<b>32</b>
<b>2.1- IF<sub>1</sub> and ROS</b> .....	<b>32</b>
<b>2.2- IF<sub>1</sub> in cancer</b> .....	<b>33</b>
<b>3- Altered pathways in cancer</b> .....	<b>35</b>
<b>3.1- SHH pathway</b> .....	<b>36</b>
<b>3.1.1- Shh pathway and Melanoma</b> .....	<b>39</b>
<b>3.2- Melanoma therapy and Drug resistance</b> .....	<b>41</b>
<b>Aim of the Study</b> .....	<b>44</b>
<b>Materials &amp; Methods</b> .....	<b>47</b>
<b>1- Cell Culture</b> .....	<b>47</b>

2- <i>Bacterial Transformation &amp; plasmid isolation</i> .....	48
3- <i>Cell Transfection</i> .....	48
3.1- <i>RNAi silencing through shRNA</i> .....	48
3.2- <i>miRNAs</i> .....	49
4- <i>Cell Growth Evaluation</i> .....	50
5- <i>Cell viability and Annexin V assays</i> .....	50
5- <i>Flow Cytometric Assessment</i> .....	51
6- <i>Mitochondrial membrane potential</i> .....	51
7- <i>Brightfield and Fluorescence Microscopy</i> .....	52
8- <i>Protein concentration</i> .....	52
9- <i>Mitochondria Isolation</i> .....	53
10- <i>BN-PAGE and Western Blot Analysis</i> .....	53
11- <i>In-gel ATPase Activity</i> .....	54
12- <i>SDS-PAGE and Western Blot Analysis</i> .....	54
13- <i>Citrate Synthase Activity</i> .....	55
14- <i>Intracellular steady-state ATP</i> .....	56
15- <i>ATP synthesis Rate</i> .....	56
16- <i>ATP hydrolysis</i> .....	57
17- <i>Glucose consumption and Lactate release assay</i> .....	58
18- <i>Analysis of Intracellular ROS in Live Cells (CellRox® Orange &amp; CellRox® Deep Red)</i> .....	58
19- <i>Oxygen Consumption Rate</i> .....	59
20- <i>Dual Luciferase Assay</i> .....	59
21- <i>miRNAs-gene targeting prediction</i> .....	60
22- <i>Real-time quantitative RT-PCR</i> .....	60
23- <i>Data Analysis</i> .....	61

<b>Results - 1<sup>st</sup> part: IF<sub>1</sub></b> .....	62
<b>1- IF<sub>1</sub> expression and shRNA-mediated stable silencing</b> .....	62
1.1- Cell model: Human osteosarcoma 143B cells.....	63
1.2- Assessment of the most efficient shRNA sequence.....	64
1.3- IF <sub>1</sub> silencing: stable clones IF <sub>1</sub> -KD were established.....	65
<b>2- Biochemical characterization of IF<sub>1</sub> - silenced clones</b> .....	68
2.1- Cell viability .....	68
2.2- Glucose consumption and Lactate release.....	69
2.3- Mitochondrial parameters and ATP content.....	70
<b>3- Bioenergetic changes in IF<sub>1</sub>-silenced clones</b> .....	73
3.1- Oxygen consumption rate.....	73
3.2- OXPHOS .....	75
3.3- Mitochondrial membrane potential.....	76
3.4- ATPase activity .....	78
<b>4- ROS and IF<sub>1</sub></b> .....	79
4.1 - Evaluation of intracellular ROS.....	79
<b>5- Dimerization of F<sub>1</sub>F<sub>0</sub> ATP synthase and IF<sub>1</sub></b> .....	80
5.1 Distribution of monomers and oligomers of F <sub>1</sub> F <sub>0</sub> -ATPase.....	80
5.2 IF <sub>1</sub> binds to the dimeric form of ATP synthase.....	82
<b>Results - 2<sup>nd</sup> part: miRNAs</b> .....	84
<b>6- miRNAs profiling pattern of expression in cancer</b> .....	84
6.2 SUFU is down-regulated in resistant cells.....	86
6.3 SHH pathway activation .....	87
<b>7- Variation of miR-136 expression</b> .....	88
7.1- SUFU.....	89
7.2- SHH pathway.....	91
7.3- Cell growth evaluation.....	93

<b>8- The effect of BRAF-I treatment on melanoma cells expression.....</b>	<b>96</b>
<b>8.1- BRAF-I decreases proliferation rate in melanoma cells .....</b>	<b>96</b>
<b>8.2- BRAF-I effect in sensitive melanoma cells .....</b>	<b>98</b>
<b>Discussion and conclusions.....</b>	<b>104</b>
<b>List of References.....</b>	<b>113</b>

# Abstract

---

Metabolic reprogramming in cancer cells has recently been connected to  $IF_1$ , a key regulator of ATP synthase activity, which is found to be overexpressed in many human carcinomas. Considering the pivotal role of mitochondria inside the cells, mitochondrial alteration is crucial for tumors to grow and  $IF_1$  may help tumor progression by conserving cellular ATP in hypoxic conditions. Although the inhibitor has been deeply investigated, its role in tumorigenesis and/or cancer progression is still debated. Therefore, we prepared stable  $IF_1$ -silenced clones from the human osteosarcoma 143B cell line and assayed the main bioenergetic parameters, to examine both the role played by  $IF_1$  and the mechanism the inhibitor adopts in tumor cells to control mitochondrial mass, structure and function, besides regulate energy homeostasis. In our model, overall data indicate that the inhibitor protein can enhance the rate of ATP synthesis via OXPHOS, thus representing a successful strategy used by cancer cells to produce more energy and proliferate under oxygen availability.

In addition, recent literature has clearly evidenced that epigenetic alterations play a crucial role in modifying genes expression and modulating cancer cell metabolism, sustaining tumor growth and dissemination. Moreover, these molecules have been recently addressed as responsible for chemoresistance in several common therapies, prompting further investigations over miRNAs-driven metabolic alterations. However, compelling data emerging from a microRNA expression profiling, revealed an up-regulation of four miRNAs in BRAF(V600E) mutation-carrying melanomas, when developing resistance to BRAF-I, the major breakthrough in the treatment of these poor-prognosis malignancies. Intriguingly, three of these miRNAs target SUFU, a protein inhibiting the Shh pathway, which is altered in various forms of cancer. Since therapeutic failure still accounts for death in over 90% of patients with

metastatic cancers, we also focused on the role exerted by these miRNAs in the molecular mechanisms of drug-resistance.

# Introduction

---

## 1- Cancer and metabolism

Classically, cancer has been considered as a set of diseases driven by progressive genetic abnormalities, including mutations in oncogenes and tumor-suppressor genes, as well as chromosomal abnormalities: as a result, these changes lead cancer cells undergoing uncontrolled cell division and evasion from mechanism of cell death, along with a high potential to spread and metastasize in other parts of the body.

Particularly, in the last decades, an increasing attention has been given to the metabolic signature of cancer cells, as evidenced by plenty of data reporting that a metabolic reprogramming occurs in these cells, resulting in a predominantly glycolytic phenotype (1). The importance of these metabolic changes was initially highlighted by Sir Otto Warburg, who first postulated that changes in metabolism are fundamental in the origin and progression of cancer (2). Actually, he first hypothesized that such changes enable cancer cells to meet the large biosynthetic demand associated with rapid cell growth and division, along with the high energy requirements of tumor cells; however, this hypothesis was only marginally considered for long time. Indeed, unlike non-transformed cells, which typically rely on oxidative phosphorylation to supply the majority of energy demand, cancer cells are often characterized by mitochondrial dysfunction and a higher glycolysis rate, even in presence of abundant oxygen.

This metabolic reprogramming in cancer cells may stem from several mechanisms, like the above mentioned mutations in somatic genes, that play a role in promoting or suppressing malignant progression, or result from adaptation to low-oxygen environment within tumor. However, it is

important to note that OXPHOS activity, even though reduced, is not suppressed in tumor cells and that mitochondria are the main crossroads of important metabolic regulation in cancer: up-regulation of OXPHOS has been recently demonstrated in breast cancer (3) and an increase in oxygen consumption, together with a prominent expression of mitochondrial function genes have also been reported (4). Furthermore, mitochondria are the main intracellular producers of reactive oxygen species (ROS), that are typically increased in cancer and may interact with mtDNA, producing mutations in mitochondrial encoded protein that are crucial for mitochondrial functioning, including alteration of the bioenergetic and biosynthetic state of cancer cells.

All these features, often referred as “hallmarks of cancer” have recently been connected to IF<sub>1</sub>, an endogenous protein encoded by nuclear DNA, which plays a crucial role in regulating ATP synthase activity inside mitochondria. Long investigated in the mechanisms of ischemia and reperfusion, indeed, this inhibitor is now under investigation for other potential roles, spanning from physiological and pathological payrolls, that may contribute to modulate energy metabolism, as will be further addressed in the following sections, with particular relevance in cancer formation and progression.

Additionally, despite large evidence support the idea that oncogenic activation of signal transduction pathways and transcription factors are responsible for metabolic reprogramming, it has more recently become apparent that cancer is also driven by epigenetic alterations (5), functionally relevant modifications to the genome that do not involve a change in the nucleotide sequence, but are critical for gene expression and tumor cell reprogramming at cellular, genetic, biochemical and metabolic levels.

Particularly, great relevance has been recently given to the small RNAs molecules, known as microRNAs (or miRNAs), short, non-protein-coding RNAs of about 20 nucleotides in length, recognized to alter gene expression at a post-transcriptional level, targeting protein-coding genes and playing a role in almost all aspects of cancer biology (6).

Since it was discovered that miRNAs are abnormally expressed in cancer, in

2002 (7), accumulative studies showed that miRNAs play important roles in tumor growth and a large number of miRNAs have been identified to regulate cancer metabolism. Actually, several studies demonstrated that a large number of microRNAs are under the control of various metabolic stimuli, including nutrients, hormones, and cytokines (8) and have recently emerged as key regulators of metabolism. Particularly, some specific miRNAs in mitochondria, often referred as mitomiRs, are crucially involved in regulating mitochondrial metabolism, morphology and biogenesis, by modulating mitochondrial proteins encoded by nuclear genes.

Moreover, it has also been reported that the extracellular vesicles - known as exosomes - represent a vital communication between different cell types: carrying information to reprogram the recipient cells, miRNAs can facilitate the crosstalk between cancer and stromal cells in the tumor microenvironment, thus favoring tumor progression at all levels and perspectives (9).

Since important cellular signaling pathways are mediated by mitochondria, both in normal and transformed cells, an increasing number of human diseases is now correlated with morphological and functional changes occurring in these important organelles, including neurodegenerative diseases and cancer (10). For these reasons, research over the last decades largely focused on mitochondrial studies, in order to fully understand their implications in malignant progression and dissemination and, hopefully, to find new therapeutic approaches for severe malignancies.

## **1.1- Mitochondria**

Mitochondria are key organelles of nearly all eukaryotic cells, including plants, animals, fungi and protists (11).

Large enough to be observed with a light microscope, the first observations of intracellular structure, probably representing mitochondria, date to the 1840s (e.g. Henle 1841; Aubert, 1852; Flemming 1882, among others).

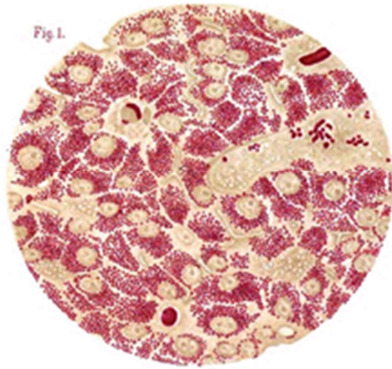


**Figure 1: Representation of “Bioblasts” observed by Richard Altmann.**  
(from *Die Elementarorganismen*, 1890)

In his book *Die Elementarorganismen* of 1890, Richard Altmann (1852-1900) referred to those “bioblasts” he observed using a special staining technique with fuchsine (*Figure 1*), as “elementary organisms” that secreted various cell substances, carrying out vital functions for the cells (12).

Comparing them to free-living bacteria, Altmann suggested that mitochondria were originally prokaryotic cells, that implemented oxidative mechanisms in eukaryotic cells. Nevertheless, his theory was rejected by his contemporaries, and the origin of these organelles has been long debated. However, based on similarities between mitochondria and bacteria, several decades later Altmann’s idea of symbiotic origin of mitochondria was accepted, and it is nowadays the most accredited. Further confirmation of this view is supported by the analysis of the gene sequences of mtDNA and the genome of *Rickettsia Prowazekii*, etiological agent of typhus, suggesting that mitochondria existing today derive from an ancestor of *R. Prowazekii*, as a result of an endosymbiotic single event (13).

The term “mitochondrion” was introduced in 1898 by Carl Benda, stemming from the Greek “*mitos*” (thread) and “*chondros*” (granule), that reflect the appearance of the organelles when observed, according to cellular requirements. Actually, these organelles are specialized structures that play a pivotal role in cell metabolism: often described as the “*powerhouse of the cell*” (14), they convert oxygen and nutrients into adenosine triphosphate (ATP), which is then used as a source of chemical energy for the cells (15). Being the chemical connection between catabolism and anabolism, ATP is a high energy compound required for many cellular processes, like muscle contraction, cell migration, secretion, and the maintenance of the ion

gradients that underlie membrane excitability (16).

In addition, mitochondria have an essential role in calcium homeostasis, in free radical signaling (17), and they are fundamental to cell life and death, as they harbor both pro- and anti-apoptotic proteins (18). Furthermore, they control cell cycle and cell growth, they may play a role in the aging process and are also implicated in several human diseases, including mitochondrial disorders and cardiac dysfunctions (19).

### 1.1.1- Mitochondrial structure

Mitochondria can be seen in the light microscope, but their detailed internal structure (*Figure 2, B*) is only revealed by electron microscopy (*Figure 2, A*).

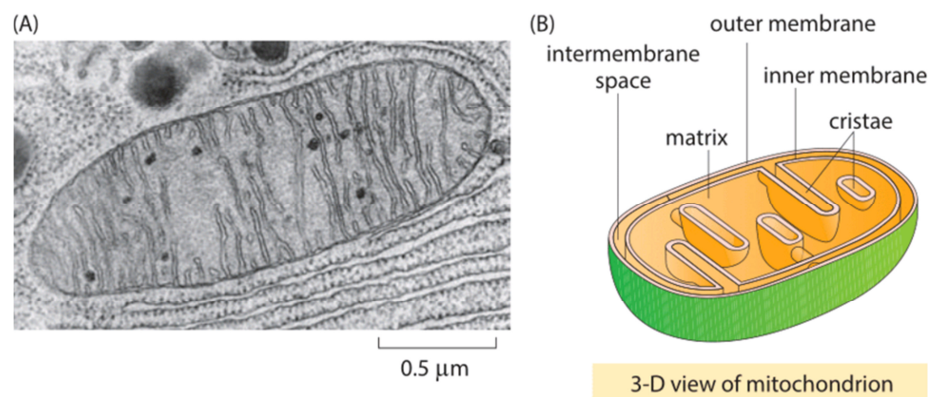


**Figure 2: Mitochondrial structure.**

**(A)** Electron microscopy of a mitochondrion **(B)** Schematic representation of a mitochondrion.

As shown in the image, they are pleomorphic and dynamic organelles, that reflect the cell type and the functional state of the tissue of origin. Indeed, according to the energetic demand of the cell, number and size of mitochondria vary widely, with a diameter ranging from 0.5 to 1.0 μm. Moreover, a recent study showed that mitochondria are functionally heterogeneous, thus resulting in a wide range of morphologies: different areas of the cytoplasm may, therefore, present subpopulations of specialized mitochondria in a different functional status, characterized by granular or rod-like aspect (20).

Despite their plasticity, all mitochondria are double-membrane-systems, including two phospholipid bilayers with embedded proteins that define four compartments, where different metabolic processes take place: the mitochondrial outer membrane (MOM), the intermembrane space, the mitochondrial inner membrane (MIM) and the matrix, enclosed by the inner membrane (21).

#### **1.1.1.1- MOM**

The outer mitochondrial membrane is around 6-7 nm thick and encloses the entire organelle. MOM is porous and barely selective to ions and other small molecules, therefore no membrane potential is registered across the outer membrane. Proteins localized in the MOM are integral membrane proteins involved in solute exchange between the cytosol and intermembrane space, protein import into mitochondria, docking sites for cytosolic proteins, and uptake of activated fatty acids into the mitochondria.

This membrane has a protein-to-phospholipid ratio close to 4:6, and contains large number of integral proteins, such as porins, forming channels to allow the diffusion of molecules less than 5000 Da, and translocases.

#### **1.1.1.2- Intermembrane Space**

The equivalent of the periplasm in the bacterial ancestors of mitochondria is the intermembrane space. There, concentration of small molecules - such as ions and sugars - is the same as in cytosol, because of the outer membrane permeability.

The protein content of this space is much lower than the matrix (about 6% of the total mitochondrial protein). Moreover, protein composition of the intermembrane space differs from cytosol and matrix, partially due to the specific amino acid sequences needed to cross the outer as well as the inner membrane. In this area, the main protein is cytochrome c, which is involved in cellular respiration and apoptosis. Other potential apoptotic inducers are present, as well as enzymes such as adenylate kinase and creatine kinase.

### 1.1.1.3- MIM

Approximately 21% of the total mitochondrial protein is localized in the MIM; in contrast to the MOM, it has a high protein-to-phospholipid ratio and is rich in cardiolipin, which is important to stabilize the respiratory chain supercomplexes (22). Also, the MIM is highly impermeable to ions and all anidrous molecules, a critical property for the maintenance of the proton gradient that supports the oxidative phosphorylation. Thus, solutes require specific transporters to enter or exit the matrix and it also contains the translocase of the inner membrane (TIM) complex, which catalyzes the import of proteins into the matrix together with the translocase of the outer membrane (TOM) complex.

To note, the inner membrane folds within the matrix (*Figure 3*) forming a series of invaginations called "*cristae*" that greatly increase the mitochondrial membrane surface, and so the number of sites for oxidative phosphorylation. These invaginations appear as tubular structures associated in layers, forming lamellar *cristae* of varying dimensions and forms, connected to the intermembrane space through small tubular joints (diameter of about 28 nm), called "*cristae junctions*" (23).

The *cristae* membranes contain the fully assembled complexes of the ETC and the ATP synthase (24) and are, therefore, the main site of biological energy conversion in all non-photosynthetic eukaryotes.

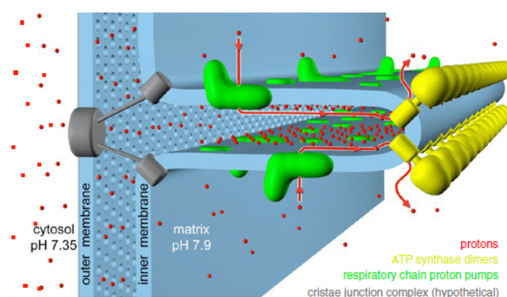


**Figure 3: Internal mitochondrial membrane folds into the matrix forming invaginations called *cristae*.** At the *cristae* ridges, the ATP synthases (yellow) form a sink for protons (red), while the proton pumps of the electron transport chain (green) are located in the membrane regions on either side of the dimer rows.

These structures have an important bioenergetic role, since they limit the passage of metabolites and expand the membrane surface for oxidative phosphorylation.

Moreover, as noted by Hackenbrock, the system of the inner membrane has a dynamic structure, reflecting the oxidative capacity of the tissue: mitochondria of high energy demand cells, such as muscle cells, contain more *cristae* and the volume of intra-cristal portions increases (25); conversely, *cristae* are less closely stacked in lower energy demand mitochondria, leaving more space for the matrix and its biosynthetic enzymes.

Nonetheless, the mechanisms that lead to their formation are not firmly established: recent studies highlighted a possible involvement of the enzyme  $F_1F_0$ -ATP synthase dimers in determining the folding and invagination of the internal membrane, but more studies are currently ongoing to further elucidate these mechanisms.

#### **1.1.1.4- Matrix**

The inner mitochondrial membrane delimits the mitochondrial matrix, which has a gelatinous consistency due to the high protein concentration (about 500 mg/ml), as it contains about 2/3 of the total protein in a mitochondrion. This area is the site of organellar DNA replication, transcription, protein biosynthesis and numerous enzymatic reactions (24). Several metabolic processes take place in the mitochondrial matrix, such as the cycle of citric acid and oxidation of pyruvate and fatty acids, vitamins and steroid hormones biosynthesis, etc. Moreover, it is also implicated in the calcium and ROS signaling and contains the mitochondrial DNA (mtDNA), ribosomes and other proteins, including those involved in the cell aging and apoptotic process (26).

### **1.1.2- Mitochondrial homeostasis: fission and fusion**

The functional integrity of mitochondria is strictly dependent on the molecular dynamics that controls their size and structure. Therefore, a sequence of alternative fusion and fission events (*Figure 4*) guarantee morphological and functional homeostasis of the mitochondrial reticulum

(27).

The fusion/fission machineries are modulated in response to changes in the metabolic conditions of the cell (28), enabling cells to generate a heterogeneous multitude of mitochondria or a highly dynamic tubular network, depending on the physiological conditions and on the functional state of the cell. Large mitochondrial networks, generated by the fusion of more mitochondria (*Figure 4*, left side), are usually present in cells with active metabolism, while quiescent cells mitochondria typically have numerous small spheres or short rods (*Figure 4*, right side), morphologically and functionally distinct (29).

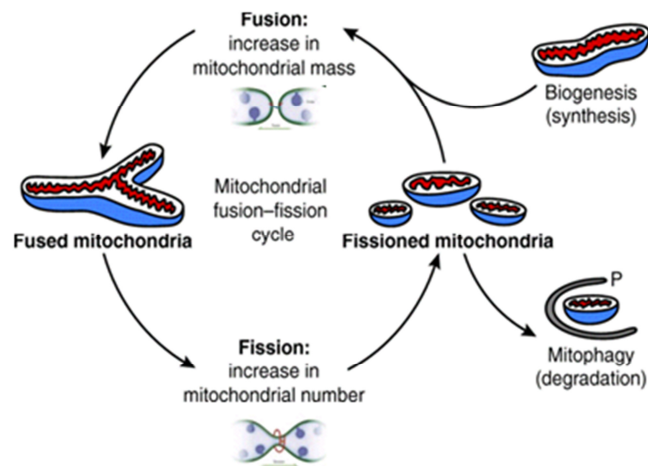


**Figure 4: Fusion and fission: interlinked processes critical for mitochondrial health.**

Moreover, fission is involved in the inheritance process and division of organelles during cell division, in the release of pro-apoptotic factors from the intermembrane space, into the intracellular translocation of organelles themselves and in the turnover of damaged organelles. Conversely, fusion is important for the complementation of the gene products of the mitochondrial DNA in heteroplasmic cells and to counteract the decline of mitochondrial function during aging. This process offers the advantage of limiting and correct mitochondrial dysfunctions caused by mutations accumulated in the

mitochondrial proteins.

### 1.1.3- Mitochondrial genome

Mitochondria have their own genetic system and protein translation machinery, complete with ribosomes, tRNAs and associated protein factors. Nevertheless, in the course of evolution, they have transferred almost all their genes for mitochondrial structure, intermediate metabolism, and biogenesis, to the nucleus: specifically, the core circuit genes for mitochondrial energy generation are encoded by mitochondrial DNA (mtDNA), whereas all of the genes for mitochondrial structure, intermediate metabolism, and biogenesis are encoded by nuclear DNA (nDNA).

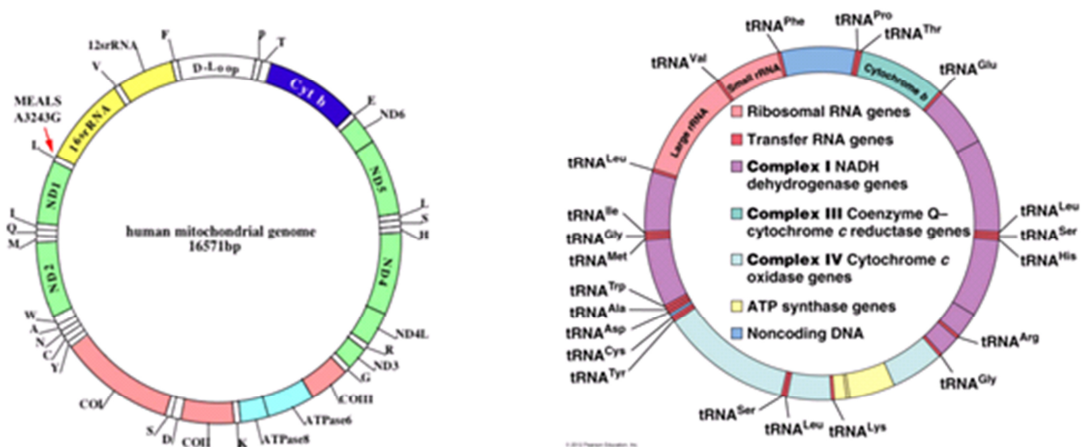


**Figure 5: Human mitochondrial genome.**

The human mtDNA is a double stranded, closed circular molecule of 16,569 nucleotides, containing only 37 genes (Figure 5). The two strands of mtDNA are differentiated by their nucleotide content, with a guanine-rich strand, referred to as the heavy strand (or H-strand), and a cytosine-rich strand, referred to as the light strand (or L-strand). Besides the structural genes, mtDNA contains the origin of H-strand replication and a control region (CR), that encompasses the promoters for both H- and L- strand transcription.

In humans, only 13 mitochondrial proteins are organelle-encoded; remarkably, all these polypeptides are hydrophobic subunits of ETC or ATP synthase. Along with the core OXPHOS polypeptides, the mtDNA encodes the 22 tRNA and 12S and 16S rRNA genes for mitochondrial protein synthesis. In addition, the mitochondrial genome contains more than 1000 nDNA-encoded mitochondrial genes, including the remaining structural subunits of the OXPHOS complexes, the structural polypeptides to assemble the mitochondrion, the mitochondrial intermediate metabolism proteins, and the proteins for mitochondrial biogenesis proteins, as well as the mitochondrial-specific DNA, RNA polymerases, and the ribosomal proteins (30).

Unlike nDNA, mtDNAs are maternally inherited and are present in multiple copies, depending on the bioenergetic demand of the cell. Moreover, mtDNA replicates independently from cell cycle and does not contain noncoding sequences among genes, since large mRNA is translated (there are no untranslated regions at 5' and 3'). Lastly, the mtDNA has a higher mutation rate compared to the nuclear DNA (nDNA): when a mutation arises, it creates a mixed population of normal and mutant mtDNAs, a state known as *heteroplasmy* and, at time of cell division, the two types of mtDNAs are randomly distributed into the daughter cells, contributing to accumulate mtDNA mutations over aging.

To note, an increase in mutant mtDNA declines the mitochondrial energetic function: poor quality mitochondria may enhance cellular oxidative stress, generate apoptosis signals and induce cell death. The bioenergetic crisis may also be further exacerbated by reactive species damage to glycolytic and glutathione-mediated antioxidant pathways. Therefore, selective removal of a subset of dysfunctional mitochondria is a needed and highly regulated process for mitochondrial quality control and damaged or dysfunctional mitochondria are either complemented with an undamaged part of the mitochondrial network, by fusion, or sorted out for mitophagy (31).

### 1.1.4- ETC

The respiratory chain, or electron transport chain, is a well-organized system of electron transporters located in the inner mitochondrial membrane. Basically, it consists of a series of protein complexes cooperating to generate redox reactions, which couples electron transfer between an electron donor and an electron acceptor to the transfer of proton  $H^+$  across the membrane, thus establishing an electrochemical proton gradient (*Figure 6*).

The system receives electrons from reducing equivalents NADH (nicotinamide adenine dinucleotide) and  $FADH_2$ , generated by catabolic processes, and the electrons are transferred in an exergonic process unto the final conversion of molecular oxygen into water.

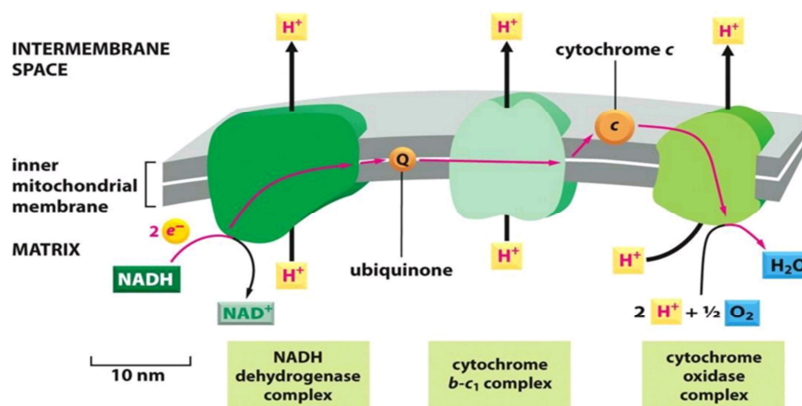


**Figure 6: The electron transport chain (ETC).**

*A series of compounds in the inner mitochondrial membranes transfer protons from electron donors to electron acceptors via redox reactions and couples this transfer with transfer of protons ( $H^+$ ) ions across the membrane.*

The respiratory chain complexes have been studied in great detail for decades: there are four transporter protein complexes and two electron carriers, named NADH-Q oxidoreductase (complex I), succinate-Q reductase (Complex II), Q-cytochrome  $c$  oxidoreductase (Complex III) and cytochrome  $c$  oxidase (complex IV), besides the lipophilic coenzyme Q (or ubiquinone), and the hydrophilic cytochrome  $c$  (cit  $c$ ), that diffuse into the mitochondrial

membrane.

Far from being randomly distributed in the membrane, it has been shown that the complex I, III and IV are associated together to form supramolecular assemblies (32), in a way that is essentially conserved from yeast to humans. Actually, studies conducted by Schagger and Pfeiffer on bovine mitochondria revealed that the complex I is associated in a fixed stoichiometry with a dimer of complex III and that this supercomplex is - in turn - associated with a variable number (usually four copies) of complex IV (33). Other electrophoretic studies have revealed the existence of supercomplexes in the form of respirasome in bacteria (34), fungi (35), higher plants (36), as well as in rats (37) and human mitochondria (38).

Albeit a clear functional role of mitochondrial supercomplexes is not yet established, it has been proposed that this supramolecular organization may have a functional significance, since their existence would capture the electron transfer between the various components of the mitochondrial respiratory chain (39).

#### 1.1.4.1- Complex I: NADH dehydrogenase

Complex I is an L-shape large enzyme, consisting of a soluble and transmembrane part formed by 46 polypeptide chains, with a horizontal arm localized in the membrane and a vertical arm that protrudes in the matrix (*Figure 7*).

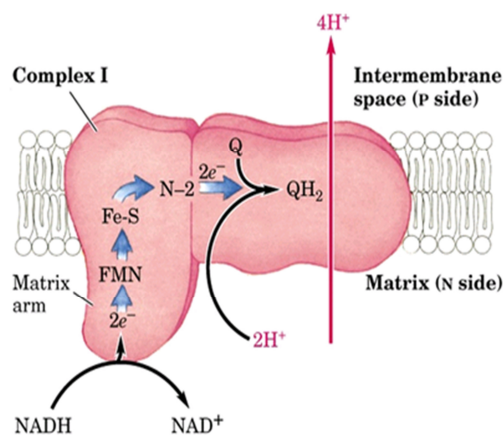


**Figure 7: NADH dehydrogenase (complex I)**

As shown in the figure, the process begins with the binding of NADH and the transfer of its two electrons to the prosthetic group of the enzyme, flavin mononucleotide (FMN), which is thus reduced to FMNH<sub>2</sub>.

Then, electrons are transferred to a series of Fe-S centers, whose iron ions are cyclically converted from the reduced  $\text{Fe}^{2+}$  to the oxidized  $\text{Fe}^{3+}$  state. Eventually, the electrons flow to the coenzyme Q, which is reduced to ubiquinol ( $\text{QH}_2$ ) and freely diffuses within the membrane towards Complex III. To note, the energy released in the electron transfer reaction between NADH and quinone is used for pumping four protons from the matrix into the *crista lumen*: this proton flux from the matrix to the intermembrane space is the first step to produce a proton gradient across the membrane, necessary to synthesize ATP. However, the way in which electron transfer from NADH to ubiquinone in complex I is coupled to proton translocation is still unknown, and much else remains to be discovered (40) (24).

#### 1.1.4.2- Complex II: Succinate dehydrogenase

Complex II, or succinate dehydrogenase, is the only enzymes involved in both citric acid cycle and the electron transport chain (41).

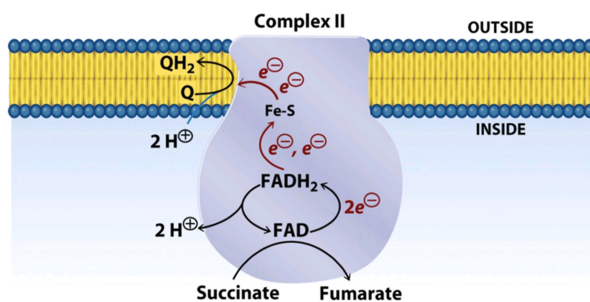


Figure 14-9 Principles of Biochemistry, 4/e  
© 2006 Pearson Prentice Hall, Inc.

**Figure 8: Succinate dehydrogenase (complex II)**

Bound to the inner mitochondrial membrane, facing the matrix (*Figure 8*), this enzyme oxidizes succinate to fumarate, with the reduction of ubiquinone to ubiquinol.

The electron transfer is mediated by a chain of redox centers, including FAD and the Fe-S clusters, that connect succinate and ubiquinone sites. However, since the complex does not transport protons, the production of ATP is lower when compared to the oxidation of NADH by the complex I.

### 1.1.4.3- Coenzyme Q

The Coenzyme Q or Ubiquinone is a para-benzoquinone, with a side chain in position 6, consisting of a variable number of isoprenoid units. Mitochondrial CoQ is inserted into the lipid bilayer of the internal membrane, where it diffuses freely between the respiratory complexes.

CoQ is the collection point for the electrons from different dehydrogenase complexes, receiving electrons from Complexes I and II, as previously described, but also from the glycerol 3-phosphate dehydrogenase and ETF-dehydrogenase. Upon receiving the first electron, ubiquinone (Q) is partially reduced to semi-quinon ( $\text{QH}^\cdot$ ), whereas the second electron fully reduced the radicalic form to ubiquinol (or hydroquinone,  $\text{QH}_2$ ). At this point, ubiquinol diffuses across the membrane and transfers electrons to the Complex III, being reoxidized to ubiquinone, and diffusing back towards Complex I and II.

### 1.1.4.4- Complex III: Complex bc1

Complex III is a multisubunit transmembrane protein that catalyzes electron transfer from  $\text{QH}_2$  to the oxidized cytochrome c, while pumping two protons in the intermembrane space (Figure 9).

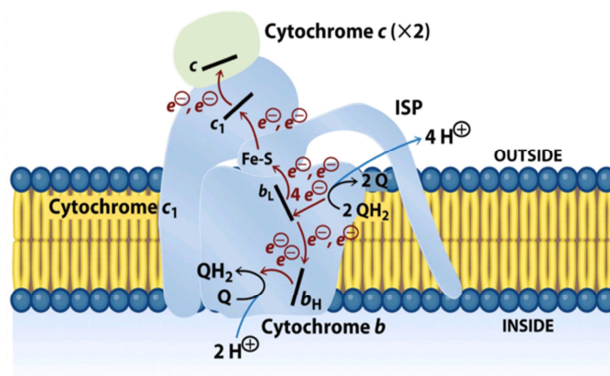


Figure 14-11 Principles of Biochemistry, 4/e  
© 2006 Pearson Prentice Hall, Inc.

**Figure 9: bc1 complex (complex III)**

Additionally, it contains an iron-sulfur protein with a 2Fe-2S center, called *Rieske* center, in which one of the iron ion is coordinated by two histidines,

This complex contains two types of cytochromes, containing heme as a prosthetic group: cytochrome b, having two b-type hemes (b<sub>L</sub> and b<sub>H</sub>) and cytochrome c, having one c-type heme (c<sub>1</sub>).

rather than two cysteines, thus stabilizing the center in its reduced form: this increases the reduction potential, so that the complex can easily accept electrons from QH<sub>2</sub>.

Complex III catalyzes the reduction of cytochrome c, by oxidation of coenzyme Q (ubiquinone), together with the concomitant translocation of four protons from the mitochondrial matrix to the intermembrane space (Q cycle process). Essentially, two QH<sub>2</sub> molecules consequentially bind to the complex, each one releasing two protons and two electrons, that are driven into two different directions. As a result, in the Q cycle two electrons are passed to cytochrome c, two protons are consumed from the matrix and four protons are released into the intermembrane space, contributing to generate the proton gradient across the membrane (42).

#### **1.1.4.5- Cytochrome c**

The Cytochrome c is a small soluble protein, with a molecular mass of about 13000 u, consisting of about 100 highly conserved residues. Located in proximity of the outer side of the inner mitochondrial membrane - to which is bound by electrostatic interactions - this other mobile electron-carrier of the respiratory chain transports electrons between the Complex III and Complex IV.

Electrons transferring from complex III to complex IV is related to the reversible oxidation of the iron in the heme group (Fe<sup>2+</sup>-Fe<sup>3+</sup>): when the heme group of cytochrome c accepts an electron from Complex III, cytochrome c moves to the Complex IV to donate the electron to a binuclear cupric center of this enzyme.

#### **1.1.4.6- Complex IV: Cytochrome c oxidase**

Finally, complex IV is a large transmembrane protein complex that catalyzes the transfer of electrons from each of four cytochrome c molecules and transfer them to one molecular oxygen, the last acceptor, that is converted into water (*Figure 10*).

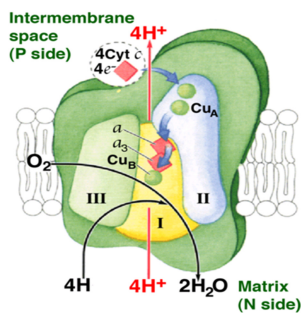


**Figure 10: Cytochrome c oxidase (complex IV)**

The bovine enzyme structure was deduced by crystallography: with a molecular mass of approximately 200 kDa, it appears as a Y-shaped dimer, wherein each monomer consists of 13 subunits.

The three major subunits (I, II, and III) are encoded by mitochondrial DNA and form the enzyme's catalytic core, surrounded by the remaining ten subunits, smaller and encoded by the nuclear DNA.

### 1.1.5- Oxidative phosphorylation

The majority of ATP in most mammalian cells is produced in the inner membrane by the central mitochondrial energy transformation system: the oxidative phosphorylation (OXPHOS). Practically, substrates oxidation in the ETC generates a proton gradient across the inner membrane, over the electron flow through the ETC, and the OXPHOS system couples this proton motive force ( $pmf$ ) with the phosphorylation of ADP in ATP.

Sir Peter D. Mitchell was the pioneer of the so-called *chemiosmotic theory*, proposed in 1961, assuming that the energy released during electron transport in the respiratory chain is used to pump protons from the mitochondrial matrix to the intermembrane space, thereby creating a difference in proton concentration on the two sides of the inner mitochondrial membrane. In this way, an electrochemical proton gradient - resulting from the difference in pH ( $\Delta pH$ ) - and an electrical gradient ( $\Delta \Psi_m$ ) - given by the difference in charge - is established between the two sides of the inner mitochondrial membrane. This electromotive force proton pushes the

protons back to the matrix, through the  $F_0$  section of ATP synthase (complex V of OXPHOS, Figure 11).

During this flow across the inner membrane, energy is provided for adenosine diphosphate (ADP) to combine with inorganic phosphate and form ATP (as described in the following section), which is then exchanged by cytosolic ADP via the adenine nucleotide translocators (ANTs), to let the ETC continuing its cycle (in absence of ADP and  $P_i$ , the electron flux through the ETC would be otherwise interrupted).

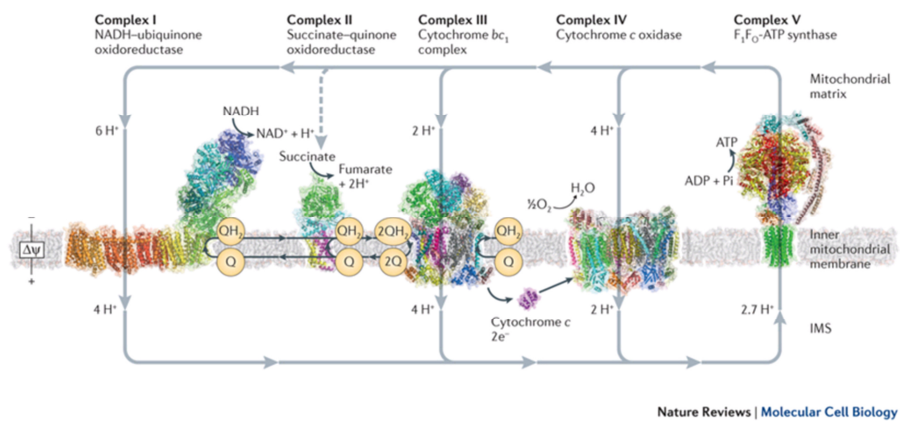


**Figure 11: Oxidative phosphorylation (OXPHOS) in mitochondria.**

Complex I (NADH/ubiquinone oxidoreductase), II (succinate dehydrogenase), III (cytochrome c reductase), IV (cytochrome c oxidase) and the mitochondrial ATP synthase (also known as complex V, *tan*) work together in oxidative phosphorylation to harness energy for the cell. Complexes I, III and IV pump protons across the cristae membrane, creating the proton gradient that drives ATP synthesis.

Mitochondrial OXPHOS powers a wide range of energy-based cellular functions, including maintaining the oxidation–reduction balance of the cell, generating a capacitance across the mitochondrial inner membrane, converting this potential energy into chemical energy, in the form of ATP, using the mitochondrial capacity to import calcium and modulate cellular and mitochondrial reactions, producing reactive oxygen species (ROS) as signal transduction molecules, and initiating cell death by activation of the mitochondrial permeability transition pore (mtPTP) to destroy those cells with defective mitochondrial energy production.

## 1.1.6- ATP synthase: structure and function

The  $F_1F_0$ -ATPase is a transmembrane enzyme complex found in the plasma membranes of bacteria, in the thylakoid membranes of chloroplasts and in the inner membranes of mitochondria.

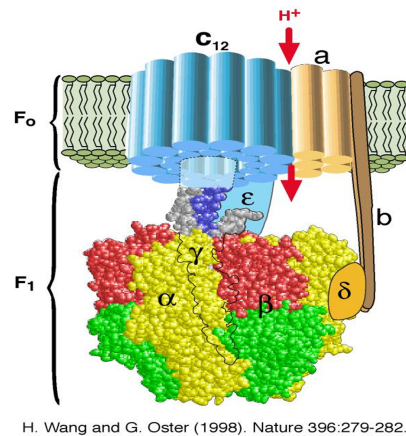


**Figure 12:  $F_1F_0$  ATP synthase**

The architecture of the enzyme is shown in Figure 12: it is a large mushroom-shaped asymmetric protein complex, with a total mass of about 550-650 kDa. Specifically, it consists of two main structural sections, distinct both structurally and functionally, linked by a central and a peripheral stalk (43).

The globular catalytic  $F_1$  domain is an assembly of five globular proteins, in a stoichiometry of three copies of each subunit  $\alpha$  and  $\beta$ , and one of  $\gamma$ ,  $\delta$  and  $\epsilon$ . The  $\gamma$  subunit and the associated  $\delta$  and  $\epsilon$  of  $F_1$  constitute the central stalk of the complex, being part of the  $\gamma$ -subunit completely enveloped in the  $\alpha_3\beta_3$  domain, while the rest protrudes to form a sort of “foot” that firmly attaches that complex to the cylindrical structure  $F_0$ .

The proton-translocating membrane-embedded  $F_0$  portion, instead, consists of a subunit c-ring, plus one copy each of subunits a, b, c, d, F6 and the oligomycin sensitivity-conferring protein (OSCP). Subunits b, d, F6 and OSCP, form the peripheral stalk, an elongated and largely  $\alpha$ -helical structure that extends from the  $F_0$  membrane domain to the topmost extremity of the  $F_1$ -domain, where it binds to the N-terminal region of an  $\alpha$ -subunit (44). Its  $\alpha$ -helical N-terminal domain provides the binding site for the N-terminal region of one of the three  $\alpha$ -subunits of  $F_1$ , whereas its C-terminal domain interacts with the C-terminal region of the b-subunit and with  $F_0$  (45)

The enzyme catalyzes the synthesis of adenosine triphosphate (ATP) from

adenosine phosphate (ADP) and inorganic phosphate (Pi), through the “binding-change” mechanism (

**Figure 13**), first proposed by the Nobel prize-winner Paul Delos Boyer (46).

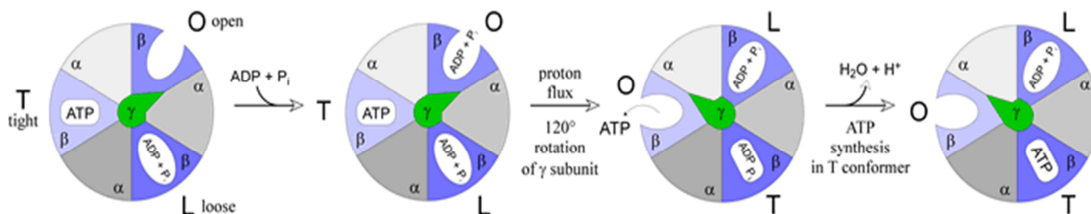


**Figure 13: Binding-change mechanism proposed by P.D. Boyer in 1975.**

The binding-change mechanism as seen from the top of the  $F_1$  complex. There are three catalytic sites in three different conformations: loose, open, and tight. Substrate ( $ADP + P_i$ ) initially binds to the open site and is converted to ATP at the tight site. A  $120^\circ$  rotation of the  $\gamma$  subunit causes a conformational change, resulting in a change in the formation of the sites. As a result, ATP is released from the enzyme. Then, a second  $120^\circ$  rotation occurs, substrate again binds to the open site, and another ATP is synthesized at the tight site

According to Boyer’s theory, each of the three  $\beta$  subunits switches cooperatively through conformations in which ADP and Pi bind, ATP is formed and released (O: Open, T: Tight, L: loose). These transitions are accomplished by rotational catalysis driven by the rotating inner core of the enzyme, which is in turn driven by the protons crossing the mitochondrial membrane (47).

Being a reversible nanomotor, the enzyme can also catalyze the opposite reaction. Indeed, when the membrane potential collapses the enzyme hydrolyzes ATP to pump protons through the membrane, in order to restore  $\Delta\Psi_m$ . Since depletion of ATP precipitates cell death, wasteful hydrolysis of ATP must be prevented when respiration is compromised: for this reason, the action of the enzyme need to be precisely regulated.

### 1.1.6.1- Regulation of ATP synthase

As mentioned above, the main function of  $F_1F_0$ -ATPase is the synthesis of

ATP. Given the intrinsic characteristics of the ATP synthase, the directionality of the enzymatic reaction is determined by the balance between the energy supplied by the phosphorylation potential and the  $\Delta\psi_m$ : the removal of ATP by ANT in normal conditions ensures relatively low phosphorylation potential and high  $\Delta\psi_m$ , thus facilitating the synthesis of ATP. However, when the mitochondrial homeostasis is compromised, the decrease in  $\Delta\psi_m$ , along with the reversion ANT - that starts importing glycolytic ATP - promotes the hydrolysis of ATP to restore physiological levels of  $\Delta\psi_m$ .

In many species, like bacteria, the reverse reaction of ATP hydrolysis is vitally important: when neither respiratory nor photosynthetic chains can generate *pmf*, the ATP synthase can work as a proton pump, at the expense of ATP, supporting important cellular functions, including flagella motility, or nutrients transmembrane transport. Nevertheless, the ATP hydrolysis activity is mostly a potential danger to living cells: when the fall of  $\Delta\psi_m$  is extreme, the only effect is the gradual depletion of cellular ATP, that leads to cell death. For this reason, futile ATP wasting must be prevented, as ensured by a precisely regulation of the enzyme activity through several mechanisms, like transcription factors, modulation of the citric acid cycle, as well as the regulation of the electron transport chain, the inhibition of ADP or ANT and proteins regulation, including the inhibitory factor 1 (IF<sub>1</sub>) (48).

Although recent evidence has also suggested that the oncoprotein Bcl-XL interacts with the F<sub>1</sub>F<sub>0</sub>-ATP synthase (49), IF<sub>1</sub> is the only molecular regulator of the enzyme characterized both biochemically and functionally.

### **1.1.6.2- Dimerization of ATP**

The structure of several subcomplexes of ATP synthase has been determined by X-ray crystallography, revealing that many organisms display extensive rows of dimers along the highly curved *cristae* ridges in mammals, plants, and fungi. Moreover, electron cryotomography of mitochondria and mitochondrial membranes from six different species showed that the two F<sub>1</sub> subcomplexes within each dimer are consistently 28 nm apart, whereas the

distance between adjacent dimers along the rows was variable, indicating that the dimers do not interact directly (50).

Oligomeric state of ATP synthase has been suggested to determine the arrangement of mitochondrial *cristae*, therefore determining mitochondrial morphology. In addition, it has been proposed that an alteration in pH occurs in the curvature of the inner mitochondrial membrane, suggesting that this proton trap is able to ensure appropriate ATP synthesis when the availability of protons is limited (51). However, the mechanisms underlying this supramolecular organization and the functional role of this assembly are not yet definitively established.

The first appearance of oligomerization dates back to 1989, when Allen (52) suggested that the dimeric form is the starting point for the construction of oligomeric form. In his work, Allen proposed that the dimers form a rigid bow, which promotes the formation of *cristae* by protruding from the planar surface of the mitochondrial membrane, in line with molecular dynamics simulations performed by Kuhlbrandt and co-workers, showing that an individual ATP synthase dimer causes a marked deformation of the surrounding lipid bilayer, inducing a positive, convex curvature in one direction and a concave curvature in the perpendicular direction (50). Therefore, the dimers seem to be responsible for the formation of the highly curved *cristae* ridges, and an essential element of normal mitochondrial morphology.

To note, more recent studies investigated on the involvement of the inhibitor of the ATP synthase, IF<sub>1</sub>, to form dimers of the enzyme, thereby contributing to modify mitochondrial morphology: since the active form of IF<sub>1</sub> is a dimer with its two N-terminal domains at both sides of the structure, free to interact with the F<sub>1</sub>-ATPase, questions have raised to define whether IF<sub>1</sub> promotes the dimerization of the ATP synthase, or at least stabilizes the dimeric form of the complex, but further studies are needed to elucidate this association.

## 2- IF<sub>1</sub>

In 1963, M.E. Pullman and C.G. Monroy discovered a soluble, heat-stable protein in mitochondria from bovine heart, that inhibits the ATP hydrolase activity of the F<sub>1</sub>F<sub>0</sub>-ATPase (53). This protein is activated in response to acidification of the mitochondrial matrix, which usually accompanies the inhibition of mitochondrial respiration (*i.e.* during hypoxia/ischaemia), with the consequential collapse of  $\Delta\Psi_m$  and the reversal of F<sub>1</sub>F<sub>0</sub>-ATP (54). However, as soon as the mitochondrial inner membrane gets re-energized and the proton gradient is rebuilt across the membrane, the enzyme restarts to catalyze the ATP synthesis and the inhibitor is rejected, acting – therefore – as an unidirectional valve (19).

Highly conserved throughout evolution, the mammalian IF<sub>1</sub> is a small, basic protein of about 10 kDa, encoded by the nuclear gene ATP1F1. This polypeptide is  $\alpha$ -helical along most of its length and contains 106–109 amino acids, depending on the species of origin, including a 25-residues mitochondrial targeting pre-sequence (that is cleaved within the mitochondria to form the mature IF<sub>1</sub> of 84 aminoacids) and the inhibitory portion from residues 48 to 70 (bovine numeration), with homologues in birds, nematodes, yeasts and plants mitochondria.

This latter domain is highly conserved throughout the species, so that the inhibitory function of the protein is maintained across F<sub>1</sub>F<sub>0</sub>-ATPases of different species, albeit with different efficacy (55). More importantly, this domain is sensitive to pH, and is thus responsible for the molecular switching between the active form, in acid conditions, and the inactive form, above neutrality (*Figure 14*). In alkaline conditions, indeed, inactive tetramers or higher oligomers are held together by antiparallel coiled-coils in the *N*-terminal regions, masking the inhibitory regions (56). Conversely, when pH is low (*i.e.* 6.7 or below), residues 48 to 56 are involved in the formation of an antiparallel double-stranded coiled-coil region between two IF<sub>1</sub> molecules, to generate the active inhibitory dimer that binds two F<sub>1</sub> domains of the enzyme, further stabilized by complimentary hydrophobic interactions

between the two helices.

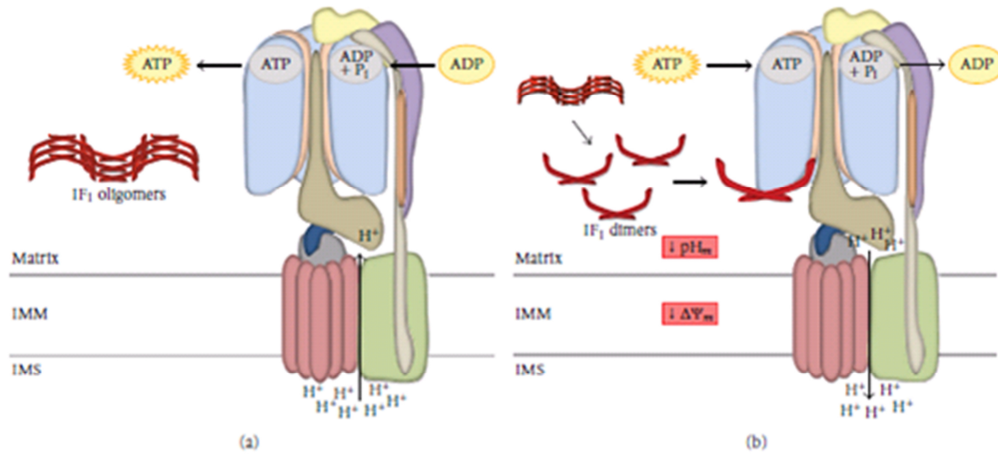


**Figure 14: Inactive (a) and active (b) structures of IF<sub>1</sub> (from (57))**

As proposed by Walker, the inhibitor binds to the soluble F<sub>1</sub> domain, via the most accessible of the three catalytic interfaces (between the  $\alpha_E$ - and  $\beta_E$ -subunits, where no nucleotide is bound) in the presence of  $\text{Mg}^{2+}$  and ATP. When the first 120° rotational step occurs, the  $\beta_E$ - $\alpha_E$  interface is converted to the  $\beta_{\text{TP}}$ - $\alpha_{\text{TP}}$  interface; then, a second 120° rotational step follows, and the inhibitor can enter its binding site in the hydrophobic pocket in the adjacent  $\beta$ -subunit and augment the binding of the inhibitor to F<sub>1</sub>-ATPase, with further interactions taking place between the  $\gamma$ -subunit and the shorter  $\alpha$ -helix (residues 14-18 of IF<sub>1</sub>) and the region linking it to the longer  $\alpha$ -helix (residues 19-21), therefore inhibiting other rotations (58).

However, upon the reversal of rotation - from the counterclockwise direction that accompanies ATP hydrolysis, to the clockwise direction required for ATP synthesis - the interactions of IF<sub>1</sub> with the F<sub>1</sub>-domain of the inhibited enzyme are destabilized, leading to the ejection of the inhibitor from the catalytic interface.

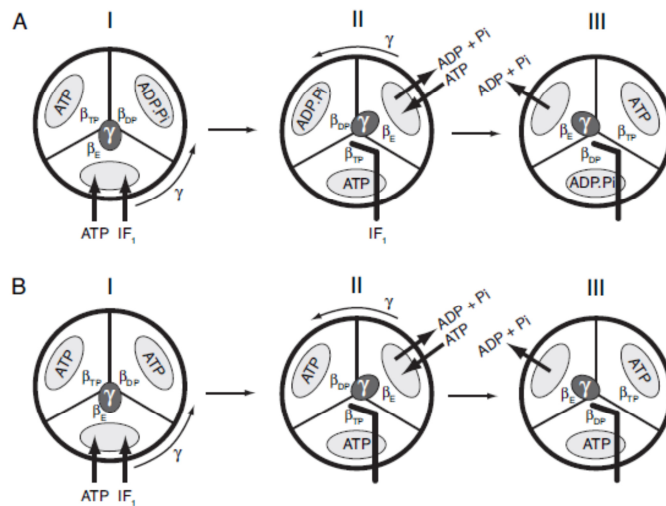


**Figure 15: The inhibitory binding of IF<sub>1</sub> to the catalytic interface of the enzyme.** The two schemes differ by ADP being bound to the  $\beta_{DP}$ -subunit in (A) and ATP in (B).

Long investigated for its ability to inhibit the hydrolytic activity of the enzyme F<sub>1</sub>F<sub>0</sub>-ATPase, IF<sub>1</sub> is now examined for other potential roles, with a large attention given to its possible contribute in pathophysiological conditions. Indeed, the homodimeric conformation binds two F<sub>1</sub> domains simultaneously, encouraging many hypothesis on the involvement of IF<sub>1</sub> in defining the oligomeric state of the F<sub>1</sub>F<sub>0</sub>-ATPsynthase – thus influencing the activity of the enzyme – and, far beyond, in remodeling mito-ultrastructure and morphology of mitochondria, leading to the formation of mitochondrial *cristae*.

More intriguingly, several groups recently focused on the overexpression of this protein found in many human carcinomas, prompting interesting speculations about the role of IF<sub>1</sub> in tumor metabolism. Furthermore, the protein has been likely related to an increase malignancy of tumors, by helping cells to survive in hostile conditions, protecting cancer cells from death, by escaping apoptosis, and increasing tumor ability for invasion and metastasis.

## **2.1- $IF_1$ in dimerization**

The role of  $IF_1$  in the oligomerization of the ATP synthase is much debated. Many studies in the literature propose that  $IF_1$  contributes to stabilize the dimeric form of the  $F_1F_0$ -ATPase, since the active form simultaneously binds two  $F_1$  portions, consequently promoting the formation of mitochondrial *cristae* and, hence, the ultrastructure of mitochondrial morphology (59).

Garcia and co-workers (60) first highlighted the possible involvement of the inhibitor in the dimerization of the ATP synthase and in the biogenesis of the mitochondrial *cristae*, reporting an increase in the dimer/monomer ratio when increasing the expression of  $IF_1$ , whereas the silencing of the inhibitor resulted in a switched ratio, in favor of the monomeric form of the enzyme.

Consistently, a number of studies by Campanella and co-workers reported that  $IF_1$  increases  $F_1F_0$ -ATP synthase activity in respiring mitochondria, promoting its dimerization and increasing the density of mitochondrial *cristae* and mitochondrial volume fraction (59) (61). However, this ideas have been rejected by others, reporting that the organization of the ATP synthase in the dimeric form was independent from the inhibitor (62). More studies are therefore needed to elucidate the influence of the inhibitor to the activity of the  $F_1F_0$ -ATPase and to define mitochondrial content.

## **2.1- $IF_1$ and ROS**

As a byproduct of OXPHOS, mitochondria generate much of the cellular ROS, highly unstable compounds with an unpaired electron in their chemical structure. One of the major compounds in mitochondria is the superoxide radical: specifically, complexes I and III likely have the primary responsibility for its generation during the electrons transfer through their redox centers.

ROS concentration inside the cell must be finely controlled, since small amount can mediate different cellular signaling pathways, whilst higher concentrations can damage cell structures, enzymes, nucleic acids and lipids,

besides inducing mitogenic pathways and stimulating carcinogenesis. Although under physiological conditions the production of ROS is well balanced by cellular antioxidant mechanisms, different diseases can alter this balance, ultimately triggering the mechanisms of apoptosis and cell death. By preventing the production of ROS,  $IF_1$  may protect cancer cells from ROS-mediated apoptosis. Moreover, it was recently reported that autophagy was dramatically increased in the  $IF_1$ -siRNA treated cells, but this phenomenon was prevented by the superoxide dismutase mimetic, indicating that the inhibitor may limit mitochondrial ROS generation, therefore reducing autophagy. In this view, variations in  $IF_1$  expression level may therefore play a significant role in defining both resting rates of ROS generation and cellular mitochondrial content (63). However, recent evidence have also shown that ROS play a key role as a messenger in normal cell signal transduction and cell cycling and the mitochondrial ATPase inhibitory factor 1 has been described as a ROS-mediated retrograde pro-survival and proliferative response activator (64).

## ***2.2- $IF_1$ in cancer***

Energy metabolism, apoptosis, as well as the production of reactive oxygen species (ROS) and important cellular signaling pathways are mediated by mitochondria, which play a crucial role in cell physiology. For this reason, an increasing number of human diseases is now correlated with morphological and functional changes occurring in these important organelles, including neurodegenerative diseases and cancer (10). Numerous studies conducted in the last decade, indeed, clearly indicate that mitochondrial dysfunctions are one of the most recurrent characteristics in cancer cells, as proven by microscopic and genetic alterations, as well as by biochemical and molecular analysis.

Particularly, in recent years, it has been rediscovered the importance of energy metabolism in cancer biology: oxidative phosphorylation (OXPHOS)

covers almost the whole of the energy demand of many differentiated cells, while many evidence report an increase of the consumption of glucose in the neoplastic cells (*Warburg effect*), therefore suggesting that transformed cells experience a metabolic reprogramming, resulting in a predominantly glycolytic phenotype.

As  $IF_1$  is upregulated in a large proportion of human cancers, this protein is currently under investigation for its involvement in cellular energy metabolism and oncogenesis. Actually, the expression of the protein varies widely in different normal human tissues, but many data reported its increased expression in many types of cancer (65) (66), along with a decreased OXPHOS activity, mitochondrial hyperpolarization and simultaneous increase of glycolysis. In this view, the over-expression of  $IF_1$  in human tumors may contribute to the onset the peculiar energy metabolism of mitochondria in cancer, acting as a molecular switch for a metabolic shift from oxidative phosphorylation to glycolysis phenotype that characterizes cancer cells.

Moreover, considering that most of the tumors rely on a poor vascularity, with highly variations of oxygen levels from the perivascular regions to the anoxic necrotic centers, the  $IF_1$  over-expression in several human cancers could play an important role in the pathology of tissue ischemia and tumor growth, by helping cells to conserve ATP. Actually, when the cells are deprived of oxygen and glucose, cells with a silenced-expression of the  $F_1F_0$ -ATPase inhibitor rapidly deplete ATP and dye more rapidly than control ones, indicating the role of  $IF_1$  in maintaining the concentration of ATP in energy crisis situations. However, the contribution of this protein in tumor mitochondrial bioenergetics is still debated and data in the literature are controversial.

A recent study (64) also reported that  $IF_1$  leads to chemotherapy resistance and promotes the proliferation of cancerous cells via signaling pathways mediated by the transcription factor NF $\kappa$ B. In addition, the inhibitor protein has been explored in relation to the progression of apoptosis:  $IF_1$  expression has been reported to serves as a checkpoint for the release of cytochrome c

and, hence, the completion of the apoptotic program. Considering also its possible role in inducing dimerization of the ATP synthase, the inhibitor of the enzyme could play a key role in avoiding the fragmentation of the mitochondrial network and the release of cytochrome c from the mitochondrial *cristae*, further protecting cells from apoptotic death (27).

However, little is still known on the effects associated with IF<sub>1</sub> and the hypothesis proposed are highly controversial at present, underlying the emergent need of a deeper investigation over the role of this protein, in order to define how IF<sub>1</sub> can affect mitochondrial activity and, more intriguingly, how this protein can contribute to cancer cell survival and progression, escape apoptosis and affect cancer cell metabolism.

### **3- Altered pathways in cancer**

As reported above, alterations in oncogenes, tumor-suppressor genes and stability genes are responsible for tumorigenesis. Mammalian cells, however, have multiple safeguards to protect them against cancer gene mutations, and only when several genes are defective an invasive cancer can develop.

Albeit all genes are potentially affected by the resultant increased rate of mutations, alterations in cancer genes that directly control cell cycle and cell proliferation can affect net cell growth, thereby conferring a selective growth advantage to the mutant cell. For example, the oncogene cdk4, cyclin D1 (67), and the tumor suppressor gene Rb (68) and p16 can respectively be activated or inactivated by mutations. In addition, others pathways are frequently involved in many tumor types, including developmental pathways involving glioma-associated oncogenes (GLI), or hypoxia-inducible transcription factor (HIF)-1 (28), among others, eventually resulting in uncontrolled rate of proliferation, cancer development and progression (69).

### 3.1- SHH pathway

Normal development during embryogenesis requires a number of complex signaling cascades, including the Hedgehog (Hh) pathway, a key mediator of many fundamental processes in vertebrate embryonic development that controls cell fate, patterning, proliferation, survival and differentiation of many different regions.

First described in 1980 by Christiane Nusslein-Volhard and Eric F. Wieschaus, (70) in their genetic analysis of the fruit fly *Drosophila melanogaster*, the name Hedgehog (Hh) originates from the short and 'spiked' phenotype of the cuticle of the Hh mutant *Drosophila* larvae, which resembled the spikes of a hedgehog (71). Although many of the key components are conserved in vertebrates, the mammalian Hh signaling pathway is incompletely understood and harbors some additional components, suggesting that the mechanism of Hh signal transduction have evolved differentially after separation of the vertebrate and invertebrate lineages, approximately 1 billion years ago (72). Moreover, mammalian Hh signaling relies on several compounds involved in the formation of the primary cilia - not required in *Drosophila* - that would act as a "signaling center" where the biochemical events of signal transduction take place (73).

In vertebrates, the canonical Hh pathway contains several key components, including Hh glycoproteins *Desert Hedgehog* (Dhh), *Indian Hedgehog* (Ihh), and *Sonic Hedgehog* (Shh), three Hh gene homologs discovered in the early 1990s (74) (75) (76). Hh proteins act as morphogens, controlling multiple different developmental processes. Particularly, Dhh and Ihh have been shown to play important roles in normal tissue development, being Dhh expression largely restricted to gonads, while Ihh is specifically expressed in a limited number of tissues, including primitive endoderm (77), and prehypertrophic chondrocytes in the growth plates of bones (78). By contrast, Shh is the most potent of these ligands and the most widely expressed mammalian Hh signaling molecule, inducing cell proliferation in a tissue-specific manner: during early vertebrate embryogenesis, it is

expressed in midline tissues such as the node, notochord and floor plate controls patterning of the left-right and dorso-ventral axes of the embryo (79); later in organogenesis, Shh affects development of most epithelial tissues, and in adults it remains active, regulating tissue homeostasis, continuous renewal and stem cells maintenance, as well as preserving tissue polarity (80).

In humans, the Hh cascade in the target cell is triggered by the Hh ligand binding to the Patched receptor (Ptch), a 12-span transmembrane protein that exists as two isoforms in vertebrates, Ptc1 and Ptc2. In absence of the ligand, Ptch inhibits downstream signaling by catalytically inactivation of the seven-transmembrane-span-receptor-like protein, Smoothed (Smo) (81), affecting its localization to the cell surface, or by eliciting endogenous Smo agonists to prevent its binding. Conversely, upon secretion of Shh glycoproteins, Ptch is inactivated and Smo is activated, resulting in the transduction of the Hh signaling to the cytoplasm and the nuclear localization of the terminal effectors of the Shh signaling, the glioma-associated (GLI) transcription factors.

In vertebrates, the GLI factors exist as three separate zinc-finger proteins: GLI1 and GLI2, functioning as transcriptional activators, and GLI3 as a transcriptional repressor (82). Once in the nucleus, GLI transcription factors can activate target genes involved in HH pathway feedback (e.g., GLI1, Ptc1), proliferation (e.g., Cyclin-D1, MYC), apoptosis (e.g., Bcl-2), angiogenesis (e.g., ANG1/2), epithelial-to-mesenchymal transition (e.g., SNAIL), and stem cell self-renewal (e.g., NANOG, SOX2) (83) (84) (85).

Moreover, genetic evidence from *Drosophila* indicate that the full activation of the pathway in response to Hh stimuli also requires the Fu protein kinase, which blocks the negative influence of the Suppressor of Fused (SUFU). Unlike the fruit fly, in which this latter component has only a minor role, mammalian Hh signaling critically depends on SUFU, that negatively regulates the pathway: in the absence of ligand, SUFU directly binds to GLI transcription factors and anchors them in the cytoplasm, thus facilitating their degradation and, more importantly, inhibiting Shh pathway signaling by

preventing the activation of GLI target genes. In addition, SUFU has also been shown to form a repressor complex leading to interaction with DNA-bound GLI1 and suppression of GLI1-induced gene expression (86).

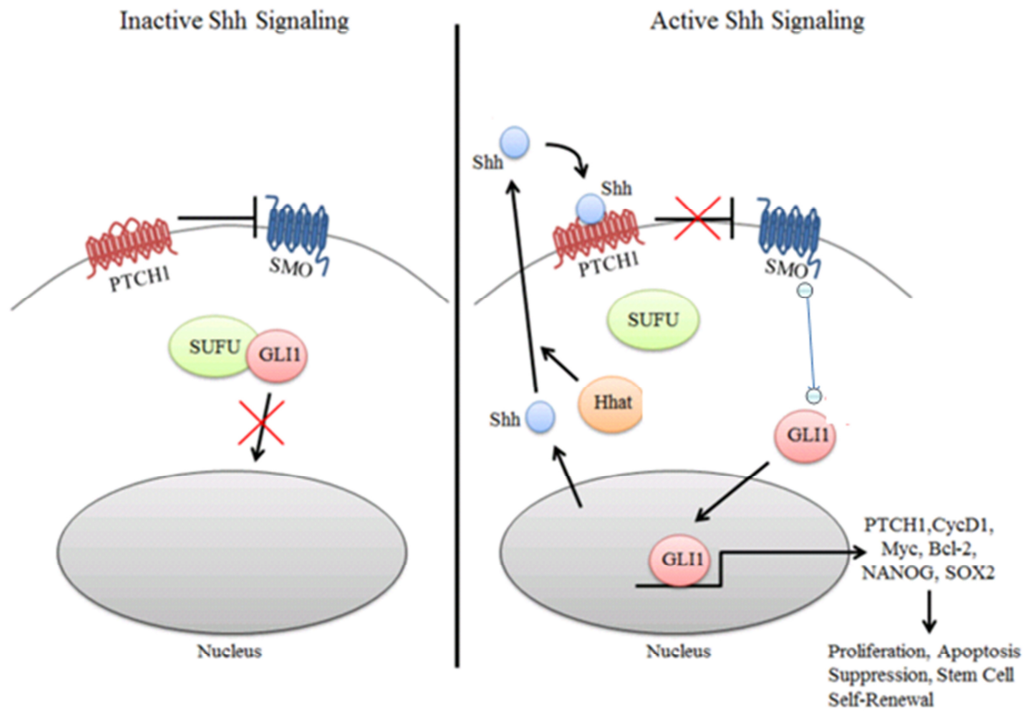


**Figure 16: Shh Pathway in mammals.**

*The interaction between Shh and Ptch1 leads to the ciliary localization of Smo, which is otherwise inhibited by Ptch1. A Gli-Sufu complex is also localized to the cilium and it is believed that Gli proteins are proteolytically processed in the absence of Shh. Conversely, in the presence of Shh, activated Smo promotes the dissociation of Gli proteins from Sufu and turns Gli proteins into transcriptional activators.*

Thus far, it is important to note that Hh signaling is crucial in development, as evinced by the dramatic consequences in human fetuses with inherited or sporadic mutations in the Shh signaling pathway, resulting in a number of human birth defects, like holoprosencephaly, microencephaly, cyclopia, absent nose or cleft palate (87) (88). Moreover, abnormal activation of the Shh pathway has been recently shown to affect tumorigenesis, apoptosis, migration, and angiogenesis of various cancer that usually originate from endoderm, enclosing gastric, pancreatic, colon, lung, prostate, and

hepatocellular cancer (89). Furthermore, Hh might also promote tumorigenesis or tumor growth acceleration in a wide variety of tissues, by signaling in a paracrine manner from the tumor to the surrounding stroma, or in cancer stem cells (CSCs).

### ***3.1.1- Shh pathway and Melanoma***

In recent years, it has become increasingly clear that abnormal Shh signaling can lead to cancer: the role of deregulated Shh signaling in cancer was first characterized by studies of basal cell nevus syndrome, also known as Gorlin syndrome, an autosomal dominant disorder leading to craniofacial and skeletal abnormalities, together with a notably increased risk of advanced basal cell carcinoma and medulloblastoma (90). Specifically, it has been proposed that a ligand-independent Hh pathway-activating mutation was responsible for aberrant Shh pathway activity, leading to the development of BCCs and medulloblastomas (91). Alternatively, it has been observed that Shh pathway can be altered in a ligand-dependent manner, either with autocrine or paracrine signaling, in multiple tumor types including lung (92), pancreatic, colorectal (93), prostate (94) metastatic carcinomas, and gliomas (95).

In this sense, it is quite clear that tumor growth and metastatic dissemination of tumor cells strictly rely on reciprocal interactions between cancer cells and the surrounding stroma (96). As revealed by studies in epithelial cancers, indeed, tumor cells secrete Shh ligand, that stimulates production of secondary growth factors driving tumor angiogenesis, tumor cell proliferation, and survival (97). Thus, identifying novel mechanisms critically regulating tumor–stroma interactions may be therapeutically relevant in aggressive types of cancer, like cutaneous melanoma, that requires secretion of growth factors and cytokines to grow and disseminate (98).

Melanoma represents approximately 4% of human cutaneous neoplasm (99), especially common among Caucasians, with a rapidly increasing incidence in

Oceania, North America, Europe, South Africa and Latin America (100). Despite this low rate of incidence with respect to other types of cancer, however, it is a highly aggressive and poor prognosis tumor, that yet accounts for almost 80% of deaths related to skin cancer (101).

Research over the last decade showed that multiple genetic alterations play a role during the progression of this complex genetic disease: among these, activating mutations in the oncogenes BRAF and NRAS - ultimately involved in cell growth, proliferation and survival - are a genetic hallmark of melanoma, being present in 70% and 15% of melanomas, respectively. As a result, these mutations can cause unintended and overactive signaling inside the cell (*e.g.* in the absence of incoming signals), leading to increased and uncontrolled cell proliferation and resistance to apoptosis (102). More in detail, studies on melanoma revealed that over 50% of metastatic melanomas harbor the BRAF(V600E) point mutation (103), with a substitution in position 600 of a glutamate with a valine, that cause a constitutively active protein serine kinase, thus sustaining the BRAF→MEK1/2→ERK1/2 MAP kinase pathway, critically implicated in the regulation of gene expression, as well as cell proliferation and survival, all involved in the initiation and progression of melanoma (104).

Since the discovery of *BRAF(V600E)* mutation in melanoma, scientists and clinicians have learned much about mechanisms that underlie melanoma origin and progression, but many questions remain unanswered, with attention given to other developmental pathways that may be involved in both formation and progression of the disease. Interestingly, a recent study suggested that Shh-GLI activity could be a basal, yet essential, requirement in melanoma: Stecca et al. previously reported that GLI1, a direct GLI2 target, is required for normal melanocyte proliferation as well as for growth and metastasis of melanoma cells. The acquisition of oncogenic RTK-RAS-RAF-MEK and/or AKT signaling could result in cell-intrinsic enhancements of GLI1 transcriptional activity, and such increases may then participate in disease progression (105).

Additionally, the Hh pathway may induce PDGFR $\alpha$  up-regulation (106), thus

helping melanoma progression in a positive autocrine/paracrine feedback on GLI1 function. Moreover, GLI2 has been found overexpressed in human melanoma and associated with melanoma cell invasion, matrix metalloproteinase (MMP) secretion, expression of E-cadherin, and metastasis to bone (107), indicating that GLI2 could be a common target of the developmental machinery and a progression factor in melanoma.

However, although progress has been made in understanding the genetics of the molecular events underlying melanoma oncogenesis, the clinical challenge remains enormous: molecules that inhibit mitogen-activated protein kinase pathway-associated kinases, like BRAF and MEK, as well as Shh inhibitors, have shown only limited efficacy in the treatment of metastatic melanoma (108). Thus, a deeper understanding of the cross talk between signaling networks and the complexity of melanoma progression should lead to more effective therapy.

### **3.2- Melanoma therapy and Drug resistance**

Metastatic melanoma is a rapidly progressing disease with an 8-month median overall survival and a 25% 1-year survival rate. The majority of melanoma lesions are diagnosed early and are mostly excised and curable, with excision and lymph node resection if involved, but advanced melanomas are really hard to cure and current therapies include chemotherapy, radiotherapy, immunotherapy, or a combination of them (109). Moreover, many clinical trials are currently ongoing, aiming to improve treatments and reduce side effects with the help of target therapies, in order to mark only the typical genetic hallmarks of melanoma cells rather than any quickly dividing cell.

Development of therapeutics for the canonical Shh signaling pathway has primarily focused on targeting Smo, through natural and synthetic antagonists, with varying degrees of success. Among these, one of the first investigated was the natural steroidal alkaloid cyclopamine, followed by a

number of derivatives, in the hopes of increasing specificity and pharmacological potency. In addition, GLI1 was singled out as a therapeutic target - as it is the most characterized GLI transcription factor associated with activation of Shh target genes - and GLI2 was also considered a potential mark, leading to a rapid expansion of GLI small-molecule inhibitors, attempting to provide the basis for other therapeutic approaches. However, Shh antagonists only have little effect on melanoma cells: likely because of deregulation of this stimulatory signaling mechanism, tumor cells often become Shh independent, and endogenous or exogenous Shh has no effect on melanoma growth and migration.

Likewise, target therapies over the last decade have been deeply focused on targeting the BRAF signaling cascade, by blocking the constitutive activation of this oncogene caused by the typical BRAF gene mutations. On this side, a number of papers reported the efficacy of the BRAF inhibitor (vemurafenib) - as well as other inhibitors in its class - in inducing tumor regression in more than 50% of the patients with BRAF(V600E) mutated metastatic melanoma. For these reasons, in 2011 the FDA approved vemurafenib as the major breakthrough in the treatment of these types of melanoma, with improved progression free and overall survival of a large number of patients supported by many clinical trials. However, monotherapy regimens with these new pharmaceuticals are hampered by the emergence of dose-limiting toxicity and secondary cancers: although some of these concerns are addressed by the combination therapies, complete responses to these targeted therapies (e.g., vemurafenib) are only observed in a small percentage of patients, as a consequence of intrinsic BRAF-I resistance. More importantly, the median time to disease progression is really short, since patients acquire resistance to therapy and tumor recurs much more aggressively, with the inevitable death of patients.

As tumor is continuously evolving during its progression, it is important to note that cancer cells have a continuous turnover in this process, allowing an ongoing selection of the fittest cells, able to escape different mechanisms of apoptosis, induced by their microenvironment, and yet to proliferate widely,

regardless possible hostile conditions prompted by the treatment. In this view, resistance to therapy might be considered as a consequence of reduction of several distinct cell death mechanisms, as well as from an increased ability to regenerate. Thus far, mechanisms by which tumor cells resist the action of anticancer drugs have been deeply investigated in the last decades: cancer drug resistance, either intrinsic or acquired with therapy, encompasses various mechanisms, including altered expression of drug influx/efflux transporters, altered role of DNA repair and impairment of apoptosis, as well as epigenomics and altered levels of microRNAs, that may lead to alterations in upstream or downstream effectors, among others. MicroRNAs are small, noncoding RNA molecules of about 20-22 bases in length, that bind to the 3'-untranslated region of target mRNA, affecting important cellular processes, like cell proliferation and differentiation, cell cycle, and other hallmarks of cancer, such as inhibition of apoptosis, epithelial-to-mesenchymal transition (EMT), cell invasion and metastases, more recently addressed as responsible for chemoresistance in several common therapies (110). Although the mechanism of microRNA-mediated drug resistance is not fully understood, an increasing number of evidence suggests their involvement in the acquisition of tumor cell drug resistance, pointing towards the need for novel and more innovative therapeutic approaches. Indeed, this aspect is particularly relevant, since therapeutic failure still accounts for death in over 90% of patients with metastatic cancers, indicating that a deeper understanding of the mechanisms underlying resistance to therapy is urgently needed, in order to increase chances of survival and improve quality of life in poor prognosis metastatic patients.

# Aim of the Study

---

Cancer is a multifactorial disease, deriving from a combination of genetic, environmental and lifestyle factors. Particularly, plenty of data reported that tumor cells exhibit profound genetic, biochemical and histological difference when compared to non-transformed cells of origin, and large attention is nowadays dedicated to the metabolic reprogramming of cancer cells, resulting in a predominantly glycolytic phenotype (the so-called *Warburg effect*).

Considering the pivotal role of mitochondria, that supply nearly the total amount of energy to the cells and are fundamental key mediators in cellular life and death processes, in the last decades it has become increasingly clear their involvement in many diseases, including cancer (10). Moreover, the effect of several conventional therapeutic drugs on cancer metabolism pushed research over the last years to develop new strategies to identify new potential therapeutic targets, like key metabolic enzymes with a central role in the energy metabolic pathway.

In this view, it has been recently reported, by Cuezva and co-workers, that the endogenous inhibitor protein of the ATP synthase ( $IF_1$ ) is over-expressed in different human cancers, when compared to non-transformed cells of the same origin. This small and evolutionary highly conserved protein is the master regulator of the ATP hydrolytic activity of the ATP synthase, activated in response to the acidification of the mitochondrial matrix - which usually accompanies the inhibition of mitochondrial respiration (*i.e.* during hypoxia/ischaemia) - and in response to the reversal of  $F_1F_0$ -ATP synthase activity. Furthermore, this protein has been recently investigated for its role in inducing the dimerization of ATP synthase, thereby promoting the formation of mitochondrial *cristae* and influencing shape and size of mitochondria. Additionally, a protective effect against ROS production and apoptosis has been proposed, therefore suggesting that the enhanced

expression of the protein may represent an advantage in cancer cells, promoting cell survival and proliferation, despite the hostile conditions experienced by cancer cells. Indeed, a limitation in oxygen and substrates availability often occurs within tumor, deriving from an inefficient development of vasculature inside the tumor mass: in these conditions, IF<sub>1</sub> may help tumor cells to preserve ATP, critically required for cancer expansion, and even act as a molecular switch in favor of glycolysis.

However, data reported in literature are highly controversial and hypothesis on the contribution of the inhibitor to modulate cancer metabolism, as well as malignant progression, are not clear. Some recent investigations have set out to explore the functional consequences of varying IF<sub>1</sub> expression levels in cancer cell lines: nonetheless, most of these studies were performed through transient modulation of IF<sub>1</sub> expression, a model which is characterized by an heterogeneous population of cells, in a dynamic condition in which cells are adapting to the change in IF<sub>1</sub> content. Therefore, to shed light over the contribution of the inhibitor and possibly clarify some ambiguities reported, the main purpose of this study was to investigate the cellular response to a fully and permanent silencing of the protein in a highly IF<sub>1</sub> expressing osteosarcoma cell line (143B cells).

In addition, recent literature has also clearly evidenced that epigenetic alterations play a crucial role in modifying genes expression, as well as in modulating cancer cell metabolism, sustaining and promoting tumor growth and dissemination. Indeed, numerous studies have provided convincing evidence on the close correlation between microRNAs and tumors (111), revealing that these molecules affect cell fate determination, apoptosis, migration and invasion, as well as the response of tumor cells to anticancer therapies (110). In addition, miRNA expression is also characteristic for different cancer types, stage, and other clinical variables, further than distinguish tumors from normal tissues.

In an attempt to explore miRNAs contribution in modulating bioenergetics of different tumor cell lines, the pattern of miRNAs expression was analyzed,

aiming to explore how these molecules alter metabolic pathways that may lead to cancer. However, compelling emerging data on different cell lines, including sensitive- and resistant-to-treatment melanoma cell lines, revealed a specific pattern of miRNAs expression, along with the acquired resistance to BRAF-I treatment, the major breakthrough in the treatment of BRAF(V600E) mutation-carrying melanomas. These data seemed quite intriguing, prompting us to further investigate over molecular mechanisms by which certain miRNAs trigger resistance to therapy in these severe, challenging and yet poor-prognosis malignancies.

# Materials & Methods

---

## ***1- Cell Culture***

Human osteosarcoma 143B cells were maintained in Dulbecco's Modified Eagle Medium (DMEM) supplemented with 10% bovine serum, 100 U/ml penicillin, and 100 µg/ml streptomycin 0.25 µg/ml amphotericin B, in presence of 25 mM glucose, 4 mM glutamine and 1 mM pyruvate. To ensure selection, IF<sub>1</sub> silenced clones were cultured in presence of 1 µg/ml Puromycin.

Cell lines were maintained at 37 °C in a humidified atmosphere with 5% CO<sub>2</sub>. During experimental procedures, cells were seeded in complete medium (*i.e.* described above) the day before the experiments, to favour adhesion. After 12 hours, the medium was replaced with fresh media and cells were cultured at 37 °C.

The substrates glucose and pyruvate were purchased from Sigma; all the other cell culture reagents were from Gibco (Life Technologies).

The parental BRAF(V600E) melanoma M21, Colo38 and SK-Mel37 cells were originated from metastatic lesions of patients with melanoma. Cells were cultured in RPMI-1640 (Life Technologies) supplemented with 10% FBS (Omega Scientific), 100 units/ml of penicillin, and 100 µg/ml of streptomycin (Life Technologies) in a humidified HERA-cell 150i incubator at 37 °C in an atmosphere of 5% CO<sub>2</sub>.

Derivative melanoma cells with acquired vemurafenib resistance (M21-R, Colo38-R and SK-Mel37-R), were generated by propagating M21 and Colo38 parental cells in increasing concentrations of BRAF-I (Vemurafenib) up to 2 and 5 µM, respectively. After two months, resistant cells were isolated from each of the two cell lines and cultured in presence of 0.5 and 5 µM PLX4032 (ChemieTek), respectively.

Both parental and derivative BRAF-I resistant melanoma cells were kindly provided by Dr. Soldano Ferrone (PhD, MD), from Harvard University.

## ***2- Bacterial Transformation & plasmid isolation***

After obtaining competent DH5 $\alpha$  - E. Coli cells, standard protocol was followed for transformation. Briefly, the ligation products were added to the bacteria, kept in ice for 10 minutes, heated at 42 °C for 45 seconds and cooled 2 minutes in ice. Then, bacteria were grown for 1 hour in 1 ml of SOC medium, composed of 20 gr/L LB broth, 1M MgCl<sub>2</sub>, 1M MgSO<sub>4</sub>, 2M Glucose (Sigma-Aldrich).

Bacterial colonies transformed with pGFP-V-RS or pCMV6-XL4 plasmid were selected in 35 gr/L LB agar plates containing 100  $\mu$ g/ml Ampicillin (Sigma-Aldrich).

Each colony was collected, expanded at 37 °C overnight in 20 gr/L LB broth with 100  $\mu$ g/ml Ampicillin and finally, the plasmid DNA was purified from bacteria using Pure Yield plasmid Maxiprep kit (Promega), according to manufacturers' instructions. The concentration was then assessed through a NanoDrop spectrophotometer (Thermo-Scientific)

## ***3- Cell Transfection***

### ***3.1- RNAi silencing through shRNA***

Human osteosarcoma 143B cells were transfected with a shRNA sequence to permanently silence the ATP1F1 gene. For transient co-transfection we used pCMV6-XL5-IF<sub>1</sub> expression plasmid, together with alternatively a single shRNA vector or a scrambled negative control constructs cloned in pGFP-V-RS plasmid (#1 GI325933, #2 GI325934, #3 GI325935, #4 GI325936 and TR30013, respectively). All the plasmids used were from Origene (Rockville, MD, USA).

Briefly, cells were seeded the day before transfection in 35 mm Petri dishes, in order to have 60-80% of confluence for the transfection procedures. The following day, equal amount of the two vectors (4 µg total DNA) were transfected overnight using polyethylenimine linear, MW ~25,000 (Polysciences, Inc.) (PEI), according to manufacturers' instructions, with a 1:7 DNA:PEI ratio. After 24h, the medium was replaced with complete DMEM and cells were cultured for further 24 hours before the analysis of IF<sub>1</sub> silencing level.

The 29 pb gene silencing shRNA sequence (5'-AAACACCATGAAGAAGAAATCGTTCATCA-3'), contained in the plasmid #4 GI325936, granted the best efficiency of transfection. Therefore, parental 143B cells were seeded and transfected - as described above - with 2 µg of either GI325936 or TR30013 plasmid DNA. 48 hours later, cells were split and selected for stable transformation in the presence of 1 µg/ml puromycin, changing the medium every day.

Single colonies were then subcloned by limiting dilution and finally all the clones obtained were assayed for the IF<sub>1</sub> expression level. Clones with the lowest expression of IF<sub>1</sub> where then expanded to perform all the experimental assays.

### **3.2- miRNAs**

The expression levels of miRNAs (*i.e.* miR-136) were altered by transient transfection with miR-136 mimic or inhibitor. After being cultured in fresh medium over-night, adherent melanoma cells were alternatively transfected with 50 nM of hsa-mir-136-5p mimic or inhibitor (Life Technologies), using scrambled sequences as a negative control. Cells were transfected using RNAiMAX Lipofectamine reagent (Life Technologies) in SFM Opti-MEM (Life Technologies), according to manufacturer's instructions. MiR-136 levels were then assayed by q-RT-PCR to verify the successful transfection.

#### **4- Cell Growth Evaluation**

Cell growth of parental and IF<sub>1</sub>-silenced 143B cells was assessed after seeding  $2 \times 10^5$  cells - in triplicate - in complete DMEM in 35 mm Petri dishes and culturing for up to 72h.

Adherent cells were trypsinized and collected, and the growth ability of cell lines was assayed using trypan blue exclusion test, counting cells every 24 h, without changing the medium.

Melanoma cell growth was assessed in three independent experiments after seeding  $1,5 \times 10^5$  cells in 6-wells plates in complete medium (three independent wells per each time point). After being cultured in fresh medium over-night, parent M21 and Colo38 cells were transfected either with scrambled or miR-136 and grown further 24h before treating with 0.5-5  $\mu$ M PLX4032 (respectively), in order to maximize miR-136 effect. Cells were counted every 24h up to 120h from the beginning of vemurafenib treatment. By contrast, resistant M21-R and Colo38-R were transfected in their normal condition (*i.e.*: under PLX4032 treatment) and counted up to 120h since transfection, either with scrambled or miR-136-inhibitor (Life Technologies). Cells were harvested together with supernatant and counted every 24h without changing the medium, to assess the total number of cells, using a Vi-CELL XR 2.03 (Beckman Coulter, Inc.).

#### **5- Cell viability and Annexin V assays**

Cell viability was assessed on fluorescent-based analysis through Muse™ Count & Viability Kit (Millipore). In the assay, both viable and non-viable cells are stained and distinguished on the basis of their permeability to the DNA-binding dyes in the reagent.

Essentially, cells were harvested and washed in PBS solution. After centrifugation, pellets were resuspended in PBS and incubated with Muse™ Count & Viability reagent for 5 minutes at room temperature, protected from

light. At least 10,000 events were acquired with Muse™ Cell Analyzer and data were expressed as Total and Viable cells/ml.

Detection of apoptotic cells was carried out exploiting the translocation of phosphatidylserine (PS) residues from the cytoplasmic face of the plasma membrane to cell surface. Annexin V-PE is used to detect PS on the external membrane of apoptotic cells.

After culturing cells, including for positive and negative controls, 143B cells were collected and resuspended in the Assay Buffer HSC (Millipore) and incubated at room temperature for twenty minutes, with the Muse™ Annexin V & Dead Cell reagent (Millipore), containing a mixture of a cell impermeant dye, as an indicator of membrane structural integrity, and a fluorescent conjugate for the detection apoptosis.

Cells were then analyzed by Muse™ Cell Analyzer, after 10,000 acquisitions and the concentration (expressed as Cells/ml) and percentage of the four distinct populations were determined: live, early and late apoptotic, dead cells.

## ***5- Flow Cytometric Assessment***

Flow cytometry of GFP positive cells was performed using a FACSaria cytometer (BD Biosciences). Excitation was at 488 nm and fluorescence emission was measured at 580/630 nm.

Data acquisition and analysis was performed with BD FACS Diva and Flowing Software, respectively.

## ***6- Mitochondrial membrane potential***

The inner mitochondrial membrane potential was measured by staining cells with 20 nM tetramethylrhodamine methyl ester (TMRM) (Molecular Probes, Eugene, OR), a lipophilic probe that enters mitochondria in a  $\Delta\Psi_m$ -dependent manner (112).

After culturing, cells were incubated with the probe for 30 min at 37 °C in the absence or presence of 0.6  $\mu$ M oligomycin and wells were then washed twice with Hanks' balanced salt solution to remove any remaining unincorporated dye. The cells were rapidly trypsinized, diluted to the optimal density (300,000 cells/ml) with Hanks' balanced salt solution supplemented with 10% FBS and immediately analyzed with the MUSE cell analyzer (Millipore, Billerica, MA).

Excitation was at 532 nm and fluorescence emission was measured at 576/28 nm. Data acquisition and analysis were performed with MuseSoft Analysis and Flowing software, respectively. A total of 10,000 events were acquired for each determination.

## **7- *Brightfield and Fluorescence Microscopy***

Brightfield and fluorescence images of controls and IF<sub>1</sub>-silenced cells were acquired using a fluorescence inverted microscope (Olympus IX50 equipped with a CCD camera).

Multiple high-power (magnification X10 and X40) images were acquired with IAS2000 software (Delta Sistemi, Roma, Italy). Fluorescence photographs of GFP-positive cells were obtained using a specific set of filters: excitation 480/30 and emission 530/30.

Mitochondrial network morphology and membrane potential were evaluated by incubating cells with 20 nM TMRM for 30 min. At least 10 different optic fields were acquired for every experimental condition tested.

## **8- *Protein concentration***

The protein concentration was determined using the Lowry method (113). Basically, the sample was treated with 5% Na-deoxycholate and subsequently incubated for 10 minutes in the presence of a reaction mixture constituted by 2 % Na<sub>2</sub>CO<sub>3</sub> and 0.1 M NaOH (Reagent 1), 2 % Na-K tartrate

(Reagent 2) and 1% CuSO<sub>4</sub> (Reagent 3) in a stoichiometric ratio of 100:1:1. The mixture was then added with the Folin-Ciocalteu to a final concentration of 3%. After 30 minutes of incubation at RT, the concentration of the reduced Folin reagent was measured at 750 nm in a V-450 Jasco spectrophotometer. The total concentration of protein in the sample was determined on the basis of a standard curve, using bovine serum albumin (BSA, Sigma) as a standard.

## **9- Mitochondria Isolation**

Coupled mitochondria were isolated from cells according to the method by Kun *et al.* (114), modified to exclude digitonin treatment, as described previously (115).

Essentially, cell homogenates were obtained using a glass Potter-Helvehjem homogenizer with a motor-driven Teflon pestle in isolation buffer (0.22 M mannitol, 0.07 M sucrose, 0.02 M HEPES, 1 mM K-EDTA, 0.1 mM K-EGTA, pH 7.4) containing 1 mM PMSF (phenylmethanesulfonyl fluoride). Crude extracts were centrifuged at 2000 *g* for 10 min (Sorvall SS34 rotor) to remove nuclei and plasma membrane fragments, and then the supernatant was centrifuged at 10,000 *g* for 10 min (Sorvall SS34 rotor) to obtain the mitochondrial pellet. Mitochondria were washed in 0.25 M sucrose, 0.02 M HEPES, 1 mM K-EDTA, and 0.1mM K-EGTA, pH 7.4, and resuspended in the same buffer to a concentration of 10 mg/ml of protein.

## **10- BN-PAGE and Western Blot Analysis**

The organization of the ATP synthase complex and the binding of IF<sub>1</sub> to the monomeric and/or oligomeric form of the enzyme were analyzed in digitonin-treated mitochondria (2.5:1 (w/w) digitonin : protein ratio) by one-dimensional blue native-PAGE (116).

Following electrophoresis under non-denaturing conditions, proteins were immediately electroblotted onto nitrocellulose membranes under denaturing

conditions. ATP synthase and IF<sub>1</sub> protein bands were detected using anti- $\alpha$  subunit and anti-IF<sub>1</sub> primary monoclonal antibodies (MitoSciences Inc.), respectively, and a secondary goat anti-mouse IgG<sub>H+L</sub> antibody labeled with horseradish peroxidase (Invitrogen).

The immunoblots were detected and quantified by chemiluminescence using the ECL Western Blotting Detection Reagent Kit (Amersham Biosciences).

### ***11- In-gel ATPase Activity***

Immediately after the electrophoretic run of the protein complexes extracted from digitonin-treated mitochondria, ATPase activity was assayed on the native gel using an enzymatic colorimetric method (117). Whitestained ATP synthase bands were acquired using a GS-800 densitometer (Bio-Rad) with a blue filter to minimize the interference from the residual Coomassie Blue.

### ***12- SDS-PAGE and Western Blot Analysis***

Cellular lysates were separated by SDS-PAGE and blotted onto nitrocellulose membranes to perform semi-quantitative analysis of protein content, according to Baracca *et al.* (118).

Cells were lysed with ice-cold RIPA buffer (pH 8.0, containing 50 mM Tris-HCl; 150 mM NaCl; 0.1% Triton, 0.1% Na-DOC, 0.1% SDS), supplemented with 5  $\mu$ L/ml of a mixture of protease inhibitors and 1 mM PMSF (Sigma).

Equal amount of protein diluted in Sample Loading Buffer (3.56 mM SDS, 36% glycerol absolute; 0.5 M Tris pH 6.8; Bromophenol Blue 10, 4  $\mu$ M;  $\beta$ -Mercaptoethanol 5%), were denatured for 5 min at 100°C and loaded into a sodium dodecyl sulfate–polyacrylamide gradient gel (12-20%).

Following SDS-PAGE electrophoresis, proteins were immediately electroblotted onto a nitrocellulose membrane (BioRad). Membranes were then saturated with a solution of fat-free milk powder (BioRad) in PBS and

0.1% Tween-20 (BioRad) for 1 hour at room temperature and incubated with primary antibodies, specific for the d-subunit of F<sub>1</sub>F<sub>0</sub>-ATPase (19 kDa) and for IF<sub>1</sub> (12 kDa), or with a mixture of five primary mouse monoclonal antibodies specific for single subunits of each OXPHOS complex (MitoSciences Inc., Eugene, OR) as reported in Sgarbi *et al.* (119). Antioxidant enzymes were detected by rabbit polyclonal primary antibodies specific for Catalase (60kDa) and Cu-Zn SOD (17 kDa), and mouse monoclonal primary antibodies targeting Mn-SOD (25 kDa), GPX-1 (22 kDa), all purchased by Abcam (MitoSciences Inc., Eugene, OR)

Samples deriving from melanoma patients were incubated with a rabbit monoclonal antibody specific for SUFU (55 kDa) and PDGFR $\alpha$  (90 kDa) primary antibody (Cell Signaling).

Actin (42 kDa) and porin (35 kDa), used as loading controls for cells and mitochondria, respectively, were immunodetected with mouse monoclonal anti-actin (Sigma) and anti-porin (Mito-Sciences Inc., Eugene, OR) primary antibodies.

Immunodetection of primary antibody was carried out with secondary goat anti-mouse or anti-rabbit IgG<sub>H+L</sub> antibody (Invitrogen) labeled with horseradish peroxidase.

Chemiluminescent detection of the specific proteins was performed with the ECL Western blotting Detection Reagent Kit (GE Healthcare, Waukesha, WI) using the ChemiDoc MP system equipped with the ImageLab software (Bio-Rad) to perform the densitometric scanning of the relative protein intensity.

### ***13- Citrate Synthase Activity***

The activity of the enzyme citrate synthase, taken as an index of mitochondrial mass, was assayed as described by Trounce *et al.*, 1996, (120), by following spectrophotometrically the reduction of 5,5' - dithiobis 2 - nitrobenzoic acid (DTNB) in a reaction coupled with acetyl - CoA and oxaloacetate. Essentially, the reaction catalyzed by citrate synthase produces

CoA-SH, which react with the DTNB by breaking the disulfide bridge, and producing the ion 2-nitro-5-thiobenzoate (NTB) in a stoichiometric ratio.

The assays were conducted at 30 °C by incubating 20–30 µg protein in Tris-HCl buffer 125 mM (pH 8), 0.2% triton, 0.1 mM acetyl-coenzyme A, 0.1 mM 5,5'-dithio-bis(2-nitrobenzoic acid) (DTNB), and 0.5 mM oxaloacetate. The activity was assessed by monitoring the release of 2-nitro-5-thiobenzoate at 412 nm ( $\epsilon=13.6 \text{ mM}^{-1} \text{ cm}^{-1}$ ), as previously described (121) (122). After the determination of protein concentration, by the Lowry method, the activity was expressed as nmol/min/mg protein.

#### ***14- Intracellular steady-state ATP***

The intracellular steady state of ATP was determined by the luciferin - luciferase bioluminescent method (ATP bioluminescent assay kit CLS II; Roche; Basel, Switzerland), using an internal standard with a known amount of ATP (33 pmol), as described before (123).

Cells were seeded ( $4 \times 10^5$ ) in complete medium and the following day fresh media were replaced to all samples. Then, cells were washed in PBS, rapidly resuspended in a buffer containing 10mM Tris-Hcl, 100mM KCl, 5 mM  $\text{KH}_2\text{PO}_4$ , 1 mM EGTA, 3 mM EDTA, 2 mM  $\text{MgCl}_2$  (pH 7.4) and then lysed in DMSO to release the ATP content at the intracellular level.

After determining the protein concentration of the intracellular content, ATP levels were expressed as nmol/mg protein.

#### ***15- ATP synthesis Rate***

The rate of mitochondrial ATP synthesis was measured using the method reported by Sgarbi et al., 2006. (124).

Essentially, cells were washed in PBS and then resuspended in a buffer containing 10 mM Tris, 100 mM KCl, 5 mM  $\text{KH}_2\text{PO}_4$ , 1 mM EGTA, 3 mM EDTA, 2 mM  $\text{MgCl}_2$  (pH 7.4). Cells were then incubated in the presence of digitonin

60 µg/ml (to permeabilize the plasma membrane), 2 mM iodoacetamide (to inhibit ATP synthesis from cytoplasmic glycolysis) and 1.25 mM adenosine pentaphosphate (myokinase inhibitor). Complex I driven ATP synthesis was induced by adding 10 mM glutamate/malate and 0.5 mM ADP to the sample. After 3 minutes, the reaction was stopped by adding dimethylsulfoxide (DMSO).

The amount of ATP product was then determined by means of the luciferin-luciferase bioluminescent method (ATP bioluminescent assay kit CLS II; Roche, Basel, Switzerland), using as a reference an internal standard with a known amount of ATP (33 pmol).

The ATP measured was referred to the protein content, determined by the method of Lowry, and the ATP synthesis rate was expressed as nmol/min/mg protein.

## ***16- ATP hydrolysis***

The ATPase activity was determined spectrophotometrically measuring the oxidation of NADH at 340 nm obtained coupling two reactions catalyzed by pyruvate kinase (PK) and lactate dehydrogenase (LDH) respectively in presence of phosphoenolpyruvate (PEP) in a V-450 Jasco spectrophotometer (125).

After isolating mitochondria as described before, samples were divided into two different aliquots to be assayed at two different pH (*i.e.* pH 7.4 and 6.7).

The assays were performed at 30 °C with an ATP regenerating system in 25 mM TRIS/acetate, 25 mM KCl, 5 mM MgCl<sub>2</sub>. 30 µg of mitochondria were incubated with 4mM ATP, 160 µM NADH, 5 µM Rotenon, 1,5 mM PEP and LDH/PK. F1Fo ATPase activity was calculated as the difference between total and oligomycin-sensitive ATPase activity and finally was expressed as nmol/min/mg.

## **17- Glucose consumption and Lactate release assay**

Glucose consumption and lactate production were determined by a colorimetric-enzymatic procedure, firstly described by Trinder in 1969 (126), that exploits the production of hydrogen peroxide (H<sub>2</sub>O<sub>2</sub>), peroxidized to form a colored compound, directly proportional to the amount of Glucose/Lactate in the sample.

The colorimetric determinations were conducted on the culture medium after the treatment of cells. Briefly, 4x10<sup>5</sup> cells were seeded in complete medium. After 24 up to 72 hours of cell culturing, the supernatants were extracted and dosed by Glucose liquid and Lactate PAP fluid kit (FAR diagnostic; Verona, Italy and Centronic GmbH; Wartenberg, Germany, respectively) at 37 °C, following manufacturers' instructions.

Using an internal standard of known concentration (5.55 mM Glucose standard, 30 mg/dl lactate standard), absorbance was measured spectrophotometrically (510 nm and 546 nm, respectively) to trace the amount of Glucose residue or Lactate produced. Data were then reported to the number of moles and normalized by the number of cells and expressed as μmol/10<sup>6</sup> cells.

## **18- Analysis of Intracellular ROS in Live Cells (CellRox® Orange & CellRox® Deep Red)**

Reactive oxygen species (ROS) in live cells were detected and quantified alternatively by the cell-permeant fluorogenic reagent — CellROX® Orange or CellROX® Deep-Red (both from Thermo Fisher Scientific). The reagents are non-fluorescent in the reduced state, but exhibit strong fluorescence upon oxidation and remain localized within the cell.

Briefly, cells were grown up to 72 hours, washed once with PBS and loaded with 5 μM CellROX® Orange or Deep Red probe (Thermo Fisher Scientific) in complete medium without FBS for 30 minutes in the dark. After loading, the dye was removed by washing the cells twice with PBS.

Cells were then trypsinized and intracellular ROS content was detected acquiring at least 10,000 events with the FACSaria flow cytometer (Deep Red probe) or with Muse™ Cell Analyzer (Orange probe), by measuring the fluorescence emission at 576/680 nm (excitation at 405 nm and 532 nm, respectively).

## **19- Oxygen Consumption Rate**

Parental and IF<sub>1</sub> silenced clones were assayed for the oxygen consumption rate both in intact and permeabilized cells, using an oxygen Clark-type electrode as previously reported by Baracca *et al.* (118).

Measurements were conducted at 30 °C, with a 7.4 pH buffer containing 0.25M Sucrose, 20 mM Tris, 4 mM MgSO<sub>4</sub>, 0.5 mM EDTA, 10 mM KH<sub>2</sub>PO<sub>4</sub>. In these conditions, the solubility of oxygen is equal to 204.1 mM.

Intact cells were harvested and resuspended in the aforementioned buffer and directly analyzed in the Stratkelvin's chamber for about 5 minutes, to assess endogenous respiration.

Alternatively, cells were permeabilized with digitonin (60 µg/ml) to favor the entry of 10 mM glutamate, 10 mM malate (plus 1.8 mM malonate) as substrate of NADH(H<sup>+</sup>) - dehydrogenase Complex I, or 20 mM succinate (plus 4 µM rotenone) as substrate of succinate - dehydrogenase.

State 3 and uncoupled respiration rates were measured in the presence of 0.5 mM ADP or 60 µM dinitrophenol, respectively. State 4 was established by adding 1.5 µM Oligomycin.

The oxygen consumption rate was referred to protein concentration, determined by the Lowry method, and expressed as nmol O<sub>2</sub>/min/mg protein.

## **20- Dual Luciferase Assay**

A luciferase reporter construct was generated by cloning eight repeated copies of wild-type or mutated Gli-binding sites (3'GliBS or mut3'Gli-BS, respectively) into a psiCHECK™-2 Vector (Promega), to control the

expression of a Firefly Luciferase (*Photinus pyralis*) to assess the Shh Pathway activation. The plasmid was kindly provided by Dr. Hiroshi Sasaki (Laboratory for Embryonic Induction, Japan) and was co-transfected together with Renilla luciferase (*Renilla reniformis*, also known as sea pansy) containing pRLTK vector, as internal control.

Briefly, Melanoma parent cells M21 and Colo38, as well as BRAF-I resistant derivative M21-R and Colo38-R, were seeded into 12-well plates for 24h (5 X 10<sup>4</sup> per well). Then the cells were co-transfected with 1 µg DNA of each reporter vector, and with 50 nM miR-136 mimic or scrambled control. After 24 and 48 hours from transfection, cells were lysed, and ratios between Firefly and Renilla luciferase activity were estimated using the Dual Luciferase Assay Kit (Promega) according to the manufacturer's instructions. Data were repeated at least three times, using a GloMax® 96 Microplate Luminometer (Promega) and presented as the mean value of Firefly/Renilla luciferase ratio.

## ***21- miRNAs-gene targeting prediction***

MicroRNAs databases were used to acquire information on miRNA sequence data and their genomic targets, mostly based on miRanda algorithm (v3.0) to detect potential microRNA target sites in genomic sequences (127).

The main software used were: microRNAs.org, miRbase, miRDB, miRwak2.0 (128). The provision of a p-value for each miRNA-target assignment allows the user to assess the confidence in the prediction.

## ***22- Real-time quantitative RT-PCR***

Semiquantitative reverse transcription-polymerase chain reaction (RT-PCR) was performed to assess miR-136 levels in wild type and miR-136 (either mimic or inhibitor) transfected melanoma cells.

Total RNA was isolated using TRIzol reagent (Life Technologies), according to the manufacturer's instructions.

The total RNA from each sample was reverse-transcribed into cDNA with the TaqMan® MicroRNA Reverse Transcription Kit (Applied Biosystems), according to manufacturer's instructions.

Expression analysis of miRNAs was performed with TaqMan primers and probes (Life Technologies) for miR-136 and the small nuclear U6 RNA, used as miRNA internal control.

Real time PCR was performed using a CFX96 real-time PCR system (BioRad). MiRNA relative expression levels were normalized to U6 by the  $2^{-\Delta\Delta C_t}$  method and data were presented as miR-136/U6 fold change. All reaction were performed in triplicate and repeated twice.

### ***23- Data Analysis***

Results are average  $\pm$  SD of 4-6 samples from at least two independent experiments. Statistical analyses were performed using the OriginPro 7.5 software (Origin-Lab Corporation, Northampton, MA, USA) applying the analysis of variance (ANOVA) test followed by the Bonferroni means comparison. Statistical significance was defined by  $p \leq 0.05$ .

# Results - 1<sup>st</sup> part: IF<sub>1</sub>

---

## **1- IF<sub>1</sub> expression and shRNA-mediated stable silencing**

The mammalian mitochondrial ATP synthase is finely regulated by the endogenous inhibitor IF<sub>1</sub>, a protein which binds at the  $\alpha/\beta$  catalytic sites and inhibits ATP hydrolysis. The binding of IF<sub>1</sub> to the enzyme is  $\Delta\Psi_m$  and pH dependent, being the latter optimal under neutrality: when the aerobic proton motive force declines, like in ischemia or respiratory impairment, the protein becomes active to prevent a massive and useless dissipation of energy inside the cell. Conversely, in conditions of normal electrochemical proton gradient, IF<sub>1</sub> does not inhibit the enzyme, which normally synthesizes ATP (48).

Most investigations into the pathophysiological role of IF<sub>1</sub> and the F<sub>1</sub>F<sub>0</sub>-ATPase have been done in the context of myocardial ischemia (19). To note, similar conditions might be found in tumor cells, where oxygen levels vary from the perivascular regions to the anoxic necrotic centers (129). In these conditions, IF<sub>1</sub> could play an important role in the pathology of tissue ischemia and tumor growth, by helping cells to conserve ATP. Confirmations of this hypothesis can be found in the overexpression of the protein registered in many human carcinomas (65), that prompted researchers to focus on the contribution of the inhibitor in modifying cancer metabolism.

In this context, IF<sub>1</sub> may therefore represent an efficient strategy of cancer cells to overcome hostile conditions; nevertheless the importance of this protein has not been definitively established and conflicting data have been reported, encouraging us to investigate over the bioenergetics of tumor cells following the variation of IF<sub>1</sub> levels.

### 1.1- Cell model: Human osteosarcoma 143B cells

As a starting point, a number of different cell lines was screened and immunodetected for IF<sub>1</sub>, to assess the expression levels of the protein in different cell types. Among these, we found that the human osteosarcoma 143B cell line expresses high levels of the inhibitor (*Figure 17, A and B*), so we decided to explore the cellular response to the silencing of IF<sub>1</sub>, aiming to shed light on the contribution of the inhibitor to the typical metabolic changes of the transformed cells.

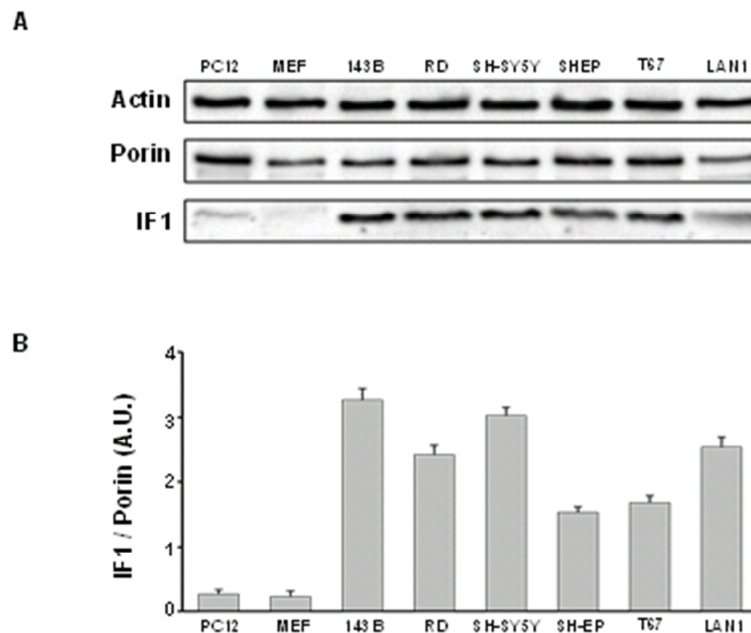


**Figure 17: IF<sub>1</sub> level in different immortalized and tumor cell lines.**

**(A)** Representative immunoblot analysis of IF<sub>1</sub> protein level in different cell lines. Actin and porin were both used as loading control and mitochondrial content respectively.

**(B)** Graph shows the densitometric analysis of IF<sub>1</sub> level normalized over the porin and bars represent the mean  $\pm$  SD of two independent experiments. Cell lines used were as follow: **PC12** = Rat adrenal pheochromocytoma cell line; **MEF** = mouse embryonic fibroblasts; **143B** = human osteosarcoma cell line; **RD** = human rhabdomyosarcoma cell line; **SH-SY5Y** = human neuroblastoma (N-type) cell line; **SH-EP** = human neuroblastoma (S-type) cell line; **T67** = human astrocytoma cell line; **LAN-1** = human neuroblastoma (N-type) cell line.

## 1.2- Assessment of the most efficient shRNA sequence

Some recent investigations in the pathology of tissue ischemia and tumor growth have been set out to explore the functional consequences of varying IF<sub>1</sub> expression levels in tumor cell lines, by transient transfection or temporary knocked-down of the protein. Nevertheless, studies on transiently transfected cells do not represent a stable steady-state metabolic condition, but a dynamic situation in which cells are adapting to the variation of IF<sub>1</sub> content, producing potentially ambiguous results, like the controversial data reported in the literature. Therefore, in the first part of our study we focused on fully silencing of the inhibitor through an RNA-interference technique, mediated by shRNA sequences directed to the ATP1F1 gene.

For this reason, four IF<sub>1</sub> gene-specific shRNA expression plasmids (Figure 18, A) were tested to identify the 29mer shRNA sequence with the highest IF<sub>1</sub> silencing competence (Figure 18, B).

A

#1 - GAGCACAGAGTAGAGAACAACACTGGCAGCT  
#2 - TCCGACATTACAGGTTATGCTTTGAGATC  
#3 - GAAATTGAGCGCCATAAGCAGAAGATCAA  
#4 - AACACCCATGAAGAAGAAATCGTTCATCA

B

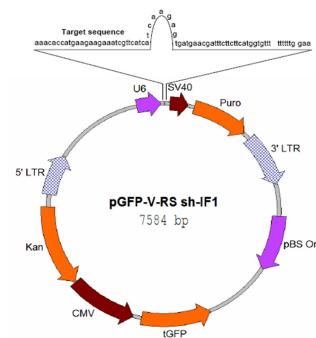


**Figure 18: Silencing of the IF<sub>1</sub> inhibitor protein: assessment of the most efficient shRNA sequence.**

(A) Nucleotide sequence of the four shRNA constructs, specific for human IF<sub>1</sub> mRNA (spanning the 3' end of the IF<sub>1</sub> mRNA) cloned in the pGFP-V-RS vector. (B) Map of the plasmid #4 showing the complete sequence of the construct (target sequence, loop and reverse complementary sequence), cloned under the control of the U6 promoter, and the termination sequence TTTTTT located immediately downstream of the shRNA construct.

The transient co-transfection of the cells with the IF<sub>1</sub> expression plasmid together with the four shRNA constructs, resulted in different efficiency of silencing, with a maximal reduction (about -70%) observed using plasmid #4 (Figure 19).

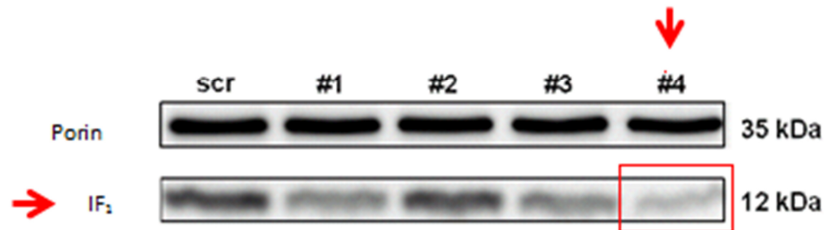


**Figure 19: Immunoblot analysis of IF<sub>1</sub> protein levels after transient co-transfection with both the IF<sub>1</sub> overexpression plasmid and alternatively one of the four shRNA or the scrambled plasmids (#1-4 plasmids as specified in Materials and Methods).**

### **1.3- IF<sub>1</sub> silencing: stable clones IF<sub>1</sub>-KD were established**

Once identified the sequence that granted the best silencing, cells were alternatively transfected with #4 or a scrambled plasmid, containing a random nucleotide sequence, (same length of G1325936 sequence, but not coding for any human mRNAs), in order to obtain a stable suppression of the inhibitor and its proper control. After 24 hours of culture, an overall 30% of population was positively transfected (*Figure 20*, lower panel), as estimated on the basis of the GFP fluorescence - GFP being encoded by each shRNA plasmid - and cells were displaying a similar morphology, independently from the presence - or absence - of the inhibitor (*Figure 20*, upper panel).

Positive transfected cells were then selected in Puromycin and subcloned by limiting dilution, to obtain several clones (starting from individual GFP-expressive-cells) from both scrambled and shRNA #4 plasmids. Clones were then assayed by SDS-PAGE to evaluate the IF<sub>1</sub> expression levels after silencing: as shown in *Figure 21*, the immunodetection of IF<sub>1</sub> exhibited a remarkable reduction of expression in all the silenced clones. To note, densitometric analysis of the bands revealed that clones A7 and D9

expressed the least IF<sub>1</sub> content, as they resulted in 6 and 9% of the controls, respectively.

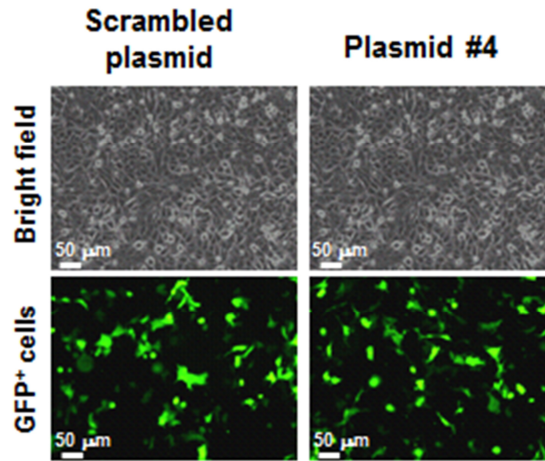


**Figure 20:** Bright-field and fluorescence microscopy images of 143B cells transiently transfected with either the scrambled or the sh-IF<sub>1</sub> #4 plasmids. The pictures are representative of several observations (magnification X10).

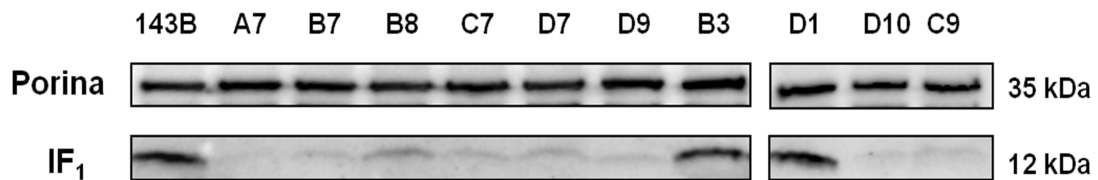


**Figure 21:** Immunoblot analysis of the IF<sub>1</sub> protein level in parental (143B cells), scrambled clones (B3 and D1), and IF<sub>1</sub>-depleted clones (A7, B7, B8, C7, C9, D7, D9, D10).

Transfection stability and cell homogeneity of IF<sub>1</sub> silenced and scrambled clones were evaluated by both fluorescence microscopy (Figure 22, A) and flow cytometry (Figure 22, B), confirming that almost the totality of cells were positive for GFP expression (around 99% on total).

At the same time, neither transfection procedures, nor the absence of the protein affected cell morphology, since both silenced and scrambled clones

maintained the same morphology of the untransfected cells (*Figure 22, A*). Indeed, the bright-field microscopy images revealed that the adhesion capacity of the clones was unaltered with respect to the parent cells (*Figure 22, A*).

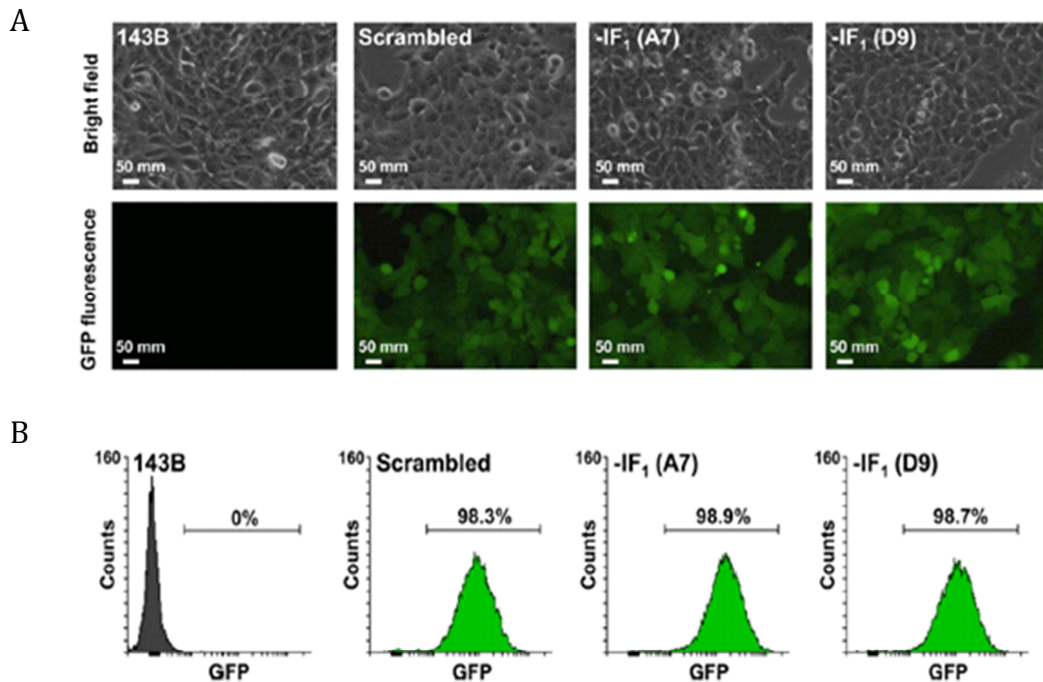


**Figure 22: Transfection stability and cell homogeneity of IF<sub>1</sub> silenced and scrambled clones.**

**(A)** Bright-field and fluorescence (GFP) microscopy images of 143B cells, scrambled clone B3 and IF<sub>1</sub>-silenced clones A7 and D9 (magnification X10). The pictures are representative of several optical fields. **(B)** Typical flow cytometry GFP-positive cells distribution in controls and IF<sub>1</sub>-depleted clones.

In addition, to avoid interferences with some probes used in the following experiments - and to verify that no artifacts resulted from the expression of the GFP - some IF<sub>1</sub>-silenced clones not expressing GFP were isolated from the starting transfected population and run on a SDS-PAGE to verify successful silencing of the protein. However, comparable amount of IF<sub>1</sub> to the aforementioned clones were immunodetected in G3 and E9 GFP<sup>-</sup> clones, confirming an efficiency of silencing of more than 90% (*Figure 23*).

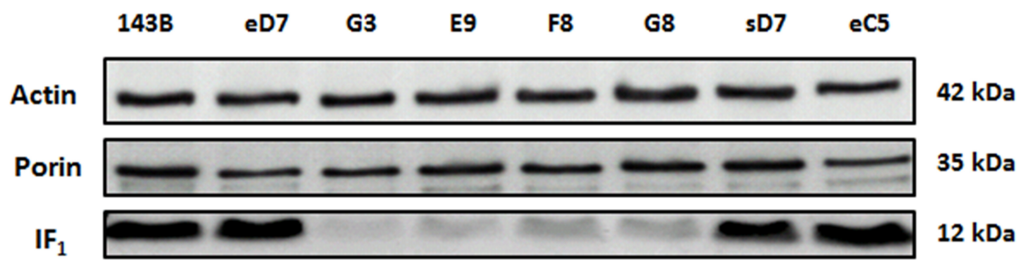


**Figure 23: Immunoblot analysis of the IF<sub>1</sub> protein level in parental (143B cells), scrambled and empty vector clones (sD7, eD7 and eC5 respectively), and IF<sub>1</sub>-depleted clones (G3, E9, F8, G8).**

## ***2- Biochemical characterization of IF<sub>1</sub> - silenced clones***

After selecting human osteosarcoma clones with a permanent silencing of the endogenous inhibitor of ATP synthase, the main bioenergetics parameters were investigated, in order to see if the presence – or absence – of the protein was critical for the bioenergetics of the cells.

### ***2.1- Cell viability***

Some studies reported that the overexpression of IF<sub>1</sub> is correlated with an augmented proliferative response of the cells (130), even in normoxic conditions; nonetheless, this has been questioned by others, in a study on permanently IF<sub>1</sub>-silenced HeLa cells, in which IF<sub>1</sub> seems not to be essential for normal cell growth (131).

To clarify these conflicting results, the first parameter assayed in our study was cell viability, in order to evaluate whether the absence of the protein could interfere with the cell proliferation rate. To that aim, cell growth of

human osteosarcoma 143B cells was assayed for up to 72 hours, counting cells every 24 hours and checking for cell viability.

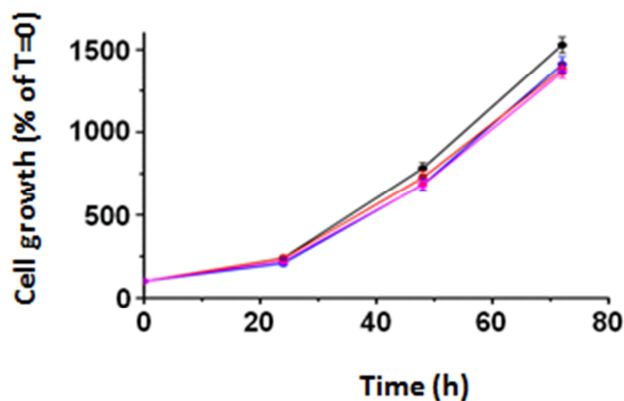


**Figure 24: IF<sub>1</sub> does not affect the Viability and Proliferation Rate of Osteosarcoma cells.** Cells were grown under normal conditions for up to 72h and counted every 24h. Parent 143B cells (black), scrambled (blue) and IF<sub>1</sub>-silenced clones (red, A7 and magenta, D9) are shown. Results are represented as the mean of each time point  $\pm$  SD of three independent experiments.

As Figure 24 clearly shows, under normal growth conditions the proliferation rate and cell viability of the two silenced clones (red and magenta line) were similar to the two control lines (143B, black line; scrambled, blue line). Therefore, we assumed that the absence of the inhibitor protein does not alter either the speed or the vitality of cancer osteosarcoma cells under optimal growth conditions.

## **2.2- Glucose consumption and Lactate release**

According to some recent studies, IF<sub>1</sub> plays a crucial role in mediating the metabolic switch experienced by cancer cells – in favor of glycolysis – therefore providing an advantageous phenotype to promote cell proliferation and invasion (132). Since we showed that the inhibitor was not involved in the proliferative response of the cells (Figure 24), nor in modifying cell morphology or adhesion capability (Figure 22), we wanted assay whether - and eventually to what extent - IF<sub>1</sub>-null cells consume the substrate glucose

and release lactate.

Nevertheless, the diagrams illustrates that, after 24 hours of cell growth under normoxic conditions, the IF<sub>1</sub>-silenced clones and controls displayed the same consumption of the substrate, as well as the same release of lactate (*Figure 25, A and B, respectively*). Incidentally, the lactate release to glucose consumption ratio was approximately two, indicating that almost all of the glucose consumed by the cells was released into the medium, in the form of lactate.

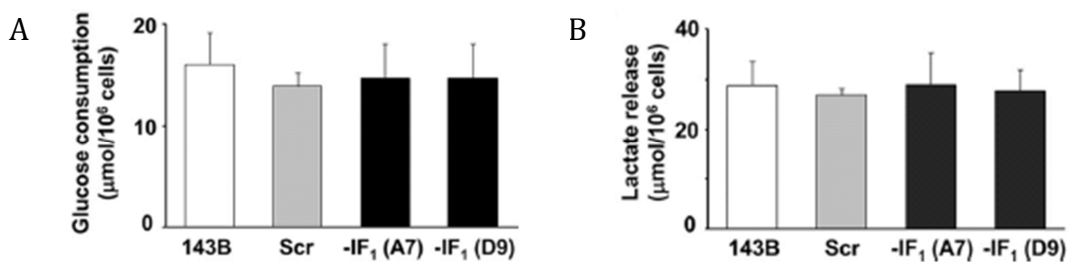


**Figure 25: No difference in Glucose consumption, nor in Lactate release.**

Cells were grown under normal conditions for 24h and media were assayed for residual Glucose (A) and Lactate produced (B), as described in Material and Method section. Data, expressed as µmol Glucose consumed/Lactate released per 10<sup>6</sup> cells, represent mean value ± SD of three independent experiments.

As expected, these data indicate that normoxic conditions do not induce the activation of hydrolytic ATP synthase, with the subsequent binding of IF<sub>1</sub>, contrarily to data reported (133).

### **2.3- Mitochondrial parameters and ATP content**

Previous studies reported that the knock-down of IF<sub>1</sub> caused stimulation of autophagy, decrease in mitochondria volume fraction in the cells and the decrease in cristae density in mitochondria (60), (63) .

However, no changes were reported in our study in absence of IF<sub>1</sub>: after incubating cells with 20 nM TMRM for 30 min, fluorescence microscopies revealed a heterogeneous mitochondrial network morphology, with spotted and filamentous mitochondria, but silenced clones displayed no prominent alteration compared to controls (*Figure 26*).

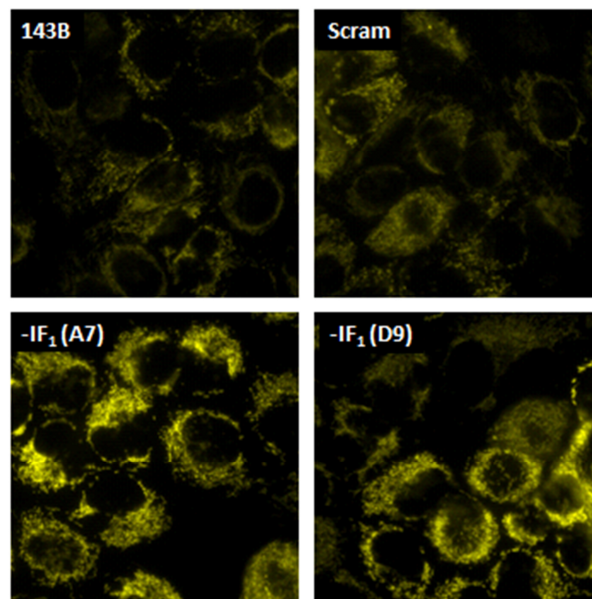


**Figure 26: Mitochondrial network was unaffected by the absence of IF<sub>1</sub>.** Parental, scrambled, and IF<sub>1</sub>-depleted cells were loaded with 20 nM TMRM and fluorescence images were obtained using an inverted fluorescence microscope (magnification X40).

In addition, the mitochondrial content of all the cells types was similar, as determined by the citrate synthase assay, taken as an index of mitochondrial mass (*Figure 27*).

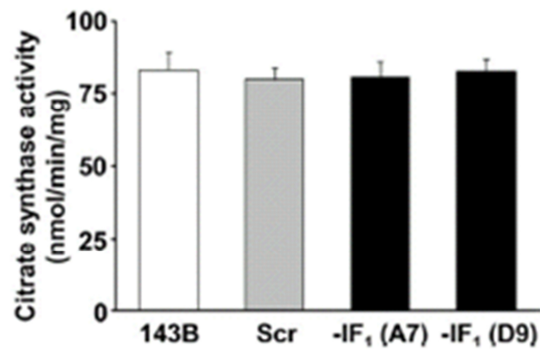


**Figure 27: Mitochondrial mass was not altered by IF<sub>1</sub>.**

Citrate synthase activity expressed as nmol/min/mg of protein. Bars show the mean  $\pm$  S.D. of five independent experiments.

Consistently, the steady state level of cellular ATP in normoxic conditions was unaltered in the absence of the protein, as it was about 25 nmol/mg of protein in all cell analyzed, independently from IF<sub>1</sub> content, as reported in Figure 28.

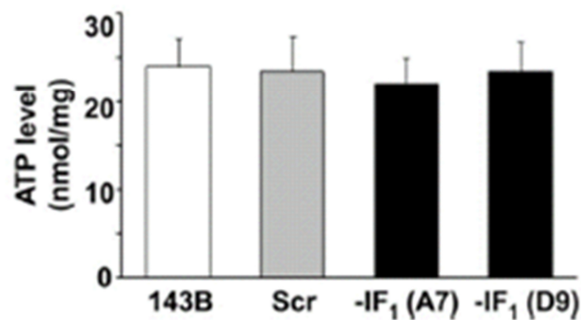


**Figure 28: Steady State levels of ATP.**

The content of ATP was measured by a chemiluminescent method and expressed as the number of moles of ATP to mg of protein. The histogram shows the mean value  $\pm$  standard deviation of three experiments independent.

Hereafter, these data suggested that IF<sub>1</sub> is not directly involved in the remodeling of these organelles, contrary to previous reports (63). On the basis of earlier studies on both isolated mitochondria and submitochondrial

particles (134) and (135), the above results were expected, since cells were grown under conditions that did not favor the binding and inhibition of IF<sub>1</sub> to the F<sub>1</sub>F<sub>0</sub>-ATPase complex. However, Fujikawa *et al.* (131) reported a nearly 40%  $\Delta\psi_m$  increase in IF<sub>1</sub> null cells and proposed that it was the result of an increased ATP hydrolytic activity of the F<sub>1</sub>F<sub>0</sub>-ATPase complex even in presence of saturating oxygen concentration.

Thus, to clarify the conflicting hypothesis on the role of IF<sub>1</sub> in cancer cell bioenergetics, the activity of both the respiratory chain and the F<sub>1</sub>F<sub>0</sub>-ATPase complex were analyzed in both parental and IF<sub>1</sub>-silenced osteosarcoma cells.

### ***3- Bioenergetic changes in IF<sub>1</sub>-silenced clones***

IF<sub>1</sub> overexpression has been observed in many human carcinomas, but the few hypothesis put forward on the associated effects are highly controversial. Data in the literature report that IF<sub>1</sub> not only inhibits ATPase activity, protecting from ATP depletion in response to respiration impairments, but it also defines the conformation of the ATP synthase and, consequentially, of mitochondrial cristae structure. In addition, it has been proposed that IF<sub>1</sub> can regulate the oxidative phosphorylation under normal physiological conditions (136).

Since the biochemical characterization of the IF<sub>1</sub>-depleted osteosarcoma cells revealed that in normoxic conditions the inhibitor was not involved in mitochondrial conformation (in terms of mass and network profile), nor in promoting cell proliferation, we decided to further investigate the role of the protein by measuring the oxygen consumption rate by the respiratory chain and the ATPase activity of the enzyme.

#### ***3.1- Oxygen consumption rate***

The role of the inhibitor was further investigated by measuring the oxygen consumption rate of the cells through polarographic techniques. To that aim, cells were permeabilized with digitonin (60 µg/ml) and energized with the

substrates of Complex I, glutamate/malate, in the presence of malonate for inhibiting the enzyme succinate dehydrogenase (state 2 respiration). Subsequently, ADP was added to induce the state 3 respiration, and then the oligomycin, inhibitor of ATP synthase, to determine the onset of the state 4 respiration. *Figure 29* shows a representative graph of the oxygen consumption rate, in three functional states described above, in the parent cell line (black trace), the scrambled clone (blue trace) and the two silenced clones (red and magenta traces).

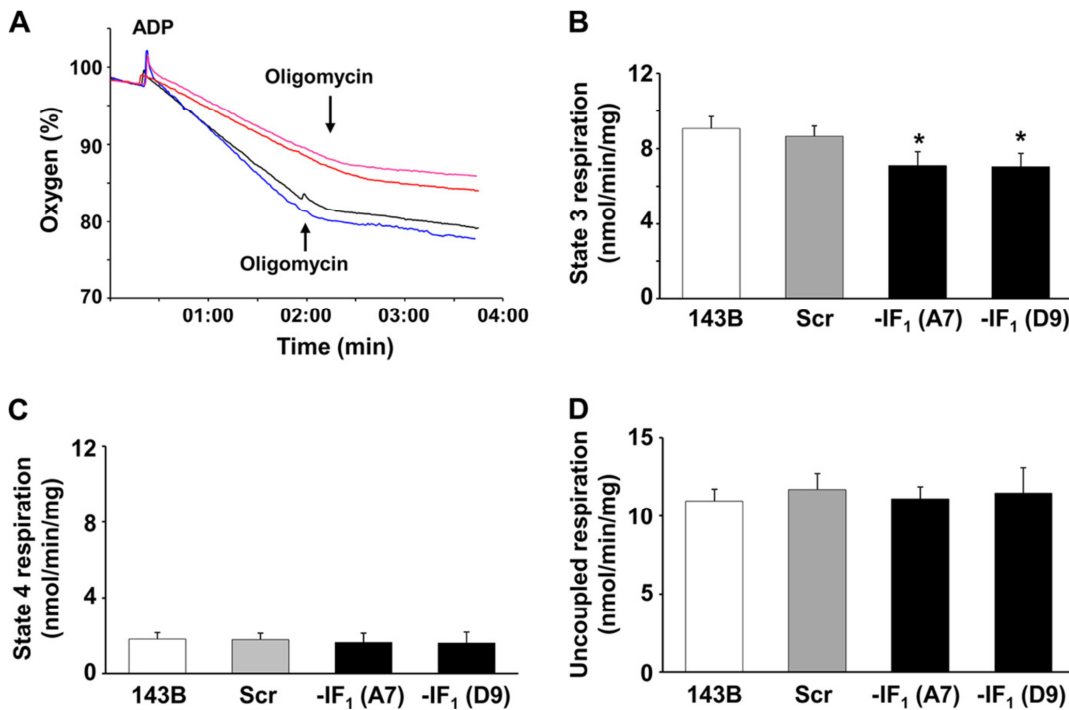


**Figure 29: Mitochondrial respiration changes in *IF<sub>1</sub>*-depleted cells.**

**(A)** Typical Complex I-driven oxygen consumption traces obtained in digitonin-permeabilized cells after energizing mitochondria with glutamate/malate, followed by addition of ADP and oligomycin. Parental (black line), scrambled (blue line), and *IF<sub>1</sub>*-depleted cells (red and magenta lines) were represented. State 3 **(B)**, state 4 **(C)**, and uncoupled **(D)** respiration rate, expressed as nanomole of  $O_2$ /min/mg of protein, were represented. Histograms show the mean  $\pm$  S.D. of three independent experiments. \*,  $p < 0.05$  indicates the statistical significance of data compared with both parental and scrambled cells.

As quantified in the graph (*Figure 29, B*), the removal of IF<sub>1</sub> from the cells caused a modest (nearly 20%) but reproducible decrease State 3 respiration rate. However, no difference was registered in presence of Oligomycin (State 4), indicating that the absence of the inhibitor did not affect the respiratory chain activity (*Figure 29, C*).

Lastly, to check whether the functional alterations detected in the state 3 respiration in the silenced clones had to be ascribed to a defect in the respiratory chain, or complex V of OXPHOS, the oxygen consumption rate was also measured in the presence of the uncoupler DNP, monitoring the maximum capability of oxygen consumption by the respiratory chain after removing the control that ATP synthase exerts on the electrons transfer (*Figure 29, D*). However, in these conditions, no difference was registered among the clones.

### **3.2- OXPHOS**

Digitonin-permeabilized cells energized with substrates for Complex I revealed a decrease in State 3 respiration in absence of IF<sub>1</sub>. To verify if such difference was an effect of a different mechanism of action of the F<sub>1</sub>F<sub>0</sub> ATP synthase in absence of the inhibitor, we first had to exclude any difference in the onset of the OXPHOS complexes. However, the immunodetection of OXPHOS complexes was unaltered in absence of IF<sub>1</sub>, as shown in *Figure 30*.

Considering that the inhibitor has been extensively defined as an unidirectional valve, active to inhibit the hydrolysis, without affecting the ATP synthesis rate, these results were quite unexpected. Indeed, these data indicate that even in normoxic conditions – thus not predicted to favor the binding of IF<sub>1</sub> to the ATP synthase - the presence of the inhibitor protein in osteosarcoma 143B cells can enhance the rate of ATP synthesis via OXPHOS, albeit not affecting the respiratory chain activity, yet increasing OXPHOS capacity to enhance ATP availability, when needed.

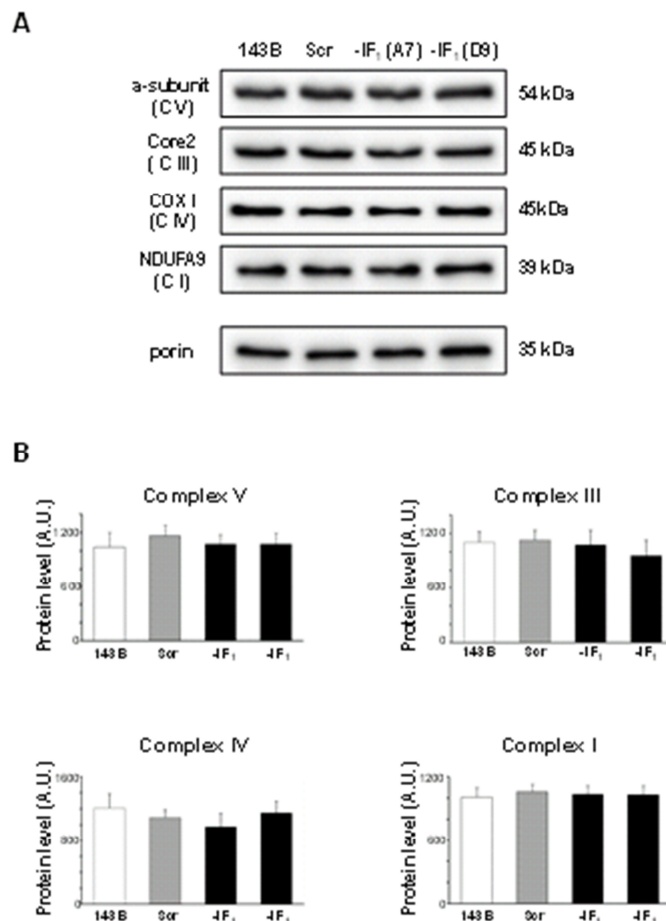


**Figure 30: Immunodetection of OXPHOS complexes after SDS-PAGE separation synthase in parental, scrambled and IF<sub>1</sub>-depleted cells.**

**(A)** Typical electrophoretic separation and immunodetection of both OXPHOS complex subunits and porin in cell lysates obtained from controls and IF<sub>1</sub>-silenced cells.

**(B)** Scanned images were quantitated by the Image Lab Software and data were normalized with respect to the porin content, taken as an internal standard. Relative protein levels of OXPHOS subunits were expressed as arbitrary units. The histograms show the mean value  $\pm$  SD of two independent experiments.

### 3.3- Mitochondrial membrane potential

Given the different bioenergetic behavior of IF<sub>1</sub> silenced cells compared to controls, we measured the  $\Delta\Psi_m$  of all cell types by examining the fluorescence of TMRM loaded cells. Consistent with the latter data, fluorescence microscopies after incubating 20 nM TMRM evidently proved that when IF<sub>1</sub> was not expressed, cells displayed a higher  $\Delta\Psi_m$  across the

inner membrane, resulting in a greatest intensity of the TMRM fluorescence (**Figure 31, A**).

These results were then confirmed and quantified by flow cytometry analysis and representative cells fluorescence distribution is reported in **Figure 31, B**: the fluorescence mean values of IF<sub>1</sub> silenced cells resulted enhanced of nearly 30% compared to controls, but such difference was nullified upon the addition of oligomycin (**Figure 31, C**), indicating that the endogenous steady-state  $\Delta\psi_m$  of the IF<sub>1</sub> silenced cells was significantly increased compared to controls, but still far below to its maximum (*i.e.* upon oligomycin exposure of the cells). To note, no difference was found in the mitochondrial content of these cells, as indicated above (**Figure 27**).

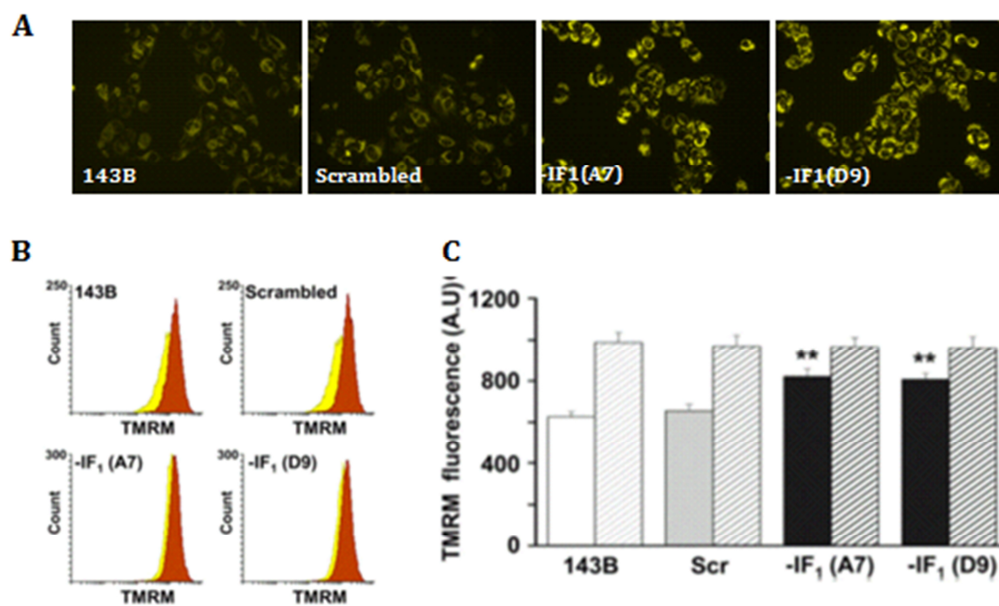


**Figure 31: IF<sub>1</sub> silencing enhances the mitochondrial membrane potential in human osteosarcoma cells.**

**(A)** Parental, scrambled, and IF<sub>1</sub>-depleted cells were loaded with 20 nM TMRM and fluorescence images were obtained using an inverted fluorescence microscope (magnification X40). **(B)** Flow cytometry analysis of cellular populations stained with TMRM, in the absence (yellow) or presence (brown) of oligomycin. **(C)** Histogram graph showing the flow cytometry semiquantitative evaluation of the mitochondrial membrane potential of controls and IF<sub>1</sub>-depleted cells in the absence (filled bars) or presence (dashed bars) of oligomycin. Bars show the mean  $\pm$  S.D. of six independent experiments; \*\*,  $p < 0.01$  indicates the statistical significance of data compared with controls.

To establish whether this difference in the bioenergetics of osteosarcoma cells among controls and  $-IF_1$  silenced cells was caused by a different mechanism of action of the enzyme, in presence and absence of the inhibitor, we analyzed the hydrolytic activity of the  $F_1F_0$  ATP synthase in presence of saturating oxygen conditions.

### 3.4- ATPase activity

To verify whether the ATP hydrolysis rate of the ATP synthase complex showed similar behavior to those earlier reported, we tested the ATPase activity of our set of cells in isolated uncoupled mitochondria (Figure 32). As expected on the bases of previous results (135) and (137), the oligomycin sensitive ATPase activity (OS-ATPase) of mitochondria was pH-sensitive, being at pH 6.7 about half than at pH 7.4.

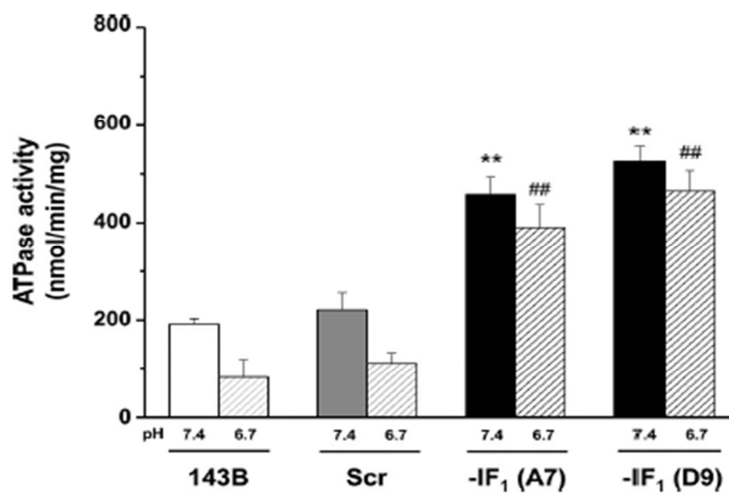


**Figure 32: Oligomycin-sensitive ATP hydrolysis activity measured in mitochondria isolated from controls and  $IF_1$ -silenced clones.**

Mitochondria were isolated using different buffers at either pH 7.4 (filled bars) or 6.7 (hashed bars) during the extraction procedure. Histograms showing the mean  $\pm$  S.D. of three independent experiments. \*\*,  $p < 0.01$  and ##,  $p < 0.01$  indicate the statistical significance of data compared with both parental and scrambled mitochondria, isolated at pH 7.4 and 6.7, respectively.

To note, the OS-ATPase activity of mitochondria from IF<sub>1</sub> silenced cells resulted 2-3 fold and 4-5 fold higher than in controls at pH 7.4 and 6.7, respectively, in agreement with data reported by Cabezon et al. (138).

## ***4- ROS and IF<sub>1</sub>***

Mitochondria are the major source of reactive oxygen species (ROS) and a target of oxidative damage during oxidative stress: initial investigations revealed that ROS can damage proteins, lipids, and DNA, thus considered tumorigenic factors inducing genomic instability. However, a recent paradigm shift has shown that mROS contributes to retrograde redox signaling from the organelle to the cytosol and nucleus, acting as signaling molecules to activate pro-growth responses and regulate cell cycle progression (64). Either way, intracellular ROS content must be regulated to avoid oxidative stress, and a number of defense mechanisms have evolved to provide a balance between production and removal of ROS in the cell.

The role of IF<sub>1</sub> in ROS production, content and effect is not clear, and requires further investigation.

### ***4.1 - Evaluation of intracellular ROS***

Although the role of mitochondria has been widely investigated, to clarify the role exerted by IF<sub>1</sub> to bioenergetics and oxidative stress in the osteosarcoma cells, we measured the intracellular ROS content, through two different cell-permeant dyes: CellROX® DeepRed and CellROX® Orange, analyzed by a FACSaria flow cytometer and Muse Cell Analyzer, respectively (*Figure 33*).

As expected on the basis of data showed above, (*i.e.* lower state 3 respiration and a higher mitochondrial membrane potential in IF<sub>1</sub>-null osteosarcoma cells), both measures confirmed that ROS content was reduced in presence of the inhibitor, suggesting that IF<sub>1</sub> may exert a protective role against ROS production and accumulation in osteosarcoma cells, reducing potential cellular damage.

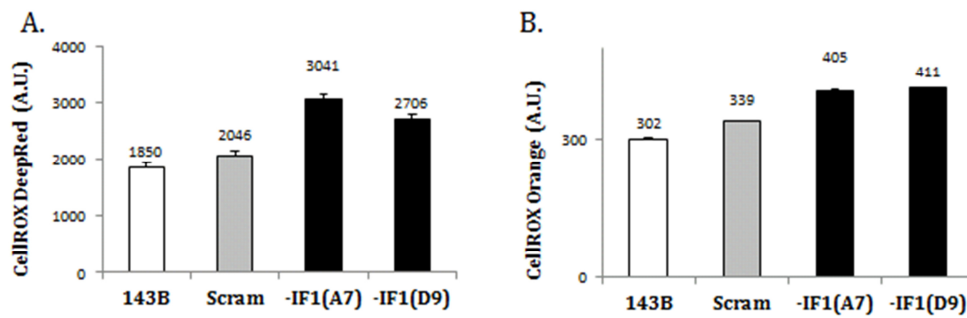


**Figure 33: Intracellular ROS content.**

Cells were harvested, washed once in PBS solution and loaded with 5  $\mu$ M CellROX® Deep Red (A) or Orange (B) probes (Thermo Fisher Scientific) in complete medium without FBS for 30 minutes in the dark. Intracellular ROS content was then detected through FACSaria flow cytometer or with Muse™ Cell Analyzer, respectively. Parental (white bars), scrambled (grey bars), and IF<sub>1</sub>-depleted cells (black bars) were represented. Histograms show the mean  $\pm$  S.D. of three independent experiments. \*,  $p < 0.05$  indicates the statistical significance of data compared with both parental and scrambled cells.

## 5- Dimerization of F<sub>1</sub>F<sub>0</sub> ATP synthase and IF<sub>1</sub>

Based on the conformation of the active form of the inhibitor, that simultaneously binds two distinct F<sub>1</sub> portions of ATP synthase, many studies in the recent literature proposed that IF<sub>1</sub> promotes the dimerization of the F<sub>1</sub>F<sub>0</sub>-ATPase (60), inducing the formation of mitochondrial *cristae* (59). This aspect has a particular relevance, since it has been proposed that IF<sub>1</sub> defines mitochondrial volume fraction, regulates autophagy (63) and protect cancer cells from apoptosis (27), attributing a crucial role to the inhibitor for cancer progression.

### 5.1 Distribution of monomers and oligomers of F<sub>1</sub>F<sub>0</sub>-ATPase

To assess whether IF<sub>1</sub> influence the oligomerization of ATP synthase – consequently contributing to define mitochondrial volume and ultrastructure – a comparative analysis was conducted, in both IF<sub>1</sub>-silenced and control cells, following a BN-PAGE electrophoretic separation of the digitonin-

extracted proteins in the four lines of interest: Parental, scrambled and the two silenced clones A7 and D9. At first, the in-gel ATPase activity of the monomeric and oligomeric forms of the enzyme was analyzed and the assay clearly showed that both monomers and dimers were ATP hydrolysis competent (*Figure 34*).

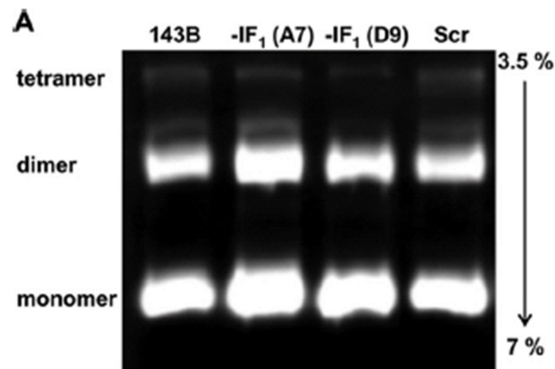


**Figure 34: Representative in-gel activity staining of the monomeric and oligomeric ATP synthase.**

Proteins were extracted from digitonin-treated mitochondria from parental, scrambled, and IF<sub>1</sub>-depleted cells after BN-PAGE separation.

Then, digitonin-extracted ATP synthase protein were transferred on a nitrocellulose membrane and immunolabeled with primary monoclonal antibody anti- $\alpha$  subunit of the ATP synthase to evaluate the distribution between monomers and dimers (*Figure 35*). As shown in the immunoblotting, and quantified by densitometric analysis of the bands, no difference was observed in the distribution of the monomeric and dimeric forms between the silenced cells and controls. Indeed, the monomeric form (black bar) ranges from 53 to 58% and the dimeric form (gray bar) from 42 to 47%, suggesting that IF<sub>1</sub> is not essential for ATP synthase dimerization, confirming data reported by Lippe G. and co-workers (62).

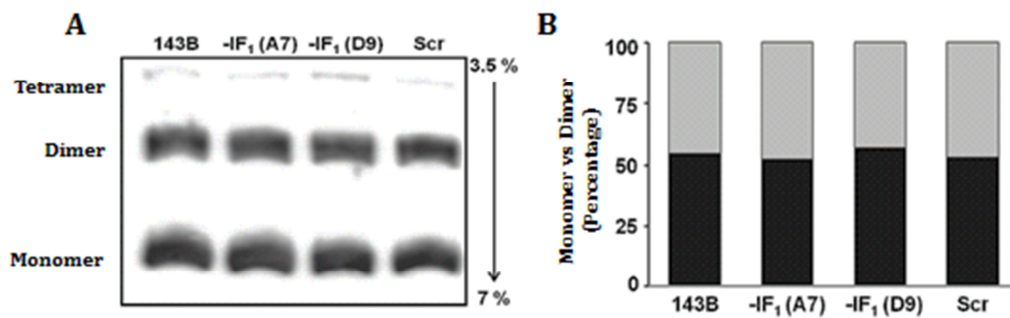


**Figure 35: Distribution of monomeric and dimeric form of the  $F_1F_0$  ATP synthase in presence or absence of  $IF_1$ .**

**(A)** Monomeric and oligomeric distribution analysis of the ATP synthase performed by immunodetection of the  $F_1$   $\alpha$ -subunit after separation of the proteins by BN-PAGE, followed by blotting of the native complexes onto nitrocellulose membrane.

**(B)** Histograms represent the densitometric analysis of the monomer (dark bar) and dimer (gray bar) of the ATP synthase complex. The representative data were confirmed in three independent experiments.

## 5.2 $IF_1$ binds to the dimeric form of ATP synthase

As well established by Walker,  $IF_1$  can exist as an active dimer or inactive oligomer, depending on the aqueous phase pH: at pH lower than 6.5 the equilibrium is forced towards the active form of the inhibitor and the  $F_1$ -ATP hydrolytic activity fully inhibited; conversely, when pH is around 8, or higher,  $IF_1$  is predominantly oligomeric and inactive (138).

Noteworthy, the immunodetection of the inhibitor protein in the four lines revealed that, even under normoxic conditions, the inhibitor protein was associated to the ATP synthase: to note, this is quite intriguing, since  $IF_1$  should not affect  $F_1F_0$ -ATPase in these conditions. Moreover, more than 90% of the inhibitor was found to be localized in correspondence of the dimers of ATP synthase (Figure 36) in both controls (*i.e.* parent and scrambled cells), indicating that the main target of  $IF_1$  is the dimeric form of the ATP synthase (obviously, no  $IF_1$  bands were detected in correspondence of the silenced cloned).

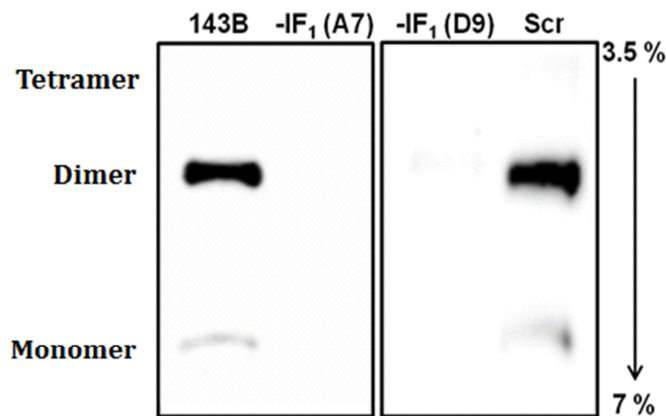


**Figure 36: IF<sub>1</sub> binds exclusively to the dimeric form of ATP synthase.**  
 Immunodetection of IF<sub>1</sub> was performed after separation of dimeric and monomeric ATP synthase by BN-PAGE (3.5–7% gradient) followed by blotting onto nitrocellulose membrane. As shown, IF<sub>1</sub> almost entirely binds to the dimeric form of ATP synthase. As expected, no bands were detected in correspondence of the IF<sub>1</sub>-silenced clones.

Overall, these data suggest that the inhibitor does not influence ATP synthase dimerization, that occurs independently from IF<sub>1</sub>; however, we can speculate that the inhibitor protein may have a role in stabilize the dimeric form of ATP synthase, thus increasing the activity of the enzyme, resulting in a higher mitochondrial membrane potential and lower respiration rate in the IF<sub>1</sub>-null cells with respect to controls, as showed above.

## *Results – 2<sup>nd</sup> part: miRNAs*

---

### **6- miRNAs profiling pattern of expression in cancer**

MicroRNAs deregulation in cancer was first demonstrated in 2002 (7), opening a new branch of investigation over cancer related issues. Since then, increasing studies have showed that microRNAs play important roles in tumor growth, by regulating oncogenes and tumor suppressor genes (139), and that cancer metabolism is greatly modulated by epigenetic alterations through miRNAs (140), stimulating researchers to address the connection between specific miRNAs and cancer metabolism. Thus far, accumulating studies indicate that many miRNAs affect the expression of key genes involved in glycolysis and energy metabolism, underlying the importance of improve our knowledge over these small molecules, to further elucidate the modulation of metabolic pathways in cancer cells and, far beyond, to assess potential new therapeutic targets - or agents - in cancers.

In order to assess microRNAs contribution to modulate cancer metabolism, an analysis of the miRNAs expression pattern was performed (data not shown). Among the lines screened, a sensitive- and a resistant-to BRAF-I treatment melanoma cell lines (*i.e.* M21 and M21-R melanoma cells) were included. Of note, we found that resistant cells displayed an up-regulation of four miRNAs when compared to the sensitive ones. Much more intriguingly, three out of four of these miRNAs were predicted to target SUFU, the negative regulator of development-related Shh pathway, which has been proved to be altered in various forms of cancer (94). Therefore, these compelling data pushed us to further investigate over the connection between miRNAs expression and refractory to treatment, pointing towards the need for novel and more innovative therapeutic approaches to by-pass anticancer drug resistance in yet poor prognosis malignancies.

## 6.1 Validation of miRNAs overexpression in resistant cells

Among the four miRNAs, miR-136 displayed the highest expression, resulting in a remarkable over-expression in M21 resistant cells (*i.e.* M21-R) with respect to the sensitive ones, encouraging us to primarily focus on the role exerted by this microRNA. However, to better elucidate this aspect, two other melanoma cell lines (both sensitive and resistant types) were included in the study, to validate the microarray data through a q-RT-PCR (*Figure 37*).

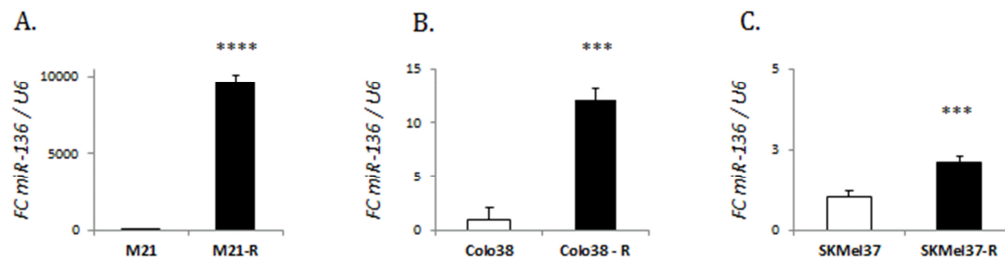


**Figure 37: miR-136 is over-expressed in melanoma BRAF-I resistant cells with respect to sensitive cells.** Upon cells harvesting, RNA was extracted and retro-transcribed, then expression analysis of miR-136 and the small nuclear U6 was performed, with TaqMan primers and probes (Life Technologies). Bars represent FC miR136 upon U6 expression, used as miRNA internal control, in BRAF-I resistant (black bars) and sensitive (white bars) cells of three different melanoma cell lines: M21 (A), Colo38 (B) and SK-Mel-37 (C). Histograms show the mean  $\pm$  S.D. of three independent experiments. \*\*\*,  $p < 0.005$  and \*\*\*\*,  $p < 0.0005$  indicate the statistical significance of resistant cells data compared to BRAF-I sensitive cells.

Quantitative Real-Time PCR confirmed the microarray data in all the cell lines tested, revealing that miR-136 is greatly expressed in BRAF-I resistant melanoma cells when compared to sensitive to treatment cells of the same type. The inhibitor of the Shh pathway, SUFU, was found to be a common target of three out of the four overexpressed microRNAs, leading to the analysis of the inhibitor in these cells.

## 6.2 *SUFU is down-regulated in resistant cells*

On the bases of the algorithm used by some miRNA databases, miR136 was predicted to target SUFU, the negative regulator of Shh pathway. Therefore, once assessed miR-136 overexpression in the resistant cells, we then screened four lines for the expression of SUFU. To that aim, an SDS-PAGE was performed, and electrophoretically separated proteins were electroblotted onto a nitrocellulose membrane, to be labeled with a rabbit monoclonal primary antibody against SUFU (*Figure 38*).

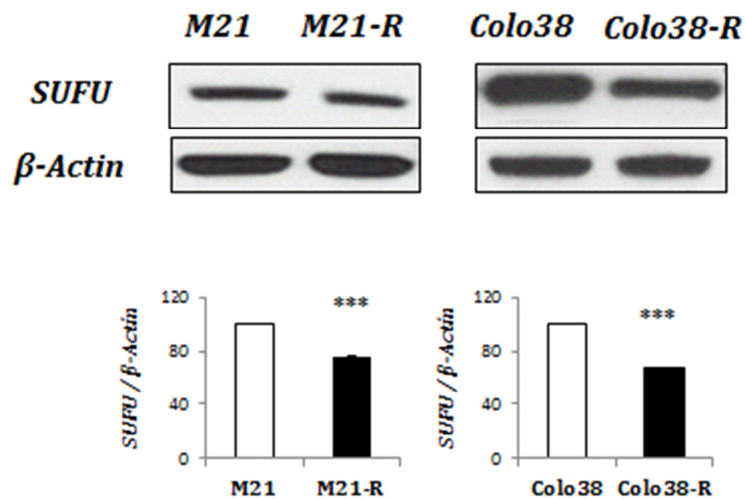


**Figure 38: Assessment of SUFU expression in melanoma cells.**

Lysed cells were separated by SDS-PAGE and electroblotted onto a nitrocellulose membrane. SUFU levels were assessed after incubating the membranes in the presence of rabbit primary monoclonal antibody, over  $\beta$ -Actin (Cell Signaling). The histogram below represent the quantification of the bands: results of three independent experiments are expressed as the mean value  $\pm$ SD of sensitive (white bars) and resistant (black bars) melanoma cells: M21 (A) and Colo38 (B). \*\*\* $p < 0.005$

As shown in the immunoblot, both M21-R and Colo38-R were characterized by a lower expression of SUFU, yet significant and reproducible (quantified in 25% and 33% reduction, respectively) in both cell lines tested, as represented in the densitometric analysis below. To further confirm whether

this reduction was able to induce the activation of the Shh pathway, the activity of this pathway in sensitive and resistant melanoma cells was also determined.

### 6.3 SHH pathway activation

Shh pathway has been proved to be deregulated in various types of cancer; moreover, a recent paper reported that melanoma resistance to BRAF-I is mediated by Shh alteration through PDGFR $\alpha$  up-regulation (106). Since we showed that the negative regulator of the pathway downregulated in the BRAF-I resistant melanoma cells, we proceeded by measuring the activity of Shh pathway through a Dual Luciferase Gene reporter assay. To that aim, eight repeated copies of wild-type or mutated Gli-binding sites (3'GliBS or mut3'Gli-BS, respectively) were cloned into a psi-check2 vector (Promega), thus controlling the activity of a Firefly Luciferase (*Photinus pyralis*). Together with this reporter gene, cells were also co-transfected with a pRLTK vector, a wild type Renilla luciferase (*Renilla reniformis*, also known as sea pansy) control reporter vector, to normalize the expression of the experimental firefly luciferase reporter gene.

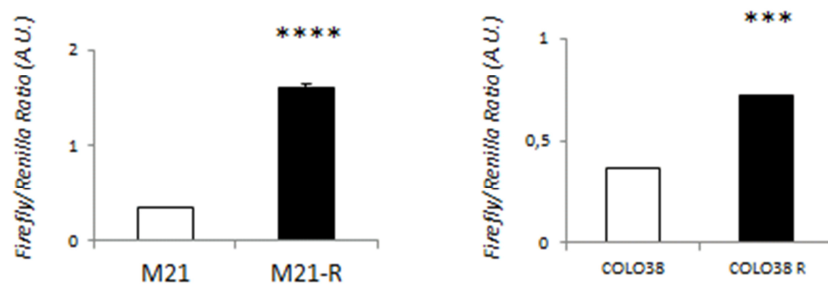


**Figure 39: Shh pathway activity.**

Adherent melanoma cells were co-transfected with a Firefly luciferase reporter gene together with a pRLTK Reporter Vector, used as an internal control. After rinse in PBS, cells were lysed for 15 minutes RT and ratios between Firefly and Renilla luciferase activity were estimated using a GloMax® 96 Microplate Luminometer (Promega). Histograms show the mean  $\pm$  S.D. of three independent experiments. \*\*\*,  $p < 0.01$  and

*p*<0,0001 indicates the statistical significance of Firefly/Renilla activity in the BRAF-I resistant cells compared to BRAF-I sensitive cells.

As shown in Figure 39, Shh pathway activity was greatly enhanced in both resistant cell lines, with respect to BRAF-I sensitive cells, indicating that the reduction of SUFU expression (25% and 33% in M21-R and Colo38-R respectively, as presented above) was sufficient to induce Shh activation, eventually resulting in a higher proneness of melanoma cells to proliferate, thus counteracting the treatment with BRAF-I.

## ***7- Variation of miR-136 expression***

On these premises, to investigate the mechanisms underlying miR-136 contribution in triggering acquired BRAF-I resistance in melanoma cells, we then proceeded verifying the cellular response to a miR-136 modulation. Sensitive melanoma cells were transfected with miR-136 mimic molecules, small, chemically modified double-stranded RNA that mimic endogenous miRNAs, thus enabling miRNA functional analysis by the up-regulation of miRNA activity. Conversely, miR-136 was downregulated in the BRAF-I resistant cells, by means of miR-136 inhibitors ( $\alpha$ -miR-136), single-stranded RNA molecules targeting (and inhibiting) the corresponding endogenous miRNAs. In both cases, a scrambled mimic RNA was used as a negative control.

After transfection, upon miR-136 levels assessment each time point considered, SUFU expression and the Shh pathway activation were evaluated. Furthermore, basing on the hypothesis that miR-136 would lead to BRAF-I resistance in melanoma cells, cell growth assays were performed under vemurafenib (*i.e.* BRAF-I PLX4032) treatment, following miR-136 up- or down-regulation, in BRAF-I sensitive and resistant cells, respectively.

## 7.1- SUFU

SUFU expression was first evaluated in M21 and M21-R cells, upon miR-136 transfection: following miR-136 levels increase in sensitive cells, SUFU was found to be reduced; conversely, enhanced content of the microRNA in the BRAF-I resistant cells (displaying a greater amount of miR-136 in wild type conditions with respect to the sensitive ones) had no substantial effect on the expression of the protein (*Figure 40*). To note, SUFU levels in the sensitive cells settled on the same levels exhibited by resistant cells in wild type conditions, again confirming that the expression of the inhibitor of Shh pathway and miR-136 were related.

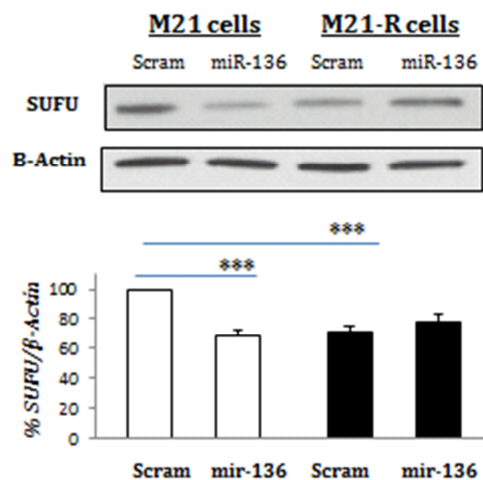


**Figure 40: SUFU is reduced in melanoma sensitive cells when miR-136 levels are increased.** BRAF-I sensitive melanoma cells were seeded and transfected either with scrambled or miR-136 mimic for 24 hours. Lysed cells were separated by SDS-PAGE and electroblotted onto a nitrocellulose membrane. SUFU levels were assessed immunolabelling protein bands with a rabbit primary monoclonal antibody (Cell Signaling). The histograms below represent the densitometric analysis of the bands, normalized over β-Actin (Cell Signaling). Results of three independent experiments are expressed as the mean value  $\pm$ SD in sensitive (white bars) and resistant (black bars) M21 melanoma cells. \*\*\* $p < 0.005$  indicates the statistical significance of miR-136 transfected cells compared to scrambled transfected ones.

Once determined this association, we explored the consequences of increasing miR-136 in the sensitive cells of both cell lines, following the expression of SUFU up to 96 hours after transfection either with scrambled or miR-136 mimics. As expected on the basis of previous results, SUFU rapidly decreased its expression upon miR-136 transfection in the sensitive cells, resulting in about 25 and 50% of reduction in the first 24 and 48 hours, in both cell lines (Figure 41).

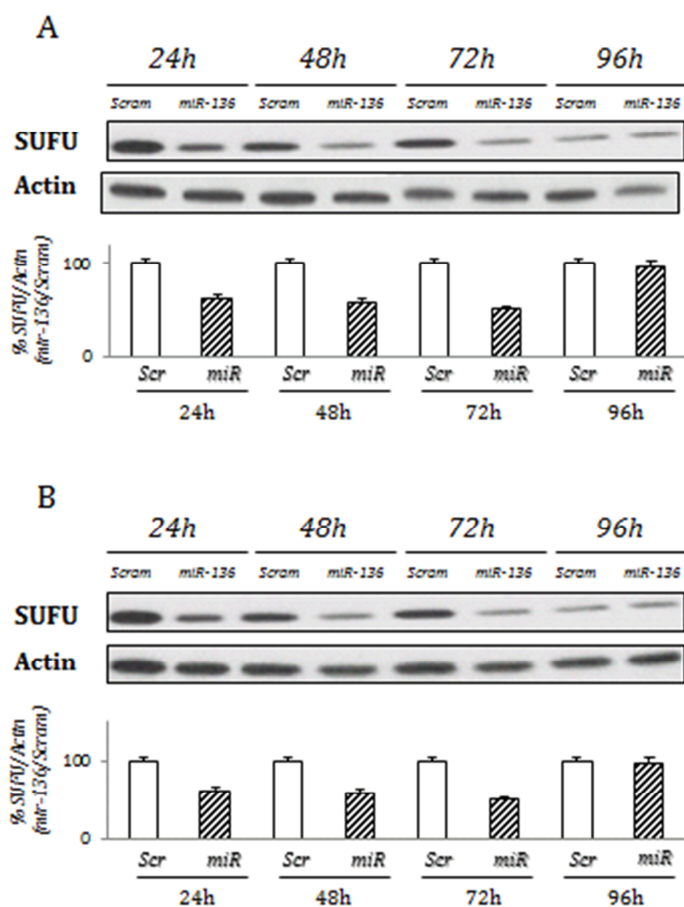


**Figure 41: SUFU trend upon miR-136 transfection.**

*BRAF-I sensitive melanoma cells were seeded and transfected either with scrambled or miR-136 mimic for up to 96 hours. Lysed cells were separated by SDS-PAGE and electroblotted onto a nitrocellulose membrane. SUFU levels were assessed immunolabelling protein bands with a rabbit primary monoclonal antibody (Cell Signaling). The histograms below represent the densitometric analysis of the bands, normalized over  $\beta$ -Actin (Cell Signaling). Results of two independent experiments are expressed as the mean value  $\pm$ SD in scrambled (white bars) and miR-136 (dashed bars) M21 (A) and Colo38 (B) melanoma cells.*

To note, following 48 hours from transfection most of the exogenous microRNA was degraded inside the cells (data not shown), likely explaining why SUFU started to increase again after 72 hours since transfection, being almost the same between scrambled and miR-136 transfected at 96h.

However, these results clearly evidenced that varying miR-136 content, SUFU was - in turn - modulated as well, thus confirming that these molecules can play a crucial role in triggering resistance mechanisms to BRAF-I in melanoma cells.

## 7.2- SHH pathway

SUFU trend assessment upon miR-136 modulation was paralleled by the Shh activity evaluation, through the Dual Luciferase assay, to verify if the variation in miR-136 content was affecting the activity of the pathway by modulating the expression of its inhibitor. To double check this association, analysis were performed in both M21 (Figure 42) and M21-R (Figure 43) cells after transfection with miR-136 and  $\alpha$ -miR-136, respectively.

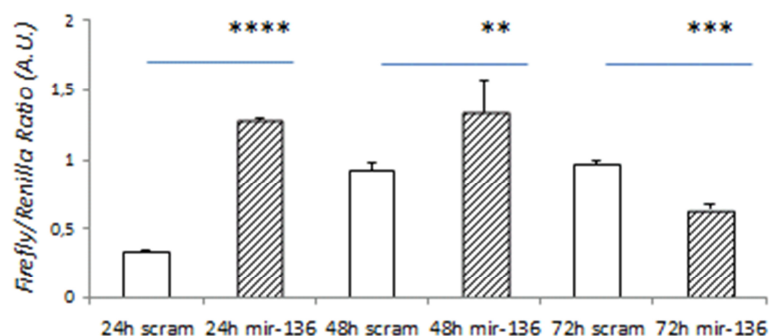


### Figure 42: Shh activation upon miR-136 transfection in sensitive cells

Adherent melanoma cells were co-transfected with a Firefly luciferase Shh pathway activity reporter gene, together with a pRLTK Reporter Vector, used as an internal control. After rinse in PBS, cells were lysed for 15 minutes RT and ratios between Firefly and Renilla luciferase activity were estimated using a GloMax® 96 Microplate Luminometer (Promega). Histograms show the mean  $\pm$  S.D. of three independent experiments. \*\*,  $p < 0.01$ , \*\*\*,  $p < 0.001$  and \*\*\*\*,  $p < 0.0001$  indicate the statistical significance of Firefly/Renilla activity in the BRAF-I resistant cells compared to BRAF-I sensitive cells.

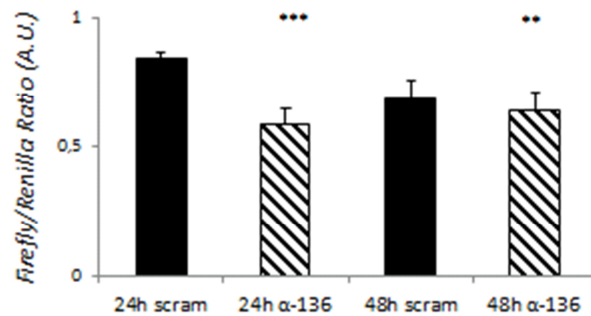


**Figure 43: Shh activity is reduced when SUFU is increased in resistant cells by inhibiting miR-136**

Adherent melanoma cells were co-transfected with a Firefly luciferase Shh pathway activity reporter gene, together with a pRLTK Reporter Vector, used as an internal control. After rinse in PBS, cells were lysed for 15 minutes RT and ratios between Firefly and Renilla luciferase activity were estimated using a GloMax® 96 Microplate Luminometer (Promega). Histograms show the mean  $\pm$  S.D. of three independent experiments. \*\*,  $p < 0.01$  and \*\*\*,  $p < 0,0001$  indicate the statistical significance of Firefly/Renilla activity in the BRAF-I resistant cells compared to BRAF-I sensitive cells.

Figure 42 shows that miR-136 transfection in M21 sensitive melanoma cells induced Shh activation, with a greatly enhanced activity in the first 24 hours post transfection with respect to scrambled controls, and the pathway was still highly active after 48 hours. Coherently, when the miR was inhibited Shh activity was reduced, as expected on the basis of the increased levels of SUFU (Figure 43).

To note, as specified above, after 72h since transfection, most of the exogenous miRNAs were degraded inside the cells, thus explaining why the Shh activity in the sensitive cells was decreased at this point.

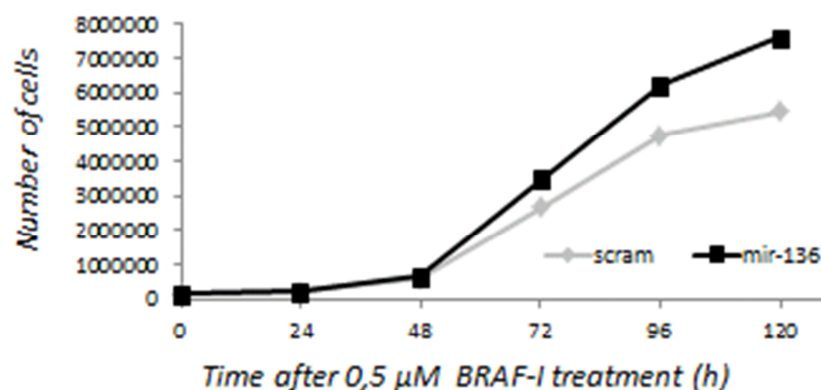
Overall, it seemed reasonable to conclude that the Shh pathway is activated by the enhanced expression of miR-136, that induce a downregulation of its inhibitor SUFU, therefore pushing BRAF-I resistant melanoma cells to overcome the effect of the drug itself and proliferate, aggressively and uncontrollably.

### 7.3- Cell growth evaluation

BRAF-I resistance has been showed to be mediated by Shh pathway activation (106), leading to a massive and aggressive proliferation of melanoma cells when developing resistance to vemurafenib. Since we showed that miR-136 was up-regulated in melanoma resistant cells, inducing a reduction in the expression of SUFU, the negative regulator of the Shh pathway, we hypothesized that an increase in miR-136 levels in sensitive melanoma cells would trigger some molecular mechanisms, eventually protecting these cells from the effect of the drug. Conversely, we assumed that the inhibition of miR-136 in BRAF-I resistant cells could restore, at least partially, sensitivity to the drug.

To verify such hypothesis, miR-136 transfected melanoma sensitive cells M21 were transfected either with scrambled or miR-136 and treated with 0,5  $\mu$ M vemurafenib, following the cell growth for up to 120 hours (A); in addition, the same experiment was performed on Colo38 cells, transfecting sensitive cells with the same amount of microRNA, but increasing the amount of drug (B). To note, since the endogenous microRNAs (both mimics and inhibitors) were rapidly degraded inside the cells, transfection procedures were repeated between 48 and 72 hours, in order to maintain high or low levels of miR-136 inside the cells.

A



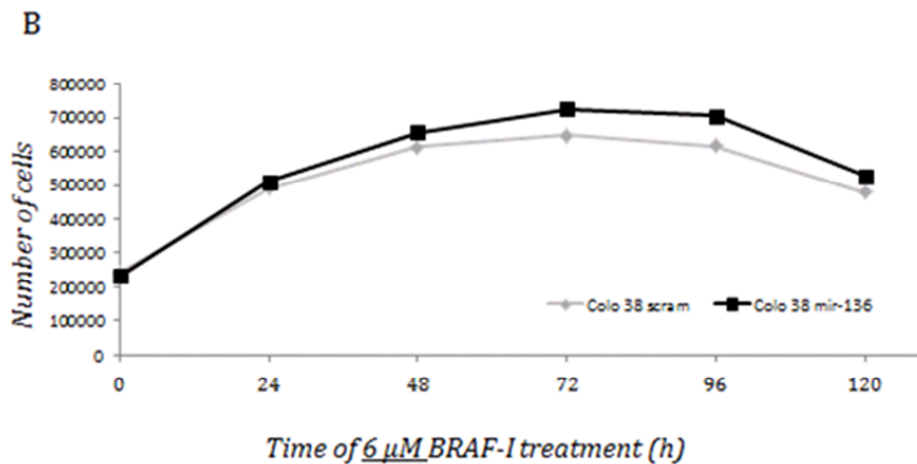


**Figure 44: Cell growth under BRAF-I treatment upon miR-136 transfection in BRAF-I sensitive melanoma cells.**

Cells were seeded in 6-wells plates and transfected with 50 nM either of scrambled (grey lines) or miR-136 mimics (black lines). After 24h from transfection, cells were treated with 0,5  $\mu$ M (M21, panel A) or 6  $\mu$ M (Colo38, panel B) of PLX4032 (Vemurafenib, BRAF-I) and grown for up to 120h. Proliferation rate was assessed every day, collecting all the cells in the plates. Results are represented as the mean of each time point  $\pm$  SD of three independent experiments.

As shown, both M21 and Colo38 melanoma cells proliferated more in presence of miR-136, with respect to the scrambled transfected cells: particularly, after 120h after treatment with 0,5  $\mu$ M miR-136 transfected M21 cells were still able to proliferate (Figure 44, A), whereas the corresponding scrambled transfected were almost arrested. The lower – yet significant - effect showed in Colo38 cells (Figure 44, B) has to be ascribed to the higher concentration of the drug, which was critical for both scrambled and miR136 transfected cells after 96h of treatment: however, even in these critical conditions, a protective role exerted by miR-136 was observed.

Coherently, we hypothesized that inhibiting miR-136, through its inhibitor, could restore the sensitivity to BRAF-I in resistant melanoma cells. Therefore, M21-R and Colo38-R were transfected with 50 nM of the anti-miR-136 and followed for up to 120 hours after transfection, using scrambled transfected

cells as control (Figure 45). Again, transfection procedures were repeated every 48 hours, in order to keep low levels of miR-136 inside the cells.

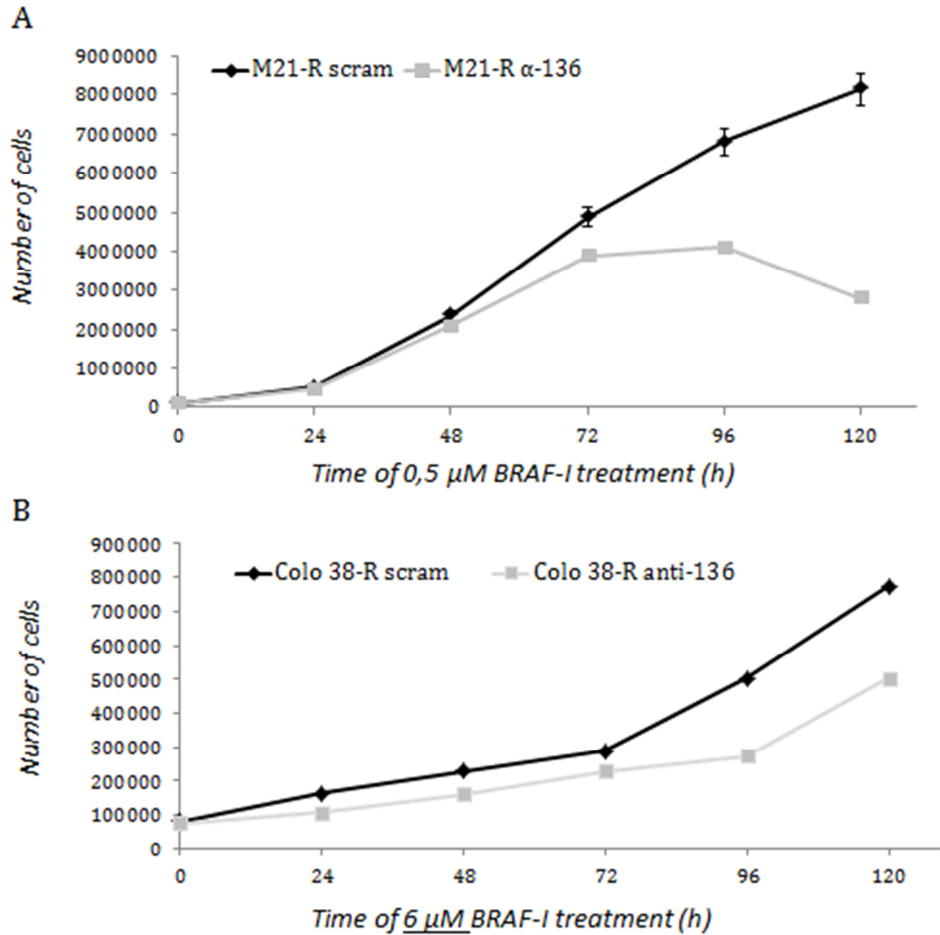


**Figure 45: Inhibit miR-136 restore sensitivity to BRAF-I in melanoma resistant cells.**

Cells were seeded in 6-wells plates and transfected with 50 nM either of scrambled (grey lines) or  $\alpha$ -miR-136 (black lines), while treated with 0,5  $\mu$ M (M21-R, panel A) or 6  $\mu$ M (Colo38-R, panel B) of PLX4032 (Vemurafenib, BRAF-I). Grown for up to 120h, proliferation rate was assessed every day, collecting all the cells in the plates. Results are represented as the mean of each time point  $\pm$  SD of three independent experiments.

As shown in the graphs above, cell proliferation rate was diminished in melanoma resistant to BRAF-I cells when miR-136 was inhibited, suggesting that miR-136 is a crucial element to trigger and maintain resistance to therapy in these cells.

## **8- The effect of BRAF-I treatment on melanoma cells expression**

Once assessed the interconnection between miR-136 and SUFU, we wanted to explore whether vemurafenib treatment could affect one of these parameters in melanoma cells. To that extent, melanoma BRAF-I sensitive cells were treated with PLX4032, whereas resistant-to-treatment cells were temporarily deprived of the drug, in order to evaluate cell growth, SUFU expression and, more importantly, miR-136 levels.

### **8.1- BRAF-I decreases proliferation rate in melanoma cells**

Melanoma M21 cells were treated with different concentration of BRAF-I and cell growth was assessed after 24 (Figure 46, A) and 96 (Figure 46, B) hours after treatment.

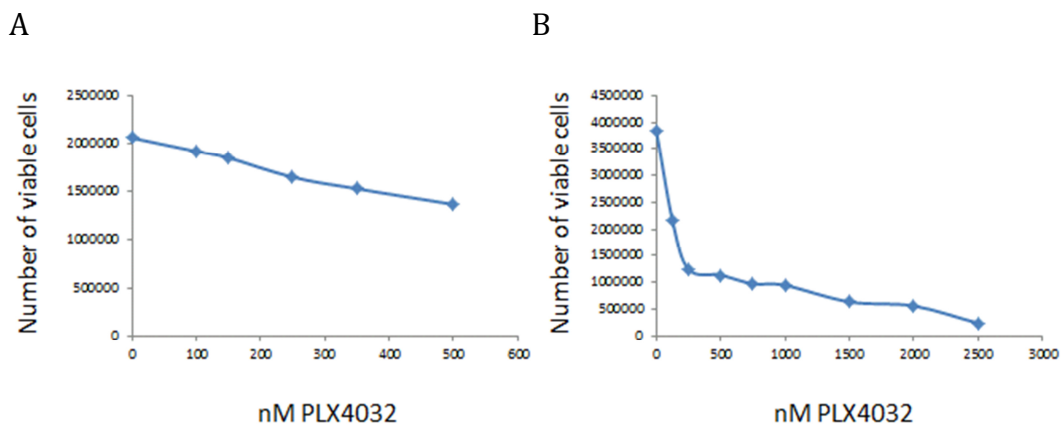


**Figure 46: Cell growth evaluation upon increasing dose of vemurafenib in melanoma BRAF-I sensitive M21 cells.**

Melanoma M21 cells were treated with increasing amount of vemurafenib and cell growth was assessed after 24h (A) and 96h (B) of treatment. Results were represented as the mean  $\pm$  SD of three independent experiments.

As expected, on the basis of vemurafenib treatment in melanoma patients, cell proliferation rate was extremely sensitive to the drug, resulting in a dose-

dependent reduction in cell growth. Specifically, a great decline was observed after prolonged time of treatment in M21 melanoma cells.

Conversely, a comparison between sensitive and BRAF-I resistant cells at two different amount of the drug, showed that BRAF-I resistant M21-R cells were obviously not affected by increasing amount of the drug, contrarily to the sensitive ones, thus confirming the time- and dose-dependent effect in the proliferation rate of melanoma BRAF-I sensitive cells in presence of the drug (Figure 47).

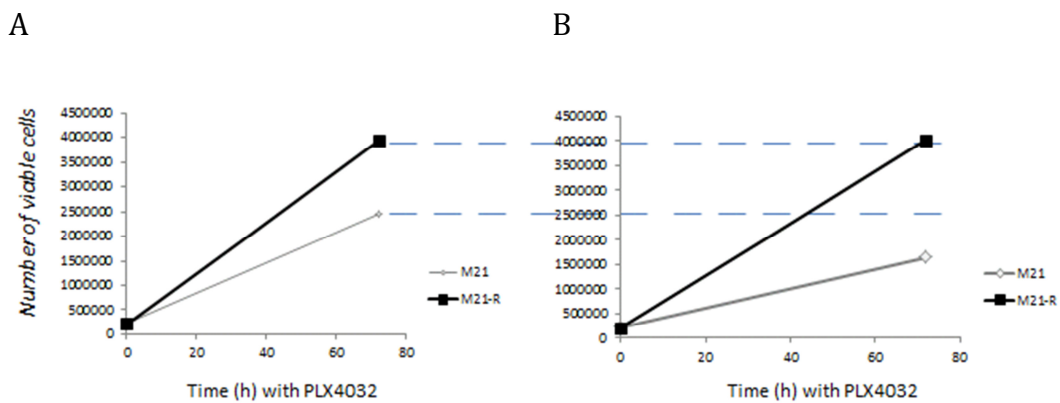


**Figure 47: Comparison between BRAF-I sensitive (M21, A) and resistant (M21-R, B) melanoma cells under two different amount of vemurafenib treatment.**

Melanoma M21 and M21-R cells were treated with 0,5 μM (A) and 1 μM (B) of PLX4032 (vemurafenib, BRAF-I) and cell growth was assessed after 72h of treatment in both cell lines. Results were represented as the mean ± SD of three independent experiments.

In these conditions, the expression of SUFU and the activity of Shh pathway were determined in BRAF-I sensitive melanoma cell lines, comparing them with miR-136 levels upon vemurafenib treatment.

## 8.2- BRAF-I effect in sensitive melanoma cells

BRAF-I sensitive melanoma cells were exposed to vemurafenib for prolonged time and the above-discussed parameters were determined. Specifically, M21 and Colo38 cells were treated with 0,5  $\mu$ M BRAF-I for 72 hours and the expression of SUFU was assessed every 24h: then, the drug was removed and cells were followed up for additional 72 hours.

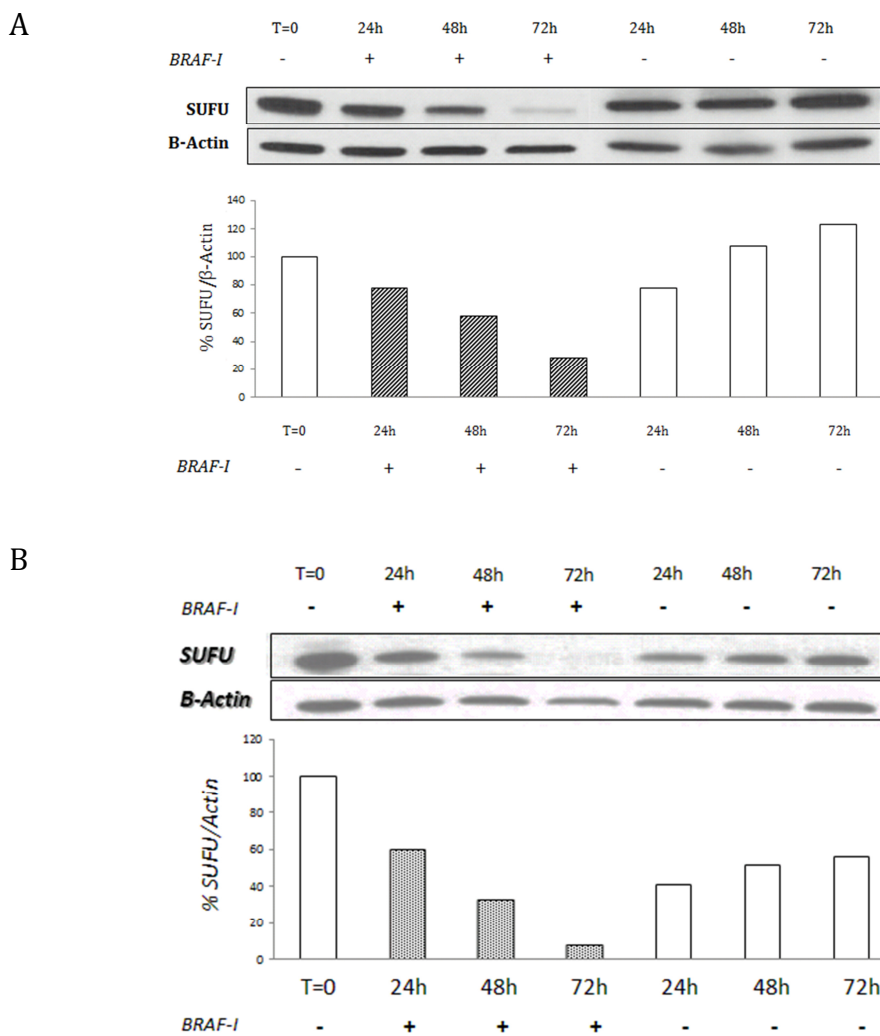


**Figure 48: SUFU expression upon vemurafenib treatment in BRAF-I sensitive melanoma cells**

BRAF-I sensitive melanoma cells (M21, A and Colo38, B) were cultured in presence of 0,5  $\mu$ M vemurafenib for 72 hours and then cells were grown for additional 72h after removal. Lysed cells were then separated by SDS-PAGE

and proteins were electroblotted onto a nitrocellulose membrane to be labeled with a rabbit monoclonal primary antibody against *SUFU* (Cell Signaling). *SUFU* expression was assessed every 24h and normalized over  $\beta$ -Actin expression (Cell Signaling). Densitometric analysis were performed and showed as the mean value  $\pm$ SD in M21 (A) and Colo38 (B) melanoma cells in presence (dashed bars) and absence (white bars) of the drug.

Surprisingly, vemurafenib treatment results in a gradual and time-dependent decrease of *SUFU* in both *BRAF-I* sensitive melanoma cell lines, M21 (Figure 48, A) and Colo38 (Figure 48, B).

Since we previously demonstrated that *SUFU* and miR-136 were related, we extracted RNA from these cells, in order to assess miR-136 levels by means of q-RT-PCR (Figure 49).

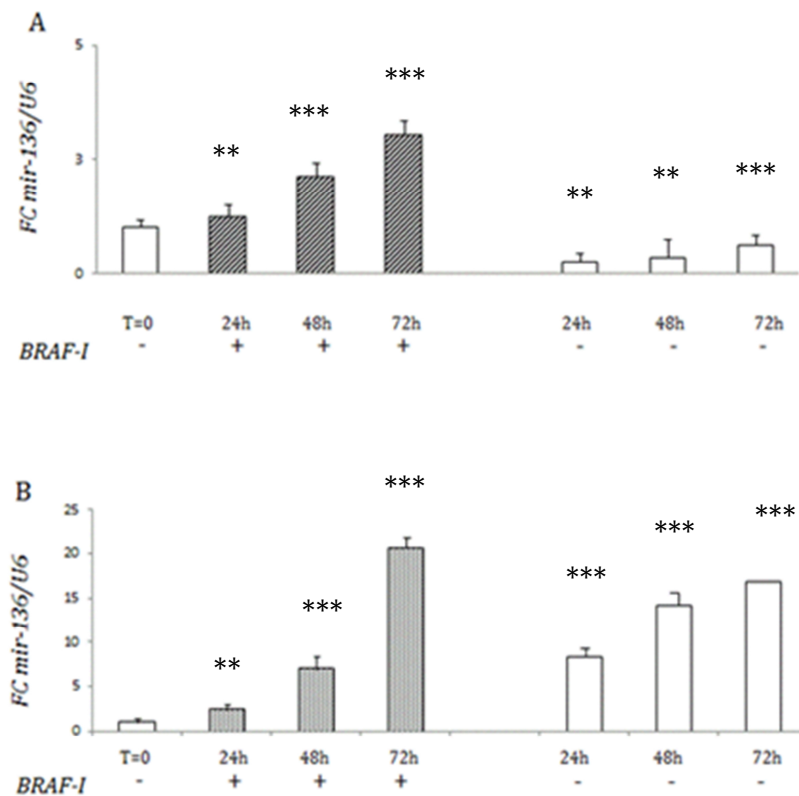


**Figure 49: miR-136 levels in *BRAF-I* sensitive melanoma cells treated with vemurafenib.**

*BRAF-I* sensitive melanoma cells (M21, A and Colo38, B) were cultured in presence of 0,5  $\mu$ M vemurafenib for 72 hours and then cells were grown for additional 72h after

removal. Upon cells harvesting, RNA was extracted and retro-transcribed, to assess miR-136 levels, with TaqMan primers and probes (Life Technologies). Bars represent FC of miR136 upon U6 expression, used as miRNA internal control in BRAF-I sensitive melanoma M21 (A) and Colo38 (B) cells in presence (filled bars) or absence (white bars) of BRAF-I (vemurafenib). Histograms show the mean  $\pm$  S.D. of three independent experiments. \*\*,  $p < 0.01$  and \*\*\*,  $p < 0.001$  indicate the statistical significance of BRAF-I sensitive melanoma treated cells compared to controls.

As expected on the basis of previous results, showing that miR-136 and the inhibitor of Shh pathway are related, the down-regulation of SUFU following vemurafenib treatment in BRAF-I treated melanoma sensitive cells, was a consequence of increased levels of miR-136 upon treatment. Therefore, the activation of Shh pathway upon the treatment was confirmed in these cells.

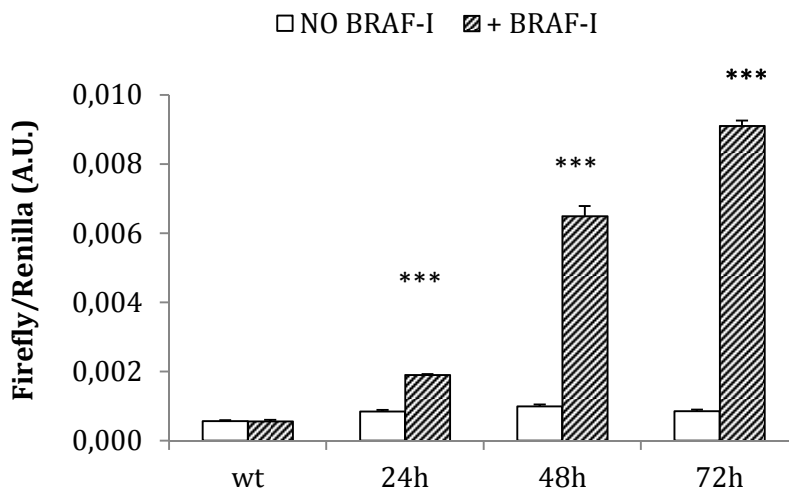


**Figure 50: Shh activation in BRAF-I sensitive cells upon BRAF-I treatment.**

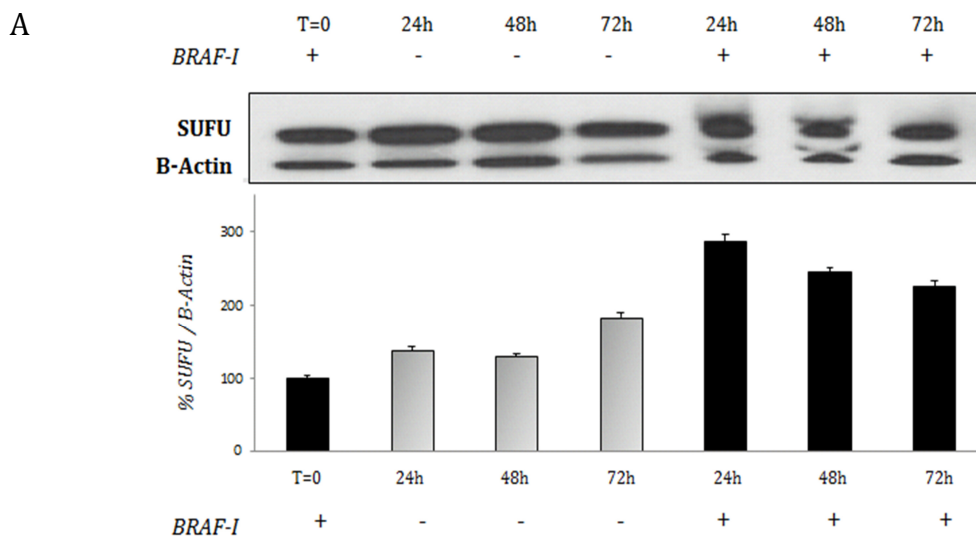
BRAF-I sensitive melanoma cells (M21 and Colo38 cells) were cultured in presence (dashed bars) or absence (white bars) of 0,5  $\mu$ M vemurafenib for 72 hours. Concomitantly, adherent melanoma cells were co-transfected with a Firefly luciferase reporter gene together with a pRLTK Reporter Vector, used as an internal control. After rinse in PBS, cells were lysed for 15 minutes RT and ratios between Firefly and Renilla luciferase activity were estimated using a GloMax® 96 Microplate Luminometer (Promega). Histograms show the mean  $\pm$  S.D. of three independent experiments. \*\*\*,  $p < 0.001$  indicates the statistical significance of Firefly/Renilla activity in the BRAF-I resistant cells compared to BRAF-I sensitive cells.

To note, the Shh pathway was activated by BRAF-I treatment in sensitive-to-treatment melanoma cells, whereas untreated cells showed no alteration in the pathway, as shown in *Figure 50*.

Quite unexpectedly, these preliminary data indicated that vemurafenib treatment induced an overexpression of miR-136 in BRAF-I sensitive melanoma cells, eventually resulting in a lowered expression of SUFU that activates Shh pathway. However, to verify such connection between the treatment with BRAF-I, these parameters were also evaluated in BRAF-I resistant cells after removal of the drug.

### **8.2- BRAF-I resistant cells upon removal of the drug**

To double confirm the effect of BRAF-I treatment on melanoma cells, levels of miR-136 and the expression of SUFU were evaluated in BRAF-I resistant cells upon removal of the treatment in these cells.



B

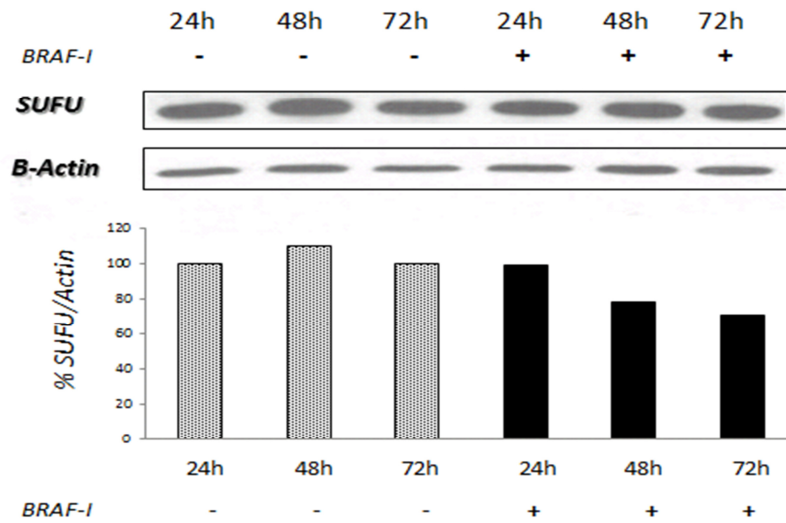


**Figure 51: SUFU expression in BRAF-I resistant cells upon removal of vemurafenib.**

Vemurafenib was removed for 72 hours in BRAF-I resistant melanoma cells (M21-R, A and Colo38-R, B) and then re-introduced for further 72h. Lysed cells were then separated by SDS-PAGE and proteins were electroblotted onto a nitrocellulose membrane to be labeled with a rabbit monoclonal primary antibody against SUFU (Cell Signaling), whose expression was assessed every 24h and normalized over  $\beta$ -Actin expression (Cell Signaling). Densitometric analysis were represented as the mean value  $\pm$ SD in M21-R (A) and Colo38-R (B) melanoma cells in presence (black bars) and absence (grey bars) of the drug.

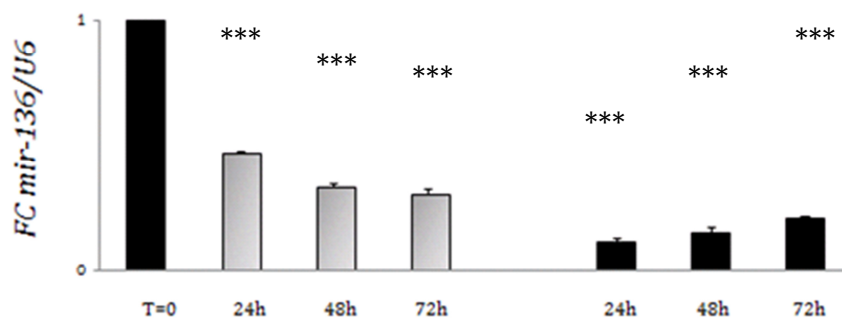


**Figure 52: miR-136 expression in BRAF-I resistant melanoma cells after removal of vemurafenib (BRAF-I).**

Vemurafenib was removed for 72 hours in BRAF-I resistant 21-R melanoma cells and then re-introduced for further 72h. Upon cells harvesting, RNA was extracted and retro-transcribed, to assess miR-136 levels, with TaqMan primers and probes (Life Technologies). Bars represent FC of miR136 upon U6 expression, used as miRNA internal control in BRAF-I resistant M21-R cells in presence (black bars) or absence (grey bars) of BRAF-I (vemurafenib). Histograms show the mean  $\pm$  S.D. of three

*independent experiments. \*\*\*,  $p < 0.0001$  was the statistical significance of resistant cells data after removal of BRAF-I compared to wild type cells.*

Overall, these preliminary data clearly indicate that vemurafenib itself induces an overexpression of miR-136 in melanoma cells, while sustaining its expression in BRAF-I resistant cells, allowing the mechanisms of resistance to therapy to take place. Actually, the overexpression of miR-136 triggers a domino effect resulting in a lowered expression of SUFU that – in turn – activates Shh pathway, leading to uncontrolled proliferation of BRAF-I resistant melanoma cells.

On the basis of the effect of vemurafenib against melanomas, as proven by many clinical trials that lead to define vemurafenib as the drug of choice to cure metastatic BRAF(V600E)-carrying melanoma patients, these emerging data were not expected. Nonetheless, although the mechanism of microRNA-mediated drug resistance is not fully understood, these emerging results could offer new perspectives to investigate over resistance to cancer therapy, that still accounts for death in over 90% of patients with metastatic cancers, due to therapeutic failure. Indeed, if the overexpression of miR-136 effectively triggers drug-resistance in these cells, it is quite conceivable to believe that the therapy itself can mediate these mechanisms, inevitably leading to BRAF-I resistance in patients. Therefore, in this view, new therapeutic strategies could be considered to approach metastatic melanomas to counteract these mechanisms, potentially offering new chances of survival in yet poor prognosis patients.

# Discussion and conclusions

---

Tumor cells exhibit profound genetic, biochemical and histological difference with respect to the non-transformed cells of the same origin. Considering the master role of mitochondria inside the cells, an increasing number of human diseases is now correlated with mitochondrial alterations, both morphologically and functionally, including neurodegenerative diseases and cancer (10). Numerous studies conducted in the last decade, indeed, clearly indicate that mitochondrial dysfunctions are one of the most recurrent characteristics in cancer cells, as proven by microscopic and genetic alterations, as well as by biochemical and molecular analysis.

Particularly, the literature over the last decade has been abundantly focusing on cancer metabolism, since many evidence reported that transformed cells are characterized by a glycolytic predominant phenotype: although the oxidative phosphorylation physiologically provides the major contribute to the ATP supply in normal cells – and yet in many cancer cell types - plenty of data reported a higher glucose consumption in the transformed cells, suggesting that a metabolic reprogramming occurs during malignant progression. Therefore, an increasing attention is now given to clarify which molecular mechanism modify energy metabolism in cancer cells, aiming to identify and inhibit one or more enzymes that play a key role in controlling metabolic alterations, in the hopes of possibly developing new potential therapeutic approaches.

As reported by the literature, different biochemical mechanism may contribute to increase glycolysis rate in tumor cells, including the over-expression of glycolytic enzymes and transporters, cellular adaptation to the hypoxic microenvironment within tumor - through HIF-1 mediated pathways - mutations in somatic genes, as well as epigenetic alterations, that drive cellular reprogramming in the altered tumoral scenario. Interestingly, it has been recently showed that the endogenous inhibitor protein of the ATP

synthase (IF<sub>1</sub>) is overexpressed in many human carcinomas: in a comparative study between healthy and cancer tissues, Cuezva and co-workers showed that the expression of the protein markedly increased in tumor cells, along with a number of metabolic features that are typically accounted in cancer cells, thereby suggesting that IF<sub>1</sub> may have an important role in tumor progression (65). Since then, a number of papers speculated over possible roles of IF<sub>1</sub> in the establishment of the so-called “cancer hallmarks”, hypothesizing that the inhibitor may act as a molecular switch of cancer metabolism, sustain cell growth in hostile conditions, mediate mechanism to escape apoptosis, further then being involved in the dimerization of the ATP synthase, thereby contributing in modifying mitochondrial structure and, hence, size and shape of mitochondria. Nevertheless, many of these issues are highly debated and no clear evidence has been yet provided to define how IF<sub>1</sub> may contribute in tumor progression, prompting our group to further investigate over this protein and its role in cancer.

As it is well established, the inhibitor protein is the master regulator of the ATP hydrolytic activity of the ATP synthase: when the electrochemical gradient across the mitochondrial inner membrane collapses and is insufficient to drive ATP synthesis - as in hypoxia/ischemia, or in general when mitochondrial respiration is compromised - the ATP synthase reverses its function and hydrolyses ATP to restore the membrane potential, thus ensuring that all the mitochondrial-potential-related process take place. Simultaneously, under these conditions, cell energy metabolism is shifted toward glycolysis, and the resulting mitochondrial pH decreases, allowing the activation and the binding of IF<sub>1</sub> to F<sub>1</sub>-ATPase domain (at the  $\alpha$ E/ $\beta$ E interface), to avoid a massive glycolytic ATP depletion and protect cells from death. On this basis, it has been hypothesized that IF<sub>1</sub> could play a key role in preventing energy dissipation when tumor cells experience hypoxic conditions, thereby promoting cell growth and survival.

To better elucidate this aspect, some recent investigations have set out to explore the functional consequences of varying IF<sub>1</sub> expression levels in different cancer cell lines. However, nearly all studies reported were

performed in normoxic conditions and, more importantly, through transient IF<sub>1</sub> over-expression or silencing: these transient models do not allow long-term changes to be studied and may also produce potentially ambiguous biochemical data, often misleading interpretations and creating conflicting data, as reported. Transient modifications of the inhibitor, indeed, only refer to heterogeneous populations of cells (due to the coexistence of transfected and control cells), in a dynamic situation in which cells are adapting to the change in IF<sub>1</sub> content.

Given these restrictions, we prepared IF<sub>1</sub>-silenced clones from the human osteosarcoma 143B cell line and assayed the main bioenergetic parameters, to examine in stable IF<sub>1</sub>-silenced human osteosarcoma cells both the role played by IF<sub>1</sub> and the mechanism the inhibitor adopts in tumor cells to control mitochondrial mass, structure and function, as well as to regulate energy homeostasis.

Short hairpin RNAs are great experimental tools for inducing gene silencing in mammalian somatic cells: under the control of a constitutive expressed promoter, IF<sub>1</sub>-targeting-shRNAs ensured a permanent silencing of the protein, resulting in more than 90-95% of gene silencing in all the clones we used for our experiments, without altering cell morphology, nor the adhesion capacity of transfected cells, with respect to parent cells. In addition, both flow cytometry and fluorescence microscopy revealed that our systems were homogeneous, resulting in 99% of GFP expression – being GFP encoded in the plasmid we used for transfection – even after two years of cell culturing, along with the reduced expression of the inhibitor, confirming the stability of transfection.

As we herein showed and recently reported (115), under normal conditions (*i.e.* normoxia) IF<sub>1</sub>-silenced cells proliferate normally, consume glucose and release lactate as controls do. On the basis of earlier studies on both isolated mitochondria and submitochondrial particles (135) and (134), these results were quite expected, since the inhibitor protein is not supposed to inhibit the ATP hydrolytic activity of the enzyme in normoxia. Coherently, analysis on stable IF<sub>1</sub>-depleted HeLa cells reported by Fujikawa et al. (131) are in line

with our results, but were debated by other groups showing that IF<sub>1</sub> promotes cell growth and progression in transiently-transfected tumor cells (these data were collected in normoxic conditions, that do not favor binding of IF<sub>1</sub> to the F<sub>1</sub>F<sub>0</sub>-ATPase complex), inducing us to suppose that transient models do not properly represent a stable steady-state metabolic condition.

IF<sub>1</sub> overexpression have been proposed to promote tumor progression by either reducing mitochondrial ATP synthase activity and increasing aerobic glycolysis (132), or inducing a  $\Delta\Psi_m$  decrease that is associated with enhanced proneness to apoptotic cell death by cytochrome c release from mitochondria (27). In our model, we showed that IF<sub>1</sub>-silenced cells intriguingly displayed an enhanced steady-state mitochondrial membrane potential, consistent with the higher  $\Delta\Psi_m$  reported by Fujikawa et al., along with a reduced ADP-stimulated respiration rate (incidentally, this reduction was not observed either in state 4, or in dinitrophenol uncoupled conditions), over the same OXPHOS content presented in all the cells. Moreover, we here showed that IF<sub>1</sub> exerts a protective role against ROS production, protecting cancer cells from ROS-related damages.

However, these data are in contrast with those reported by Sanchez-Cenizo et al. (65), who reported an increase in  $\Delta\Psi_m$  in transiently-overexpressing-IF<sub>1</sub> carcinoma cells, paralleled by retrograde ROS signal to the nucleus triggered by superoxide radical to support tumor development through the NF- $\kappa$ B. Although we cannot exclude that different types of cancer cells behave differently from HeLa (131) (59) and osteosarcoma cells, we still believe that some of these latter results may be only apparent, due to the analysis of an heterogeneous population of cells, with different IF<sub>1</sub> expression levels.

Taken together, overall data indicate that the presence of the inhibitor protein in osteosarcoma 143B cells can enhance the rate of ATP synthesis via OXPHOS, with no effect on respiratory chain activity. In addition, the inhibitor protein was found to be associated with the dimeric form of the ATP synthase complex in control cells, being the distribution between monomeric and dimeric state of the enzyme unaffected by the absence of IF<sub>1</sub> (the latter result implying that the inhibitor does not induce ATP synthase dimerization,

contrary to previous data reported (56) on IF<sub>1</sub>-F<sub>1</sub> complexes). Therefore, the interaction of IF<sub>1</sub> with the F<sub>1</sub>F<sub>0</sub>-ATPase complex either directly, by increasing the catalytic activity of the enzyme, or indirectly, by improving the structure of mitochondrial cristae, can increase the oxidative phosphorylation rate in osteosarcoma cells grown under normoxic conditions.

This aspect is of particular relevance, since the inhibitor has been long known to only inhibit ATP hydrolysis, whereas the observation that it can increase the ATP synthesis in mitochondria may represent a successful strategy used by cancer cells to produce more energy, giving a plausible explanation to the IF<sub>1</sub> overexpression in cancer. Additionally, this facet is also relevant considering that the binding of IF<sub>1</sub> is supposed to be strictly dependent on the environmental conditions to which tumor cells are exposed: as discussed above, it is well known that the inefficient development of vasculature within the tumor mass may expose tumor cells to a limited oxygen - and substrate - availability. As a consequence, both acidification of the matrix as well as a collapse in mitochondrial membrane potential may occur, inducing the binding of the inhibitor to the ATP synthase (141), but these conditions have only been marginally considered in recent studies.

Therefore, further studies are currently ongoing to define the IF<sub>1</sub> role in cancer, extending the investigation to include hypoxic and anoxic conditions, to better elucidate how the increase of the protein represents an efficacious strategy for cancer cells to survive and proliferate, facing - and successfully overcoming - all the circumstances these cells may encounter in the tumor microenvironment.

In addition, a number of papers over the last decade indicated that cancer metabolism is greatly modulated by epigenetic alterations through endogenous RNA interference molecules, known as microRNAs (miRNAs). MiRNAs are small, noncoding RNA molecules of about 20-22 base in length, that bind to the 3'-untranslated region of target mRNA, affecting important cellular processes, like cell proliferation and differentiation, cell cycle, energy metabolism and other hallmarks of cancer, such as inhibition of apoptosis,

epithelial-to-mesenchymal transition (EMT), cell invasion and metastases and, more recently, they were addressed as responsible for chemoresistance in several common therapies (110).

MicroRNAs deregulation in cancer was first demonstrated in 2002 (7), opening a new branch of investigation over cancer formation and progression: since then, accumulative studies showed that miRNAs play important roles in tumor growth by regulating oncogenes and tumor suppressor genes (142) (139). More intriguingly, a large number of miRNAs in the last few years have been identified to regulate cancer metabolism (140), pushing researchers to address the connection between cancer cells and specific miRNAs. Thus far, accumulating studies indicate that many of the well-known miRNAs relate to crucial genes that can impact metabolic pathways, both negatively and positively, by regulating the expression of genes/pathways/enzymes involved in glycolysis and energy metabolism. Therefore, studying the role of miRNAs is crucial in understanding their effect on metabolic pathways, and their ultimate effect on cancer cells, thus representing promising therapeutic targets, or therapeutic agents, in cancers. In an attempt to investigate over miRNAs contribution in regulating cancer cell metabolism in different cancer cell lines, during the permanence at the Children's Hospital of Los Angeles, the miRNAs expression pattern was analyzed, to explore how these molecules alter metabolic and developmental pathways that can lead to cancer. However, while further investigations are currently ongoing to unravel miRNAs contribution in altering cancer metabolism, compelling data emerging from a microarray on different cell lines that included a sensitive- and a resistant-to-treatment melanoma cell lines, showed a specific pattern of miRNAs in the resistant cells, when compared to the sensitive ones. On the basis of the raised attention now given to the role exerted by microRNAs in triggering resistance to therapy, this peculiar miRNAs outline prompted us to further focus over this aspect, pushing us to deeper investigate on the molecular mechanisms induced by these molecules in a severe, challenging and yet poor-prognosis malignancy, like metastatic melanoma.

Indeed, microRNA expression profiling using microarrays (refer to (143) for details) revealed an up-regulation of four miRNAs in BRAF-I resistant melanoma cells M21-R when compared to the sensitive (M21) ones. Incidentally, three out of four miRNAs were predicted to target SUFU, the negative regulator of the GLI signaling cascade in the Sonic Hedgehog (Shh) pathway, crucially involved in the development of all vertebrates and recently reported to be deregulated in cancer. In addition, a recent paper specifically reported that the resistance to treatment in melanoma is mediated by Shh activation, which is induced by PDGFR $\alpha$  up-regulation (106).

Being miR-136 the most expressed microRNA in this comparison, we primarily focus on the role exerted by this miR, validating these preliminary data, including other melanoma cell types in the study (*i.e.* Colo38 and Colo38-R and, partially, SK-Mel37 and Mel-37-R), and then analyzing the interconnection existing between the expression of miR-136 and the negative regulator of Shh pathway, SUFU, whose expression was evidently dependent on the content of the microRNA.

Specifically, we showed that miR-136 has a protective role against BRAF-I treatment in sensitive melanoma cells, while inhibiting its expression in BRAF-I resistant cells partially restore the sensitivity to the drug in these cells (as summarized in Figure 53). Although the mechanism of microRNA-mediated drug resistance is not fully understood, overall these emerging data encourage us to believe that melanoma cells trigger resistance to BRAF-I therapy by inducing the up-regulation of the three miRNAs, that down-regulate SUFU and consequently activate Shh pathway. In addition, *in vivo* experiments have already been set up to further confirm these data in animal models, while future perspectives are also intended to investigate over the role exerted by the other up-regulated microRNAs, pointing towards the need for novel and more innovative therapeutic strategies to evade cancer drug resistance and fatal prognosis in metastatic melanoma patients.

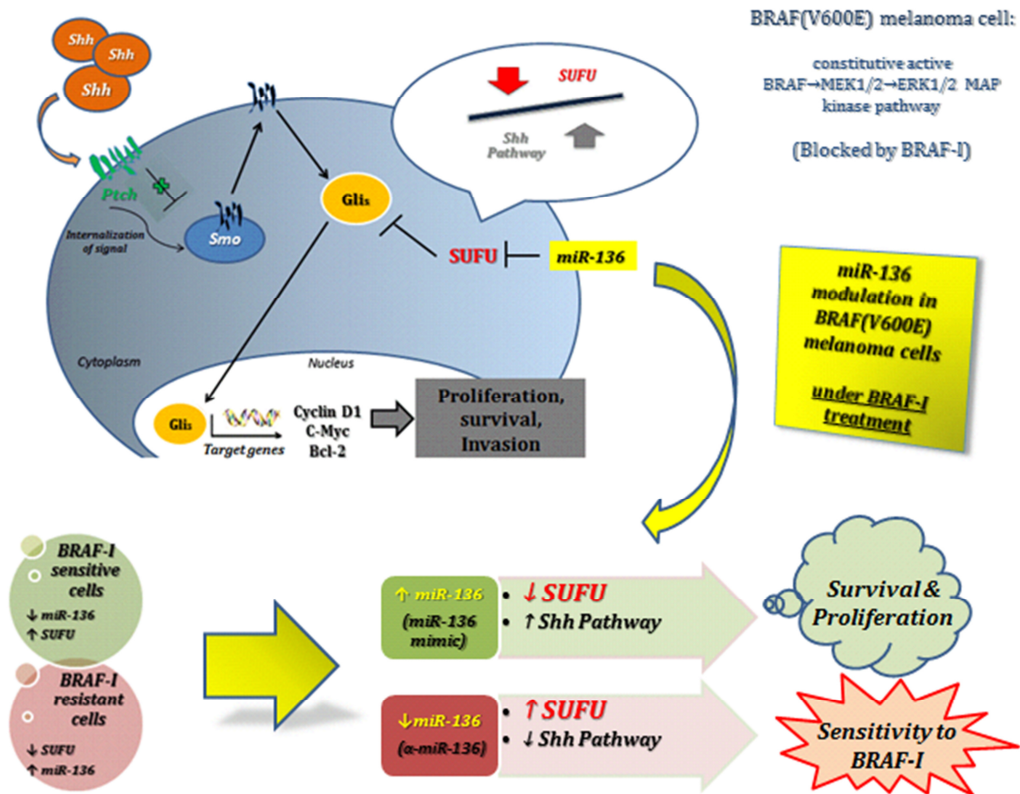


**Figure 53: miR-136 can mediate BRAF-I resistance in BRAF(V600E) melanoma cells.** Upon Sonic Hedgehog (Shh) ligand binding to its receptor Patched (Ptch), the repression of Smoothed (Smo) is relieved, resulting in the movement of Smo from the intracellular vesicles to the primary cilium. Activated Smo induces the Gli proteins, that enter the nucleus and promote transcription of the target genes, enhancing proliferation. This process is negatively regulated by the internal protein SUFU: in the absence of ligand, SUFU directly binds to GLI transcription factors and anchors them in the cytoplasm, thus facilitating their degradation (in addition, SUFU forms a repressor complex suppressing GLI1-induced gene expression inside the nucleus). BRAF(V600E) melanoma cells have a constitutive active BRAF→MEK1/2→ERK1/2 MAP kinase pathway, leading to uncontrolled proliferation of cells, which can be counteracted by BRAF-I treatment, unless cells develop drug-resistance. Since miR-136 targets SUFU (and its levels are higher in BRAF-I resistant melanoma cells, when compared to the sensitive ones), this molecule can likely modulate Shh pathway activity, affecting cell proliferation and drug sensitivity. Indeed, the induction of miR-136 partially counteracts BRAF-I treatment in melanoma sensitive cells, by decreasing SUFU and activating Shh pathway, while its down-regulation in BRAF-I resistant cells up-regulates SUFU, partially restoring sensitivity to BRAF-I treatment.

Moreover, additional studies are currently ongoing to further explore how the treatment itself mediates the up-regulation of miR-136, contributing to the establishment of the BRAF-I resistance. Much more intriguingly, indeed,

we showed that vemurafenib itself enhances miR-136 expression in melanoma sensitive-to-treatment cells, while concomitantly sustains higher levels in the under-treatment resistant melanoma cells.

Being vemurafenib the major breakthrough in the treatment of melanomas, it is conceivable to imagine that BRAF-I therapy (*i.e.* vemurafenib subadministration), initially resulting in effective reduction of the tumor mass, later seemingly turns traitor by inducing the overexpression of the miRNAs mentioned above, eventually leading to BRAF-I resistance and tumor recurrence, in a much more aggressive form. Considering this hypothesis, an intermittent therapy, like the intermittent hormone therapy for prostate cancer (144), could be considered. Even more striking, once determined the effective roles exerted by all the four miRNAs in leading resistance to therapy, a combination of vemurafenib, together with small molecules inhibiting their overexpression could be a promising strategy to be considered, in the direction of donating new chances of survival and improved quality of life in poor prognosis melanoma patients.

# List of References

---

1. *Hallmarks of cancer: the next generation.* **Hanahan, D and Weinberg, RA.** 5, 2011, Cell. , Vol. 144, pp. 646-74.
2. *The chemical constitution of respiration ferment.* **Warburg, O.** 1928, Science, Vol. 68, pp. 437-443.
3. *Mitochondria and cancer.* **Wallace, DC.** 2012, Nat. Rev. Cancer, Vol. 12, pp. 685–698.
4. *Tumors and Mitochondrial Respiration: A Neglected Connection.* **Viale, A, Corti, D and Draetta, GF.** 2015, Cancer Res., Vol. 75, pp. 3685–3686.
5. *MicroRNAs and cancer epigenetics.* **Fabbri, M.** 6, 2008, Curr Opin Investig Drugs., Vol. 9, pp. 583-90.
6. *MicroRNAs.* **Fabbri M, Croce CM, Calin GA.** 1, 2008, Cancer J. , Vol. 14, pp. 1-6.
7. *Frequent deletions and down-regulation of micro- RNA genes miR15 and miR16 at 13q14 in chronic lymphocytic leukemia.* **Calin, GA et al.** 2002, Proc. Natl. Acad. Sci. U.S.A, Vol. 99, pp. 15524–15529.
8. *MicroRNAs and metabolism crosstalk in energy homeostasis.* **Dumortier, O, Hinault, C and Van Obberghen, E.** 3, 2013, Cell Metab., Vol. 18, pp. 312-24.
9. *Exosomal microRNAs in the Tumor Microenvironment.* **Neviani, P and Fabbri, M.** 47, 2015, Front Med (Lausanne)., Vol. 2.
10. *The bioenergetic signature of cancer: a marker of tumor progression.* **Cuezva, J.M., Krajewska, M., de Heredia, M.L., Krajewski, S., Santamaria, G., Kim, H., Zapata, J.M., Marusawa, H., Chamorro, M., and Reed, J.C.** 2002, Cancer Res., Vol. 64, pp. 6674–81.
11. *Evolutionary biology: essence of mitochondria.* **Henze K., and Martin W.** 6963, 2003, Nature, Vol. 426, pp. 127-8.
12. **Altmann, Richard.** *Die Elementarorganismen.* 1890.
13. *Common evolutionary origin of mitochondrial and rickettsial respiratory chains.* **Emelyanov, VV.** 2003, Arch. Biochem. Biophys., pp. 130-41.
14. *Powerhouse of the cells.* **Siekevitz, Philip.** 1957, Scientific American.
15. *Chemiosmotic coupling: the cost of living.* **Rich, P.** 2003, Nature, p. 583.

16. *IF1: setting the pace of the F1F0-ATP synthase.* **Campanella, M. et al.** 2009, Trends in Biochemical Sciences, pp. 343-350.
17. *Mitochondria and Ca<sup>2+</sup> in cell physiology and pathophysiology.* **Duchen, M.R.** 2000, Cell Calcium, Vol. 28, pp. 339-348.
18. *Mitochondrial control of apoptosis.* **Kroemer, G. et al.** 1997, Immunol. Today, pp. 44-51.
19. *Biochemical dysfunction in heart mitochondria exposed to ischaemia and reperfusion.* **Solaini, G and Harris, DA.** 2005, Biochem J., pp. 377-94.
20. *Mitochondria are morphologically and functionally heterogeneous within cells.* **Collins TJ, Berridge MJ, Lipp P and Bootman MD.** 7, 2002, The EMBO Journal, Vol. 21, pp. 1616-1627.
21. *An electron microscope study of the mitochondrial structure.* **Palade, G.E.** 1953, J. Histochem. Cytochem, pp. 188-211.
22. *Cardiolipin stabilizes respiratory chain supercomplexes.* **Pfeiffer K, Gohil V, Stuart RA, Hunte C, Brandt U, Greenberg ML, Schagger H.** 278, 2003, J. Biol. Chem., pp. 52873-80.
23. *Insight into mitochondrial structure and function from electron tomography.* **Frey T.G., Renken C.W., Perkins G.A.** 2002, Biochim. Biophys. Acta, Vol. 1555, pp. 196-203.
24. *Structure and function of mitochondrial membrane protein complexes.* **Kuhlbrandt, W.** 2015, BMC Biology, pp. 1-11.
25. *Ultrastructural bases for metabolically linked mechanical activity in mitochondria. I. Reversible ultrastructural changes with change in metabolic steady state in isolated liver mitochondria.* **Hackenbrock, CR.** 2, 1966, J Cell Biol., Vol. 30, pp. 269-297.
26. *New Insights Into Structure and Function of Mitochondria and Their Role in Aging and Disease.* **Lenaz, G, Baracca, A, Fato, R, Genova, ML and Solaini, G.** 3, 2006, ANTIOXIDANTS & REDOX SIGNALING, Vol. 8.
27. *Mitochondrial IF1 preserve cristae structure to limit apoptotic cell death signaling.* **Faccenda D., Tan H.T., Duchon M.R., Campanella M.** 2013, Cell Cycle, pp. 2530-32.
28. *Hypoxia and mitochondrial oxidative metabolism.* **Solaini G, Baracca A, Lenaz G and Sgarbi G.** 2010, Biochim Biophys Acta, pp. 1171-7.
29. *Mitochondrial fusion and fission in cell life and death.* **Westermann, B.** 2010, Molecular Cell biology, pp. 872-884.
30. *Bioenergetic Origins of Complexity and Disease.* **Wallace, DC.** 2011, Cold Spring Harb Symp Quant Biol, Vol. 76, pp. 1-16.

31. *the interplay between mitochondrial dynamics and mitophagy*. **Twig G., Shirihai OS.** 2011, *Antiox Redox Signal*, Vol. 14, pp. 1939-51.
32. *Mitochondrial respiratory chain super-complex I-III in physiology and pathology*. **Lenaz G, Baracca A, Barbero G, Bergamini C, Dalmonte ME, Del Sole M, Faccioli M, Falasca A, Fato R, Genova ML, Sgarbi G and Solaini G.** 2010, *Biochimica et Biophysica Acta* , Vol. 1797, pp. 633–640.
33. *Supercomplexes in the respiratory chains of yeast and mammalian mitochondria*. **Schagger H and Pfeiffer, K.** 2000, *The Embo journal*, Vol. 19, pp. 1777-83.
34. *Assembly of respiratory complexes I, III, and IV into NADH oxidase supercomplex stabilizes complex I in Paracoccus denitrificans*. **Stroh, A, Anderka O, Pfeiffer K, Yagi T, Finel M, Ludwig B, Schagger H.** 2004, *J. Biol. Chem.*, Vol. 279, pp. 5000–07.
35. *Supramolecular organization of cytochrome c oxidase and alternative oxidase-dependent respiratory chains in the filamentous fungus Podospora anserina*. **Krause F, Scheckhuber CQ, Werner A, Rexroth S, Reifschneider NH, Dencher NA, Osiewacz HD.** 2004, *J. Biol. Chem.*, Vol. 279, pp. 26453-61.
36. *Respiratory chain supercomplexes in plant mitochondria*. **Eubel, H., Heinemeyer, J., Sunderhaus, S, Brau, HP.** 2004, *Plant Physiol. Biochem.*, Vol. 42, pp. 937-42.
37. *Defining the mitochondrial proteosomes from five rat organs in a physiologically significant context using 2D Blue-Native/SDS-PAGE*. **Reifschneider NH, Goto S, Nakamoto H, Takahashi R, Sugawa M, Dencher NA, Krause F.** 2006, *J. Proteome Res.*, pp. 1117-32.
38. *Significance of respirasomes for the assembly/stability of human respiratory chain complex I*. **Schagger H., De Coo R., Bauer MF., Hoffmann S., Godinot C., Brandt U.** 279(35), 2004, *J Biol Chem.*, pp. 36349-53.
39. *Is supercomplex organization of the respiratory chain required for optimal electron transfer activity*. **Genova ML, Baracca A, Biondi A, Casalena G, Faccioli M, Falasca AI, Formiggini G, Sgarbi G, Solaini G and Lenaz G.** 2008, *Biochim. Biophys. Acta*, Vol. 1777, pp. 740–746.
40. *Mitochondrial Complex I: structure, function, and implications in neurodegeneration*. **Lenaz G, Baracca A, Fato R, Genova ML, Solaini G.** 3-4, 2006, *Ital J Biochem.* , Vol. 55, pp. 232-53.
41. *The quaternary structure of the Saccharomyces cerevisiae succinate dehydrogenase. Homology modeling, cofactor docking, and molecular dynamics simulation studies*. **Oyedotun, KS and Lemire, BD.** 279, 2004, *J. Biol. Chem.*, Vol. 5, pp. 9424-31.

42. *Q-cycle bypass reactions at the Q site of cytochrome bc<sub>1</sub> (and related) complexes.* **Kramer DM, Roberts AG, Muller F, Cape J, Bowman MK (2004) Q-cycle.** 2004, *Methods Enzymol*, Vol. 382, pp. 21-45.
43. *Inhibitors of the catalytic domain of mitochondrial ATP synthase.* **Gledhill JR and Walker, JE.** 2006, *Biochem Soc Trans.*, Vol. 34, pp. 989-92.
44. *The peripheral stalk of the mitochondrial ATP synthase.* **Walker, JE and Dickinson, VK.** 2006, *Biochim. Biophys. Acta*, Vol. 1757, pp. 286-96.
45. *The ATP synthase: the understood, the uncertain and the unknown.* **Walker, JE.** 2013, Keilin Memorial Lecture, pp. 1-16.
46. *A model for conformational coupling of membrane potential and proton translocation to ATP synthesis and to active transport.* **Boyer, PD.** 58, 1975, *FEBS letter*, Vol. 15, pp. 1-6.
47. *The binding change mechanism for ATP synthase: some probabilities and possibilities.* **Boyer, P D.** 1993, *Biochim. Biophys. Acta*, pp. 215-30.
48. *The regulation of catalysis in ATP synthase.* **Walker, JE.** 1994, *Current Opinion in Structural Biology*, pp. 912-18.
49. *Post-transcriptional regulation of the mitochondrial H<sup>+</sup>-ATP synthase: a key regulator of the metabolic phenotype in cancer.* **Willers, IM and Cuezva, JM.** 06, 2011, *Biochimica et Biophysica Acta*, Vol. 1807, pp. 543-51.
50. *Structure of the yeast F<sub>1</sub>F<sub>o</sub>-ATP synthase dimer and its role in shaping the mitochondrial cristae.* **Karen M. Davies, Claudio Anselmi, Ilka Wittig, José D. Faraldo-Gómez and Werner Kühlbrandt.** 34, 2012, *PNAS*, Vol. 109, pp. 13602–07.
51. *Dimer ribbons of ATP synthase in native mitochondrial inner membranes.* **Strauss M, Hofhaus G, Schroder RR and W Kuhlbrandt.** 2007, *EMBO J.*, pp. 2870-76.
52. *An investigation of mitochondrial inner membranes by rapid-freeze deep-etc techniques.* **Allen RD, Schroeder CC and Frok AK.** 1989, *J. Cell Biol.*, pp. 2233-40.
53. *A naturally occurring inhibitor of mitochondrial adenosine triphosphatase.* **Pullman, ME and Monroy, GC.** 1963, *The Journal of Biological Chemistry*, Vol. 238, pp. 3762-69.
54. *Protonic inhibition of the mitochondrial adenosine 50-triphosphatase in ischemic cardiac muscle. eversible binding of the ATPase inhibitor protein to the mitochondrial ATPase during ischemia.* **Rouslin, W. and Pullman, M.E.** 1987, *J. Mol. Cell. Cardiol.*, Vol. 19, pp. 661-68.
55. *ATPase activity, IF1 content, and proton conductivity of ESMP from control and ischemic slow and fast heartrate hearts.* **Rouslin, W. et al.** 1995, *J. Bioenerg. Biomembr*, Vol. 27, pp. 459-66.

56. *Dimerization of Bovine F1-ATPase by Binding the Inhibitor Protein, IF1.* **Cabezón, E., Arechaga, I., Jonathan, P., Butler, G. and John E. Walker.** 2000, *J. Biol. Chem.*, pp. 28353-55.
57. **Faccenda, D and Campanella, M.** 2012, *International Journal of Cell Biology*.
58. *Binding of the Inhibitor Protein IF1 to Bovine F1-ATPase.* **Bason, JE, Runswick, MJ, Fearnley, IM and John E. Walker.** 2011, *J. Mol. Biol.*, Vol. 404, pp. 443-53.
59. *Regulation of mitochondria structure and function by the F1FO-ATPase inhibitor protein,IF1.* **Campanella M, Casswell E,Chong S et al.** 2008, *Cell Metabolism*, Vol. 8, pp. 13-25.
60. *The inhibitor protein (IF1) promotes dimerization of the mitochondrial F1FO-ATP synthase.* **Garcia, JJ, Morales-Ríos E, Cortés-Hernández P, and Rodríguez-Zavala, JS.** 42, 2006, *Biochemistry*, Vol. 45, pp. 12695-703.
61. *IF1 limits the apoptotic-signalling cascade by preventing mitochondrial remodelling.* **Faccenda, D, Tan, CH, Seraphim, A, Duchen, MR and Campanella, M.** 2013, *Cell Death and Differentiation* , pp. 1-12.
62. *Dimerization of FOF1ATP synthase from bovine heart is independent from the binding of the inhibitor protein IF1.* **Tomaseting, L, Di Pancrazio, F, Harris, DA, Mavelli, I and Lippe, G.** 2002, *Biochimica et Biophysica Acta*, Vol. 1556, pp. 133-141.
63. *IF1, the endogenous regulator of the F1Fo-ATPsynthase, defines mitochondrial volume fraction in HeLa cells by regulating autophagy.* **Campanella, M Seraphim, A, Abeti R, Casswell E, Echave P, and Duchen, MR.** 2009, *Biochimica et Biophysica Acta*, Vol. 1787, pp. 393-41.
64. *The mitochondrial ATPase inhibitory factor 1 triggers a ROS-mediated retrograde prosurvival and proliferative response.* **Formentini, L, Sanchez-Arago, M, Sanchez-Cenizo, L and J. M. Cuezva.** 6, 2012, *Molecular Cell.*, Vol. 45, pp. 731–742.
65. *Up-regulation of the ATPase Inhibitory factor 1 (IF1) of the mitochondrial ATP synthase in human tumors mediates the metabolic shift of cancer cells to a Warburg phenotype.* **Sanchez-Cenizo, L., Formentini, L., Aldea, M., Ortega, AD, Garcia-Huerta, P., Snchez-Aragò, M. and J. Cuezva.** 33, 2010, *J. Biol. Chem.*, Vol. 285.
66. *Increased content of natural ATPase inhibitor in tumor mitochondria.* **Luciakova, K. and Kuzela, S.** 1, 1984, *The FEBS Letters*, Vol. 177, pp. 85–88.
67. *Cyclin D-dependent kinases, INK4 inhibitors and cancer.* **Ortega, S, Malumbres, M and Barbacid, M.** 2002, *Biochim. Biophys. Acta* , Vol. 1602, pp. 73–87.
68. *The retinoblastoma tumour suppressor in development and cancer.* **Classon, M and Harlow, E.** 2002, *Nat. Rev. Cancer*, pp. 910–917.

69. *DNA damage and repair*. **Friedberg, EC**. 2003, *Nature*, Vol. 421, pp. 436-440.
70. *Mutations affecting segment number and polarity in Drosophila*. **Nusslein-Volhard, C and Weischaus, E**. 1980, *Nature*, Vol. 287, pp. 795-801.
71. *Hedgehog: functions and mechanisms*. **Varjosalo, M and Taipale, J**. 2008, *Genes Dev.*, pp. 2454-72.
72. *Hedgehog signaling*. **Varjosalo M. and Taipale, J**. 2007, *J.Cell. Sci.*, Vol. 120, pp. 3-6.
73. *A genome-wide RNA interference screen in Drosophila melanogaster cells for new components of the Hh signaling pathway*. **Nybakken, K, Vokes, SA, Lin, TY, McMahon, AP and Perrimon, N**. 2005, *Nat. Genet.*, Vol. 37, pp. 1323-32.
74. *Sonic hedgehog, a member of a family of putative signaling molecules, is implicated in the regulation of CNS polarity*. **Echelard, Y., et al., et al.** 1993, *Cell.*, Vol. 75, pp. 1417–1430.
75. *A functionally conserved homolog of the drosophila segment polarity gene hh is expressed in tissues with polarizing activity in zebrafish embryos*. **Krauss, S, Concordet, J.P. and Ingham, P.W.** 1993, *Cell*, Vol. 75, pp. 1431–1444.
76. *Floor plate and motor neuron induction by vhh-1, a vertebrate homolog of of hedhegoh expressed by the notochord*. **Roelink, H., et al., et al.** 1994, *Cell*, Vol. 76, pp. 761-775.
77. *Indian hedgehog activates hematopoiesis and vasculogenesis and can respecify prospective neuroectodermal cell fate in the mouse embryo*. **Dyer, MA, Farrington, SM, Mohn, D, Munday, JR and Baron, MH**. 2001, *Development*, Vol. 30, pp. 1717-30.
78. *Regulation of cartilage dufferentiation by Indian hedgehog and PTH-related protein*. **Vortkamp, A, Lee, K, Lankse, B, Segre, GV, Kronenberg, HM and Tabin, CJ**. 1996, *Science*, Vol. 273, pp. 613-622.
79. *Functional differences among Xenophis nodal-related genes in left-right axis determination*. **Sampath, K, Cheng, AM, Frisch, A and Wright, CV**. 1997, *Development*, Vol. 124, pp. 3293-3302.
80. *Communicating with Hedgehogs*. **Hooper, JE and Scott, MP**. 2005, *Nat. Rev. Mol. Cell. Biol.*, Vol. 6, pp. 306-17.
81. *Patched acts catalytically to suppress the activity of Smoothened*. **Taipale, J, Cooper, MK, Maiti, T and Beachy, PA**. 2002, *Nataure*, Vol. 418, pp. 892-97.
82. *Catching a Gli-mpse of Hedgehog*. **Ruiz-Altaba, A**. 1997, *Cell.*, Vol. 90, pp. 193-96.
83. *Gli proteins in development and disease*. **Hui, C.C.and Angers, S**. 2011, *Annu. Rev. Cell Dev. Biol.*, Vol. 27, pp. 513–537.

84. *Mechanisms of hedgehog pathway activation in cancer and implications for therapy.* **Scales, S.J. and de Sauvage, F.J.** 2009, Trends Pharmacol. Sci., Vol. 30, pp. 303–312.
85. *Context-dependent regulation of the Gli code in cancer by hedgehog and non-hedgehog signals.* **Stecca, B. and Ruiz, I.A.A.** 2010, J. Mol. Cell Biol., Vol. 2, pp. 84–95.
86. *Mammalian suppressor-of-fused modulates nuclear-cytoplasmic shuttling of Gli-1.* **Kogerman, P., et al., et al.** 1999, Nat. Cell. Biol. , pp. 312–319. .
87. *Identification of Shhas a caandidate gene responsible for holoprosencephaly.* **Belloni, E, Muenke, M, Roessler, E, Traverso, G, Siegel-Bartelt, J, Frumkin, A et al.** 1996, Nat. Gen., pp. 353-56.
88. *mutations in thr human Sh genecause holoprosencephaly.* **Roessler E, Belloni E, Gaudenz K, Berta P, Scherer SW et al.** 1996, Nat. Gen., pp. 357-60.
89. *The hedgehog response network: Sensors, switches, and routers.* **Lum, L. and Beachy, P.A.** 2004, Science, Vol. 304, pp. 1755-59.
90. *Multiple nevoid basal-cell epithelioma, jaw cysts and bifid rib.* **Gorlin, R.J. and Goltz, R.W.** 1960, N. Engl. J. Med., Vol. 212, pp. 908-12.
91. *Clinical manifestations in 105 persons with nevoid basal cell carcinoma syndrome.* **Kimonis, V.E., et al., et al.** 1997, Am. J. Med. Genet., Vol. 69, pp. 299-308.
92. *Hedhehog signalling within airway epithelial progenitors and in small-cell lung cancer.* **Watkins, DN, Berman, DM, Burkholder, SG, Wang, B, Beachy, PA and Baylin, SB.** 2003, Nature, Vol. 422, pp. 313–317.
93. *Human colon cancer epithelial cells harbour active hedgehog-GLI signalling that is essential for tumour growth, recurrence, metastasis and stem cell survival and expansion.* **Varnat, F., et al., et al.** 2009, EMBO Mol. Med., Vol. 1, pp. 338–351.
94. *Hedgehog signalling in prostate regeneration, neoplasia and metastasis.* **Karhadkar, S.S., et al., et al.** 2004, Nature, pp. 707–712.
95. *The gain-of-function GLI1 transcription factor tGLI1 enhances expression of VEGF-C and TEM7 to promote glioblastoma angiogenesis.* **Carpenter, RL, Paw, I, Zhu, H, Sirkisoon, S and Xing, F.** 2015, Oncotarget, Vol. 6, pp. 22653–22665.
96. *Tumor-host interactions: a far-reaching relationship.* **Mcallister, SS and Weinberg, RA.** 2010, J Clin Oncol, Vol. 28, pp. 4022–8.
97. *A paracrine requirement for hedgehog signalling in cancer.* **Yauch, R.L., et al., et al.** 2008, Nature, Vol. 455, pp. 406–410.
98. *Melanoma and the tumor microenvironment.* **Villanueva, J and Herlyn, M.** 2008, Curr Oncol Rep, Vol. 10, pp. 439-46.

99. *Focus on melanoma*. **Houghton AN, and Polsky D.** 4, 2002, *Cancer Cell.*, Vol. 2, pp. 275–278.
100. *Global cancer statistics, 2002*. **Parkin D, Bray F, Ferlay J, and Pisani P.** 2, 2005, *CA Cancer J Clin*, Vol. 55, pp. 74-108.
101. *Early detection and treatment of skin cancer*. **Jerant AF, Johnson JT, Sheridan CD and Caffrey TJ.** 2, 2000, *Am Fam Physician*, Vol. 62, pp. 357–68, 375–6, 381–2.
102. *BRAF as therapeutic target in melanoma*. . **Wellbrock, C and Hurlstone, A.** 2010, *Biochem Pharmacol.*, pp. 561-567.
103. *Mutations of the BRAF gene in human cancer*. **Davies H, Bignell GR, Cox C, et al.** 2002, *Nature.*, Vol. 417, pp. 949-954.
104. *A pivotal role for ERK in the oncogenic behaviour of malignant melanoma?* **Smalley, KS.** 5, 2003, *Int J Cancer.*, Vol. 104, pp. 527–532.
105. *Melanomas require HEDGEHOG-GLI signaling regulated by interactions between GLI1 and the RAS-MEK/AKT pathways*. **Stecca B, Mas C, Clement V, Zbinden M, Correa R, Piguet V, Beermann F and Ruiz IAA.** 14, 2007, *PNAS*, Vol. 104, pp. 5895-5900.
106. *PDGFR $\alpha$  up-regulation mediated by sonic hedgehog pathway activation leads to BRAF inhibitor resistance in melanoma cells with BRAF mutation*. **Sabbatino F, Wang Y, Wang X, Flaherty KT, Yu L, Pepin D, Scognamiglio G, Pepe S, Kirkwood JM, Cooper ZA, Frederick DT, Wargo JA, Ferrone S, and Ferrone CR.** 7, 2013, *Oncotarget*, Vol. 5, pp. 1926-41.
107. *GLI2-mediated melanoma invasion and metastasis*. **Vasileia-Ismini Alexaki, Delphine Javelaud, Leon C. L. Van Kempen, Khalid S. Mohammad, Sylviane Dennler, Flavie Luciani, Keith S. Hoek, Patricia Juárez, James S. Goydos, Pierrick J. Fournier, Claire Sibon, Corine Bertolotto, Franck Verrecchia, et al.** 2010, *JNCI*, pp. 1148-59.
108. *Malignant melanoma: genetics and therapeutics in the genomic era*. **Chin L, Garraway LA, and Fisher, DE.** 16, 2006, *Genes Dev.*, Vol. 20, pp. 2149–2182.
109. *Treatment of metastatic melanoma: an overview*. **Bhatia S, Tykodi SS and Thompson JA.** 2009, *Oncology.* , Vol. 23, pp. 488-496.
110. *MicroRNAs and cancer resistance: A new molecular plot*. **Fanini, F and Fabbri, M.** *Clin. Pharmacol. Ther.* : s.n., 2016.
111. *MicroRNAs as new therapeutic targets and tools in cancer*. **Gandellini P, Profumo V, Folini M and Zaffaroni N.** 2011, *Expert Opin Ther Targets* , Vol. 15, p. 265 279.
112. *Hypoxia inducible factor-1 $\alpha$  as a therapeutic target in multiple myeloma*. **Borsi, E., Perrone, G., Terragna, C., Martello, M., Dico, A. F., Solaini, G., Baracca, A., Sgarbi, G.,**

**Pasquinelli, G., Valente, S., Zamagni, E., Tacchetti, P., Martinelli, G., and Cavo, M.** 2014, *Oncotarget*, Vol. 5, pp. 1779–1792.

113. *Protein measurement with the Folin phenol reagent.* **Lowry OH, Rosebrough NJ, Farr AL, Randall RJ.** 1951, *J Biol Chem*, Vol. 193, pp. 265-275.

114. *Stabilization of mitochondrial functions with digitonin.* **Kun, E., Kirsten, E., and Piper, W. N.** 1979, *Methods Enzymol.*, Vol. 55, pp. 115-18.

115. *The Inhibitor Protein (IF1) of the F1F0-ATPase Modulates Human Osteosarcoma Cell Bioenergetics.* **Barbato S, Sgarbi G., Gorini G., Baracca A., Solaini G.** 10, 2015, *J Bio Chem.*, Vol. 290, pp. 6338-48.

116. *Oxidative phosphorylation in cancer cells.* **Solaini, G., Sgarbi, G., and Baracca, A.** 2011, *Biochim. Biophys. Acta*, Vol. 1807, pp. 534–542.

117. *Quantification of muscle mitochondrial oxidative phosphorylation enzymes via histochemical staining of blue native polyacrylamide gels.* **Zerbetto, E., Vergani, L., and Dabbeni-Sala, F.** 1997, *Electrophoresis*, Vol. 18, pp. 2059–2064.

118. *Mitochondrial Complex I decrease is responsible for bioenergetic dysfunction in K-ras transformed cells.* **Baracca, A., Chiaradonna, F., Sgarbi, G., Solaini, G., Alberghina, L., and Lenaz, G.** 2010, *Biochim. Biophys. Acta*, Vol. 1797, pp. 314–323.

119. *Mitochondria hyperfusion and elevated autophagic activity are key mechanisms for cellular bioenergetic preservation in centenarians.* **Sgarbi G, Matarrese P, Pinti M, Lanzarini C, Ascione B, Gibellini L, Dika E, Patrizi A, Tommasino C, Capri M, Cossarizza A, Baracca A, Lenaz G, Solaini G, Franceschi C, Malorni W, Salvioli S.** 2014, *Aging*, Vol. 6, pp. 296-310.

120. *Assessment of mitochondrial oxidative phosphorylation in patient muscle biopsies, lymphoblasts, and transmitochondrial cell lines.* **Trounce IA, Kim YL, Jun AS, Wallace DC.** 1996, *Methods Enzymol* , Vol. 264, pp. 484-509.

121. *Hyperoxia fully protects mitochondria of explanted livers.* **Sgarbi G, Giannone F, Casalena GA, Baracca A, Baldassarre M, Longobardi P, Caraceni P, Derenzini M, Lenaz G and Solaini G.** 6, 2011, *J Bioenerg Biomembr.* , Vol. 43, pp. 673-82.

122. *Biochemical phenotypes associated with the mitochondrial ATP6gene mutations at nt8993.* **Baracca A, Sgarbi G, Mattiazzi M, Casalena G, Pagnotta E, Valentino ML, Moggio M, Lenza G, Carelli V and Solaini G.**

123. *Glucose plays a main role in human fibroblasts adaptation to hypoxia.* **Baracca, A., Sgarbi, G., Padula, A., and Solaini, G.** 2013, *J. Biochem. Cell Biol.*, Vol. 45, pp. 1356–1365.

124. *Inefficient coupling between proton transport and ATP synthesis may be the pathogenic mechanism for NARP and Leigh syndrome resulting from the T8993G mutation in mtDNA.* Sgarbi G, Baracca A, Lenaz G, Valentino LM, Carelli V, Solaini G. 2006, *Biochem J*, Vol. 395, pp. 493-500.
125. *Tryptophan phosphorescence as a structural probe of mitochondrial F1-ATPase-subunit.* Solaini G, Baracca A, Parenti Castelli G, and Strambini GB. 1993, *Eur. J. Biochem.*, Vol. 214, pp. 729–734.
126. *Determination of blood glucose using 4-amino phenazone as oxygen acceptor.* Trinder, P. 2, 1969, *J Clin Pathol.*, Vol. 22, p. 246.
127. *MicroRNA targets in Drosophila.* Enright, A.J., John,B., Gaul,U., Tuschl,T., Sander,C. and Marks, D.S. 2003, *Genome Biol.*, p. R1.
128. *miRWalk2.0: a comprehensive atlas of microRNA-target interactions.* Dweep, H et al. 8, 2015, *Nature Methods*, Vol. 12, p. 697.
129. Sutherland, RM. 1988, *Science*, Vol. 240, pp. 177-84.
130. *Expression, regulation and clinical relevance of the ATPase inhibitory factor 1 in human cancers.* Sánchez-Aragó M1, Formentini L, Martínez-Reyes I, García-Bermudez J, Santacatterina F, Sánchez-Cenizo L, Willers IM, Aldea M, Nájera L, Juarránz A, López EC, Ciofent J, Navarro C, Espinosa E, Cuezva JM. 2, 2013, *Oncogenesis*, Vol. 22.
131. *Assessing actual contribution of IF1, inhibitor of mitochondrial FOF1, to ATP homeostasis, cell growth, mitochondrial morphology, and cell viability.* . Fujikawa, M., Imamura, H., Nakamura, J., and Yoshida, M. 2012, *J. Biol. Chem.*, Vol. 287, pp. 18781–18787.
132. *Up-regulation of the ATPase Inhibitory Factor 1 (IF1) of the Mitochondrial H<sup>+</sup>-ATP Synthase in Human Tumors Mediates the Metabolic Shift of Cancer Cells to a Warburg Phenotype.* Sánchez-Cenizo L, Formentini L, Aldea M, Ortega AD, García-Huerta P, Sanchez-Aragó M, and José M. Cuezva. 33, 2010, *JBC*, Vol. 285, pp. 25308-13.
133. *IF1 reprograms energy metabolism and signals the oncogenic phenotype in cancer.* Sánchez-Aragó M, Formentini L, García-Bermúdez J and José M. Cuezva. 16, 2012, *Cell Cycle*, Vol. 11.
134. *Lack of major changes in ATPase activity in mitochondria from liver, heart, and skeletal muscle of rats upon ageing.* Barogi, S., Baracca, A., Parenti Castelli, G., Bovina, C., Formigini, G., Marchetti, M., Solaini, G., and Lenaz, G. 1995, *Mech. Ageing D*, Vol. 84, pp. 139-50.
135. *Modification of the mitochondrial F1-ATPase epsilon subunit, enhancement of the ATPase activity of the IF1-F1 complex and IF1-binding dependence of the conformation*

of the epsilon subunit. **Solaini G, Baracca A, Gabellieri E, Lenaz G.** 327, 1997, *Biochem J.*, Vol. 15, pp. 443-8.

136. *IF1: setting the pace of the F1Fo-ATP synthase.* **Campanella M, Parker N, Tan CH, Hall AM and Duchen MR.** 2009, Cell Press, pp. 343-50.

137. *Purification and characterization of adenosine triphosphatase from eel liver mitochondria.* **Baracca, A., Degli Esposti, M., Parenti Castelli, G., and Solaini, G.** 1992, *Comp. Biochem. Physiol.*, pp. 421-26.

138. *Modulation of the oligomerization state of the bovine F1-ATPase inhibitor protein, IF1, by pH.* **Cabezón, E., Butler, P. J., Runswick, M. J., and Walker, J. E.** 2000, *J. Biol. Chem.*, Vol. 275, pp. 25460–64.

139. *MicroRNA signatures in human cancers.* **Calin, GA and Croce, CM.** 11, 2006, *Nat. Rev. Cancer*, Vol. 6, pp. 857–866.

140. *Regulation of cancer cell metabolism.* **Cairns, RA, Harris, IS and Mak, TW.** 2, 2011, *Nat. Rev. Cancer*, Vol. 11, pp. 85-95.

141. *Control of mitochondrial ATP synthesis.* **Harris, DA and Das, AM.** 1991, *Biochem. J.*, Vol. 280, pp. 561–573.

142. *The microcosmos of cancer.* **Lujambio A. and Lowe, SW.** 7385, 2012, *Nature*, Vol. 482, pp. 347–355.

143. *MicroRNA expression profiling using microarrays.* **Liu CG, Calin GA, Volinia S and Croce CM.** 4, 2008, *Nat Protoc.*, Vol. 3, pp. 563-78.

144. *Trial of combined intermittent chemotherapy in prostatic cancers. Estrogen resistant metastases.* **Chauvin, HF.** 12 Pt 2, 1973, Vol. 79, pp. 397-8.

145. *MiR 133a is functionally involved in doxorubicin resistance in breast cancer cells MCF 7 via its regulation of the expression of uncoupling protein 2.* **Yuan Y, Yao YF, Hu SN, Gao J and Zhang LL.** 2015, *PLoS One*.